BRNO UNIVERSITY OF TECHNOLOGY

VYSOKÉ UČENÍ TECHNICKÉ V BRNĚ

CENTRAL EUROPEAN INSTITUTE OF TECHNOLOGY BUT

STŘEDOEVROPSKÝ TECHNOLOGICKÝ INSTITUT VUT

RESEARCH AND DEVELOPMENT OF A TECHNOLOGY OF HARD ANODIZATION OF NONFERROUS ALLOYS

VÝZKUM A VÝVOJ TECHNOLOGIE PŘÍPRAVY TVRDÉ ANODIZACE NEŽELEZNÝCH SLITIN

DOCTORAL THESIS
DIZERTAČNÍ PRÁCE

AUTHOR   Ing. Michaela Remešová
AUTOR PRÁCE

SUPERVISOR   prof. Ing. Jozef Kaiser, Ph.D.
ŠKOLITEL

BRNO 2020

Abstract

The thesis is focused on the research and development of the technological process for the preparation of hard anodic coatings on three different non-ferrous materials, namely (i) aluminium alloy (AA1050), (ii) pure magnesium (99.9% Mg), and (iii) zinc alloy (ZnTi2). Suitable combinations of anodizing conditions (voltage, current density, temperature and composition of the electrolyte, etc.) can produce anodic coatings with different properties. The effect of pre-treatment and anodizing conditions on the appearance, morphology, thickness and hardness of the produced anodic coatings was demonstrated in the present thesis. In order to increase tribological properties and hardness, the anodic coatings were directly doped with Al_2O_3 or with a mixture of Al_2O_3/PTFE particles during the anodizing process. The theoretical part describes the basic principles of anodization, the methods used in industry and the technological process. The experimental part is divided into three basic parts. The first part is devoted to anodizing of aluminium alloy. The second part is focused on anodizing of pure magnesium, and the last part is focused on anodizing of zinc alloy, which has not been researched as thoroughly as anodizing of aluminium.

Keywords
Surface treatment, anodizing process, aluminium, magnesium, zinc, coating microstructure, hardness, wear

Abstrakt

Práce je zaměřena na výzkum a vývoj technologie přípravy tvrdých anodických vrstev na třech různých typech neželezných materiálů a to (i) hliníkové slitině (AA1050), (ii) čistém hořčíku (99.9% Mg) a (iii) zinkové slitině (ZnTi2). Vhodnou kombinací anodizačních podmínek (napětí, proudová hustota, teplota a složení elektrolytu atd.) lze vytvářet anodické vrstvy s rozdílnými vlastnostmi. V rámci předložené práce byl prokázán vliv předúpravy a anodizačních podmínek na vzhled, morfologii, tloušťku a tvrdost vytvořených anodických vrstev. Pro zvýšení tribologických vlastností a tvrdosti byly anodické vrstvy přímo dopovány Al_2O_3 částicemi nebo kombinací Al_2O_3 a PTFE částic během anodizačního procesu. Teoretická část práce popisuje základní principy anodizace, metody používané v průmyslové praxi a v práci je také popsán technologický proces. Experimentální část je rozdělena na tři základní části. První část se věnuje anodické oxidaci hliníkové slitiny AA1050. Druhá část je zaměřena na anodizaci čistého hořčíku a poslední část je zaměřena na anodizaci zinkové slitiny ZnTi2, která není tak známá jako anodizace hliníku.

Klíčová slova
Povrchová úprava, anodizace, hliník, hořčík, zinek, mikrostruktura, tvrdost, opotřebení

Bibliographic citation

REMEŠOVÁ, Michaela. *Research and development of a technology of hard anodization of nonferrous alloys.* Brno, 2020. Available online: https://www.vutbr.cz/studenti/zav-prace/detail/128704. Doctoral thesis. Vysoké učení technické v Brně, Středoevropský technologický institut VUT, Central European Institute of Technology BUT. Supervisor Jozef Kaiser.

Statement

I declare that this doctoral thesis was performed independently under the supervision of Prof. Ing. Jozef Kaiser, Ph.D. and Assoc. Prof. Ing. Ladislav Čelko, Ph.D., and it is original work with using the cited sources, literature and other professional sources which are listed in the text and reference list.

In Brno, 3.7.2020

Ing. Michaela Remešová

Acknowledgement

Contents

Introduction

Aluminium (Al), magnesium (Mg), zinc (Zn) and their alloys are used mainly in the automotive, aerospace, marine, and consumer industries, especially in fields where the weight reduction is critical, or where there are additional technical requirements for lightweight components. A disadvantage of these materials is related to the not very suitable surface properties such as corrosion resistance and surface hardness, which hinder their widespread use. For example, Mg and its alloys have poor corrosion resistance in most environments and require surface treatment or coating. Light metals such as those listed above are characterized by poor tribological properties, including low abrasion resistance and low strength. On the other hand, there has been a recent increase in the demand for non-ferrous metal components operating in extreme conditions (the influence of UV radiation, low/high temperature, and corrosive environments) together with higher requirements for improvement in their surface properties. One possibility to improve the aforementioned properties of these materials while increasing the service life of components is surface treatment [1-4].

A variety of surface treatment processes are being used to protect non-ferrous metals, including surface conversion treatment (e.g. chromating, phosphating), anodizing, and galvanizing/plating. These processes can be used alone or in combination with the application of organic coatings. In addition, further methods have been reported such as chemical vapour deposition (CVD), physical vapour deposition (PVD), plasma spraying and electron/laser beam surface treatments [2], which can act similarly. The anodizing technique was developed a long time ago, mainly with the aim to produce decorative coatings on Al and its alloys surfaces. Anodizing is one of the most popular industrial processes, which applies an anodic current or voltage to a substrate metal to produce a decorative, durable, corrosion-resistant, anodic coating [1, 2]. These anodic coatings are most commonly applied to protect Al, Mg, Ti and their alloys and less often to protect Zn and its alloys. Anodic coatings may be used to improve paint adhesion, strength, and chemical, mechanical and tribological properties of the metal, as a surface treatment before dyeing or as a passivation treatment. It is a very cost-effective method for producing a uniform and highly adhesive oxide/hydroxide coatings on metals. Two types of coatings can be produced: (i) compact barrier coating and (ii) porous coating [4-7]. The technological process includes (1) mechanical pre-treatment, (2) chemical pre-treatment (degreasing, etching, activation), (3) anodizing using direct current (DC), alternating current (AC) or pulse current (PC), (4) dyeing or post-treatment, and (5) sealing. Every stage has an influence on the final properties of coatings.

Several methods for anodizing of aluminium are used in the industry. Chromic acid anodizing (CAA, Type I) is used in aerospace, sulfuric acid anodizing (SAA, Type II) or decorative anodizing is used in architecture or for anodizing of subjects of daily necessity while hard anodizing (HA, Type III) is used in the mechanical engineering [8]. For industrial anodization of Mg and its alloys, the following three methods are most frequently used: Dow 9, Dow 17 and HAE. The least-used anodizing technology in the industry is anodizing

1

of zinc. With the increasing demands on the coating properties, Al and Mg micro-arc oxidation technologies are being developed and improved [7, 9].

Most of the commercial methods require expensive processes (e.g. high temperature of the electrolyte, high voltage, etc.) or the use of hazardous/toxic chemicals (e.g. hexavalent chromium). Therefore, new and more environmentally friendly methods are being developed. Anodically produced coatings are widely used in the automotive, aerospace, engineering and marine industries, but recently they have also been used in medicine, electrical engineering, and nanotechnology [2].

The non-uniform growth of an anodic coating is strongly influenced by the type of alloying elements or the resulting intermetallic phase and has a considerable effect on the resulting corrosion resistance, mechanical properties, and appearance of the produced coatings.

The thesis is divided into two main parts. The first part is the theoretical part that includes subchapters describing the fundamental principle, standard methods of the anodizing process of aluminium, magnesium and zinc. Also described are the properties and parameters of anodic coatings, the influence of the chemical composition of initial material on the growth of anodic coatings, and the technological process. The second part is the experimental part, which is focused on the optimization of the technological process of anodizing of aluminium alloy (AA1050), pure magnesium (99.9% Mg) and zinc alloy (ZnTi2). The effect of pre-treatment and anodizing conditions (concentration, composition and temperature of the electrolyte, current density/voltage, anodizing time, etc.) on the morphology, thickness, etc. of the produced anodic coatings were investigated. To improve the hardness and tribological properties of the produced anodic coatings, aluminium oxide (Al_2O_3) and polytetrafluoroethylene (PTFE) particles were added to the electrolyte.

1. Theoretical part

1.1. Fundamentals of anodizing

Non-ferrous metals can form native oxide/hydroxide coatings on their surfaces that offer limited protection to surface degradation. Anodizing is an electrochemical process during which a thicker, durable, corrosion and wear-resistant anodic oxide/hydroxide coating is formed [2, 8]. During anodizing, the component is immersed in an electrolyte of suitable composition and is connected as the anode (positive electrode) into an electrical circuit with (i) direct current (DC), (ii) alternating current (AC) or (iii) pulse current (PC) (Fig. 1). The counter electrode (cathode) is sheet or rod of stainless steel, carbon, lead, platinum or any other metal that is inert in the anodizing electrolyte [8, 10]. The anodizing process of Al, Mg, Zn and their alloys is based on chemical and electrochemical reactions between the substrate of initial material and the electrolyte. Such reactions for each experimental material are described in the following chapter.
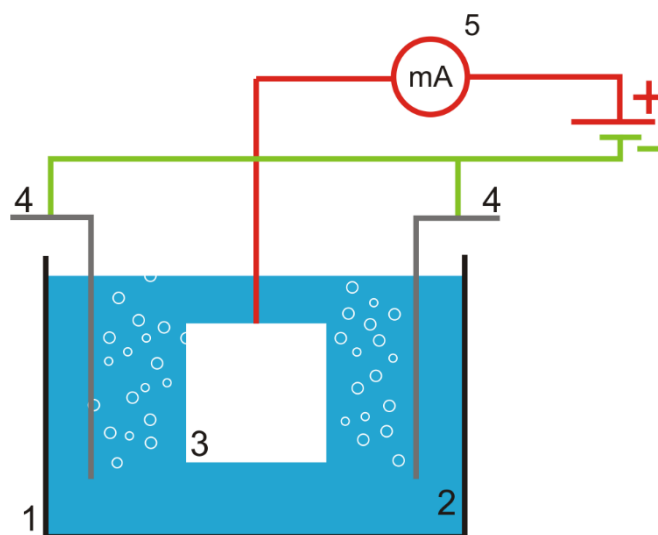
Fig. 1 *Schematic illustration of the anodizing cell: 1 - tank, 2 - electrolyte, 3 - component (anode), 4 - cathode, 5 - controlled power source.*

Although aluminium (Al), magnesium (Mg), zinc (Zn) and their alloys can be anodized, there are significant differences in their pre-treatment (degreasing, etching, deoxidizing, etc.), in the anodizing process conditions (voltage/current density, composition and temperature of the electrolyte, etc.) and in the post-treatment (sealing).

Generally, for the anodizing process of Al and its alloys, acidic electrolytes and low voltage are mostly used, whereas, for Mg, Zn and their alloys, alkaline or neutral electrolytes in combination with higher voltage are used.

The anodized coating formed on Al is regular in structure and consists of a compact barrier coating adjacent to the metal surface and/or a coating containing uniform parallel pores normal to the surface. In contrast, the anodized coatings on Mg and Zn are irregularly porous in structure [1, 2].

The final properties and quality of these electrochemically formed anodic coatings are influenced by a number of factors, in particular by the: (i) type, concentration and temperature of electrolyte, (ii) chemical composition of the initial material and its purity, (iii) current density, (iv) voltage, (v) anodizing time, (vi) homogeneity of the cooling and electrolyte agitation, and (vii) method of mounting or hanging the component [2, 11, 12].

1.2. Electrochemical process of aluminium anodizing

The chemical reaction of Al anodizing can be described simply as [13]:

$$2Al + 3H_2O \rightarrow Al_2O_3 + 3H_2. \tag{1}$$

Equation (1) represents the overall chemical reaction. However, it is also essential to understand the chemical reactions at the aluminium/oxide and electrolyte/oxide interfaces separately [13]. A schematic illustration of the process occurring during anodizing is shown in Fig. 2 [7].
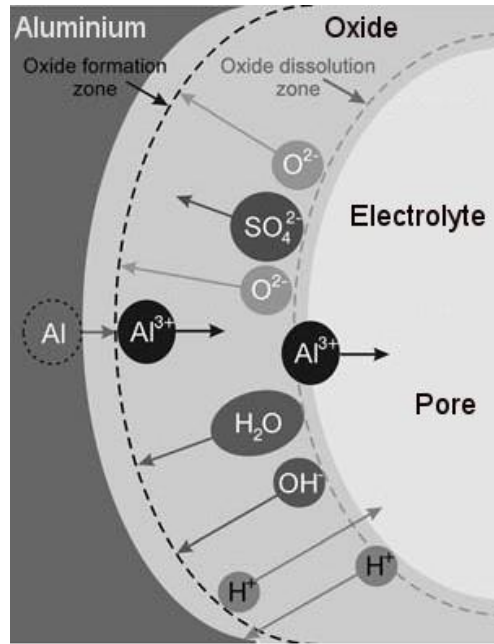
Fig. 2 *Schematic representation of the cross-sectional view of an illustration of ions move through the electrolyte/oxide and the aluminium/oxide interface during the anodizing process in sulfuric acid electrolyte resulting in porous aluminium oxide [7].*

When an electric field is applied, hydrogen ions are reduced to produce hydrogen gas at the cathode, and the aluminium anode (oxide/metal interface) is oxidized into Al^{3+} [13]:

$$Al \rightarrow Al^{3+} + 3e^-. \tag{2}$$

At the same time, the dissociation of water takes place on the cathode [7]:

$$2H_2O + 2e^- \rightarrow 2OH^- + H_2(g). \tag{3}$$

Moreover, at the electrolyte/oxide interface, the formation of OH^- and O^{2-} ions occur due to H_2O splitting or to interaction with the absorbed electrolyte anions. This can be expressed, in the case of H_2SO_4 electrolyte as [7]:

$$2H_2O + 2SO_4^{2-} \rightarrow O^{2-} + H_2SO_4 + OH^- + HSO_4^-. \tag{4}$$
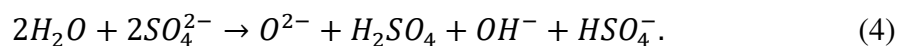
Although the anodizing of Al has been investigated widely, it is still not clear which oxygen-carrying anion species (OH⁻, O²⁻) is involved in the anodic process and reacted with Al^{3+}. Under an electric field, OH⁻ and O²⁻ ions migrate inwards through the oxide towards aluminium (anode), where they form γ-Al_2O_3, γ'-Al_2O_3 or η-Al_2O_3. The possible reactions are [7, 8]:

$$2Al + 6OH^- \rightarrow Al_2O_3 + 3H_2O + 3e^- \tag{5}$$

$$2Al + 3O^{2-} \rightarrow Al_2O_3 + 6e^-. \tag{6}$$
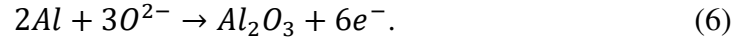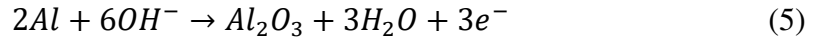
Based on reported experimental work [13-15], it has been found that some Al^{3+} cations migrate across the oxide coating and are dissolved into the electrolyte or they form an aluminium oxide at the electrolyte/oxide interface.

1.3. Electrochemical process of magnesium anodizing

The most accurate description of the Mg anodizing mechanism in a silicate-containing electrolyte is based on the theoretical description and experimental results by Shi et al. [2]. The anodizing process was classified into four different stages. A schematic illustration of the anodizing stages is presented in Fig. 3 [2].
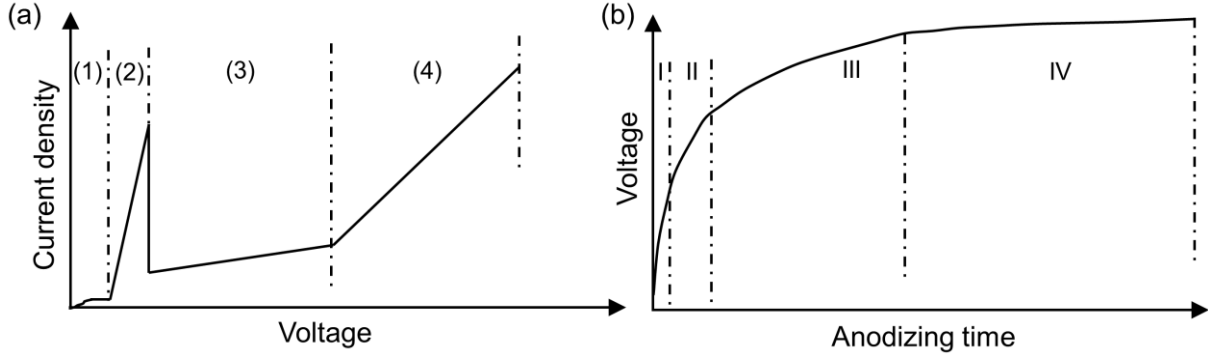
Fig. 3 *Schematic illustration of anodizing stages: (a) anodic polarization curve in the voltage control mode and (b) dependence of cell voltage on anodizing time in the current control mode [2].*

First stage

The anodizing voltage increases linearly (< 10 V) with anodizing time. At the cathode, hydrogen is evolved in the form of bubbles. At the anode, Mg dissolves in the electrolyte first and then $Mg(OH)_2$ and $MgSiO_3$ coating is formed, and oxygen is evolved at the same time. The possible reaction can be described by the following equation (7, 8, 9, 10) [2]:

$$4OH^- \rightarrow 2H_2O + O_2 + 4e^- \tag{7}$$
$$Mg \rightarrow Mg^{2+} + 2e^- \tag{8}$$
$$Mg^{2+} + 2OH^- \rightarrow Mg(OH)_2 \tag{9}$$
$$Mg^{2+} + SiO_3^{2-} \rightarrow MgSiO_3. \tag{10}$$

At this stage, the produced coatings are thin and dense because the anodizing time is only a few seconds. The reactions 8-10 which were reported by Mizutani et al. [16], and reaction (7) are insignificant at this stage [2].

Second stage

The anodizing voltage increases up to a value of ~190 V, and the evolution of some tiny gas bubbles can be observed but no sparking. It has been postulated that in addition to the anodizing reactions (7-10), another reaction (11) starts to take place [2]:

$$Mg + 2OH^- \rightarrow MgO + H_2O + 2e^-. \tag{11}$$

7
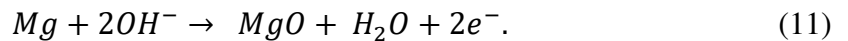
This is an electrochemical reaction resulting directly in the coating formation, and Mg is electrochemically oxidized into MgO [2].

Mizutani et al. [16] reported that the coating on Mg alloys formed at 60 V in an alkaline electrolyte contained a mixture of $Mg(OH)_2$, MgO and $MgSiO_3$. Therefore, the involvement of reaction (11) in this stage is reasonable. Reactions (9), (10) and (11) involved in this stage of anodizing can also be supported by the experimental results of Mizutani et al. [16]. Moreover, the limited oxygen evolution observed at this stage indicates that reaction (7) is still slow and therefore insignificant to the process. Kim et al. [17] studied the anodizing of Mg-Al alloys in the NaOH electrolyte at constant voltages of 3, 10, 40 and 80 V. The results showed that coatings formed at low voltages consisted of a relatively thick $Mg(OH)_2$ coating with a rough surface. In contrast, MgO coating with a smooth surface was formed at high voltage (Fig. 4). The high voltage anodizing process, especially the formation of the final multilayer coating, has not been described well yet.
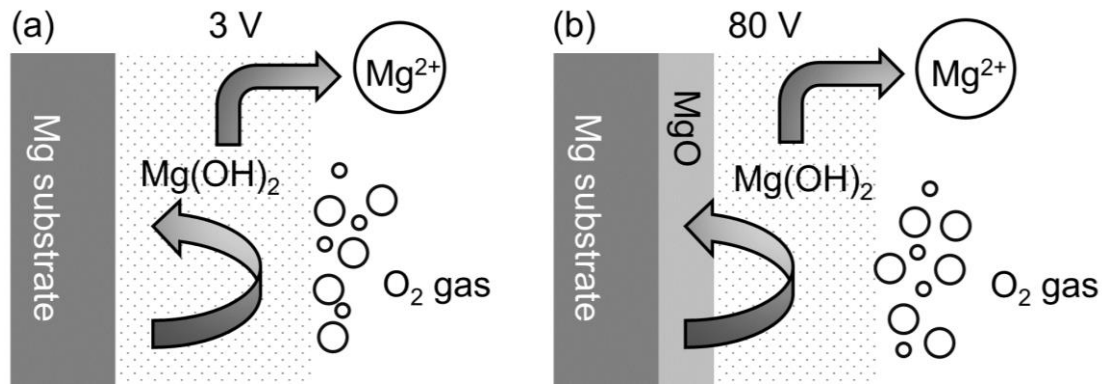
Fig. 4 Schematic illustration of the formation mechanism of anodic coatings on Mg-Al alloys at a constant voltage of (a) 3 V, and (b) 80 V [17].

Third stage

The obvious phenomena at this stage are the uniform sparking and significant gas evolution from the anodized sample surface. The voltage continues to increase up to ~330 V with anodizing time. Reactions (7-11) continue at this stage, and at the same time, the following reactions occur [2]:

$$Mg(OH_2) \rightarrow MgO + H_2O \tag{12}$$
$$2Mg + O_2 \rightarrow 2MgO. \tag{13}$$
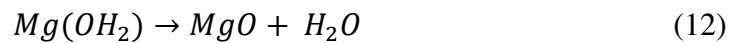
These reactions mainly describe chemical precipitation processes. Reaction (12) describes the dehydration process that can occur when the temperature is higher than 350 °C. The temperature of the sparking arc during the anodizing of Mg alloys is far above 1000 °C. Not all of the $Mg(OH)_2$ can be transformed into MgO. At the high temperature, direct oxidation of Mg is also possible, particularly with the active oxygen freshly generated by reaction (7). At this stage, there is an increasing amount of MgO in the coating and also increase in hardness and higher abrasion resistance. Therefore, reaction (13) is proposed in this stage of anodizing [2].

Fourth stage

When the voltage increases above 330 V, oxygen evolution becomes vigorous, and sparking much more intense and localized. This process is known as micro-arc oxidation (MAO) or plasma electrolytic oxidation (PEO). It is proposed that the two following reactions are also involved in the fourth stage [2]:

$$2MgO + yMgSiO_3 \rightarrow (MgO)_3 (SiO_2)_y \qquad (14)$$
$$2H_2O \rightarrow 2H_2 + O_2. \qquad (15)$$
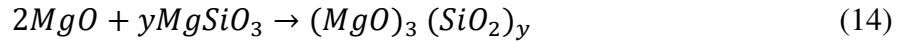
Reaction (14) describes the melting and solidification process of MgO and MgSiO$_3$ in the coating at the sparking spots. When the temperature increases during sparking, the anodized coating could be locally melted by sparking spots and mixed with some components or decomposed products of the electrolyte. Then such areas of the coating rapidly solidify into a reform coating. The sparking lasts only a few seconds and leads to the deposition of the silicates from the electrolyte directly into the coating through plasma discharge (melting and freezing), which is related to increasing ratio of the silicon particles in the coating. Reaction (15), i.e. thermal decomposition of water has not yet been sufficiently studied. There is a possibility that local areas of plasma discharge produce a sufficiently high temperature that allows decomposition of water [2].

1.4. Electrochemical process of zinc anodizing

Zinc oxide (ZnO) coatings are usually produced in aqueous solutions of NaOH, KOH, etc. As reported in many studies [18-21] in which the NaOH electrolyte was used, the possible mechanism for the process can be described as follows:

At the cathode, hydrogen gas is produced according to equation (16) [22]:

$$2H^+ + 2e^- \rightarrow H_2(g). \tag{16}$$

At the anode, the following reactions take place [18]:

$$Zn \rightarrow Zn^{2+} + 2e^- \tag{17}$$
$$Zn^{2+} + 4OH^- \rightarrow Zn(OH)_4^{2-}(aq) \tag{18}$$
$$Zn(OH)_4^{2-}(aq) \rightarrow Zn(OH)_2(s) + 2OH^- \tag{19}$$
$$Zn(OH)_2 \rightarrow ZnO + H_2O. \tag{20}$$
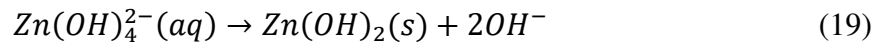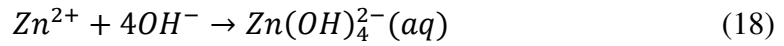
The initial stage of the process is the active dissolution of pure Zn (Eq. 17), which is attributed to the formation of $Zn(OH)_4^{2-}$ (Eq. 18). When the concentration of $Zn(OH)_4^{2-}$ exceeds the solubility of $Zn(OH)_2$, the precipitation of a compact coating of $Zn(OH)_2$ will occur on the anode surface according to Eq. 19. Finally, ZnO will form, as described by Eq. 20 [18, 22]. The coatings obtained in alkaline and carbonate electrolyte primarily consist of ZnO. The anodic coatings produced in the Na_3PO_4 electrolyte mainly consist of $Zn_3(PO_4)_2$ [21].

1.5. Commonly applied processes

1.5.1. Anodizing of aluminium and its alloys

U.S. Military Specification MIL-A-8625 describes three basic types of electrolytically formed anodic coatings on Al and its alloys. Chromic acid anodizing (CAA), or Type I, was the first large-scale commercial process for aluminium and its alloys developed by Bengough and Stuart [8]. The produced oxide coating is relatively softer, thinner and less porous than those formed by the other processes and does not lead to a deterioration of the fatigue properties of the substrate. The coating has substantial corrosion resistance and is an excellent base for paints. CAA is used by the aerospace, marine and automotive industries [23]. New environmentally friendly alternatives to the previous process were developed as a pre-treatment for paint adhesion [24-26], namely (i) phosphoric acid anodizing (PAA), (ii) boric-sulfuric acid anodizing (BSAA), (iii) phosphoric-sulfuric acid anodizing (PSA), and (iv) tartaric-sulfuric acid anodizing (TSA). The above-listed processes are more energy efficient (temperature, voltage, anodizing time, etc.) than CAA and conditions for the most commonly used processes are listed in Table 1.

Table 1 *Conventional anodizing processes of aluminium and its alloys - Type I.*

Method	Composition	Volts (V)	Time (min)	Temperature (ºC)	Thickness (µm)
CAA Bengough-Stuart	30 g/L $CrO_3^{\times}$	$0{\to}40$ 40 $40{\to}50$ 50	10 20 5-40 5	40	2.5-15
PAA	72 mL/L $H_3PO_4^{£}$	10-12	20-30	23-25	1-2
BSAA	30.5-52 g/L $H_2SO_4^{\#}$ 5.2-10.7 g/L $H_3BO_3^{*}$	15	18-22	24.5-29	3-5

$^{\times}CrO_3$ - chromium(VI) trioxide; $^{£}H_3PO_4$ - phosphoric acid; $^{\#}H_2SO_4$ - sulfuric acid; $^{*}H_3BO_3$ - boric acid

Sulfuric acid anodizing (SAA), or Type II, is the most widely used method to produce porous anodic aluminium oxide coatings on aluminium and its alloys, patented by Gower and Brien [27]. This process is primarily used for decorative or protective purposes (household appliances, furniture, architecture, sports equipment), and porous anodic aluminium oxide coating also serves well as a base for dye application [28]. Methods of dye application are further described in chapter 1.9.3. Addition of oxalic acid to the sulfuric acid electrolyte leads to the formation of harder and less porous anodic aluminium oxide coatings compared

to decorative anodizing. Therefore, it served as the background for the development of the hard anodizing process [29]. The most commonly used processes are listed in Table 2 [30].

Table 2 *Conventional anodizing processes of aluminium and its alloys - Type II.*

Method	Composition	Volts (V)	Time (min)	Temperature (°C)	Thickness (µm)
Sulfuric acid	60.44 mL/L H_2SO_4[#]	14-18	15-30	18	5-17
Oxydal	129.27 mL/L H_2SO_4	12-16	30	18	15-20
Oxal	28-147 g/L $C_2H_2O_4$[€]	60	30	20-22	10-20

[#]H_2SO_4 - sulfuric acid; [€]$C_2H_2O_4$ - oxalic acid

In the engineering industry, widespread use has been made of hard anodizing (HA), also called hard coat, engineered anodizing, or Type III [25]. Hard anodizing produces a heavier or denser coating than the general SAA or CAA processes do [30, 31]. Typical hard anodizing processes are listed in Table 3 [30]. Hard anodizing coatings are usually not sealed because sealing may deteriorate the hardness and abrasion resistance of coatings. In order to increase the sliding and static friction properties, the porous hard anodic aluminium oxide coating can be further improved by the incorporation of solid lubricants (e.g. PTFE or MoS_2) into coating [32-34].

Table 3 *Conventional anodizing processes of aluminium and its alloys - Type III.*

Method	Composition	Volts (V)	Time (min)	Temperature (°C)	Thickness (µm)
Martin Hard Coat	93.7 mL/L H_2SO_4[#]	20-75	80	-4	50
Alumilite 225 and 226	129.27 mL/L H_2SO_4 14 g/L $C_2H_2O_4$[€]	10-75	30-40	10	25-50

[#]H_2SO_4 - sulfuric acid; [€]$C_2H_2O_4$ - oxalic acid

1.5.2. Anodizing of magnesium and its alloys

Various anodizing processes have been developed to protect Mg and its alloys from corrosion. For industrial anodizing of Mg and its alloys, the following three primary processes are widely used: (i) Dow 9, (ii) Dow 17, and (iii) HAE. The Dow 9 process, also called galvanic anodizing, produces an anodic coating which is often used for optical components (telescopes, camera parts, etc.) and for heat sinks in electronic applications, as well as for applications that require a non-reflective surface. This coating also serves as an excellent base for paints [1, 8].

The Dow 17 process was developed by the Dow Chemical Company and can be used for all types of Mg alloys. For this process, DC or AC can be used. Coatings produced with DC are smoother than those using AC [1, 35].

The HAE process is effective for all Mg alloys and produces two types of coating like the Dow 17. Alternating current is applied to form the coating, and the voltage typically does not exceed 125 V. The coating produced at high voltage is very rough, relatively hard, with excellent abrasion resistance but, on the other hand, it is very brittle [1, 8, 35].

Upon sealing, the Dow 17 and HAE processes provide excellent anti-corrosion properties. The most commonly used processes are listed in Table 4 [8, 31]. Currently, Dow 17 and HAE are being replaced by processes which do not require the use of hexavalent-chromium or other heavy metals and operate below room temperature and at a high voltage (more than 150 V), for example Tagnite process, Megaoxide process, etc. [1, 2, 35]. The high voltage causes sparking, and the ongoing reactions are complicated.

Table 4 *Conventional anodizing processes of magnesium and its alloys - alternating current.*

Method	Composition	Volts (V)	Time (min)	Temp. (ºC)	Thickness (µm)	Colour
Dow 17	240 g/L $(NH_4)HF_2$[#] 100 g/L $Na_2Cr_2O_7\cdot2H_2O$[€] 90 mL/L H_3PO_4[£]	60-75* 90-100	4-5* 25	70-80	2.5-7.5* 23-38	light green* dark green
HAE	120 g/L KOH[×] 10.4 g/L $Al(OH)_3$[$] 34 g/L KF[@] 34 g/L Na_3PO_4[¥] 20 g/L K_2MnO_4[°]	65-70* 80-90	7-10* 60	< 35	5-10* 25-80	light* dark brown
Tagnite	4-8 g/L KOH 5-20 g/L KF 15-25 g/L K_2SiO_3[‡]	150-400	> 2	10-20	< 25	white

[#]$(NH_4)HF_2$ - ammonium hydrogen difluoride; [€]$Na_2Cr_2O_7\cdot2H_2O$ - sodium dichromate dihydrate; [£]H_3PO_4 - phosphoric acid; [×]KOH - potassium hydroxide; [$]$Al(OH)_3$ - aluminium hydroxide; [@]KF - potassium fluoride; [¥]Na_3PO_4 - triammonium phosphate; [°]K_2MnO_4 - potassium manganate; [¶]KOH - potassium hydroxide; [‡]K_2SiO_3 - potassium silicate; *thin coating

1.5.3. Anodizing of zinc and its alloys

Anodizing of Zn and its alloys was introduced into the industry under the trade name Iridize. Not many applications in the industry use it for cost reasons (high requirements for heating, equipment, etc.) [36]. In the last few years, anodizing of zinc has become more popular due to the development of technologies, and future applications including the solar cells, gas sensors, biosensors, optoelectronics or corrosion-resistant coating in mechanical engineering, antibacterial material in medicine, etc. [18, 37].

Anodizing of pure zinc in the KOH [38], NaOH [39], and H_2O [40] electrolytes and in the electrolytes with other additives was studied in [38, 41]. The resulting oxide coatings exhibit higher corrosion resistance than pure zinc does [42]. In order to increase wear resistance, service life coatings may be doped with submicron and nanometric particles.

1.6.   Types of anodic coating

In general, anodizing of non-ferrous metals can result in two different types of anodic coatings, depending on the type and concentration of electrolyte, current density or voltage: (i) compact barrier type (Fig. 5a) or (ii) porous type (Fig. 5b) [7, 14, 43, 44].
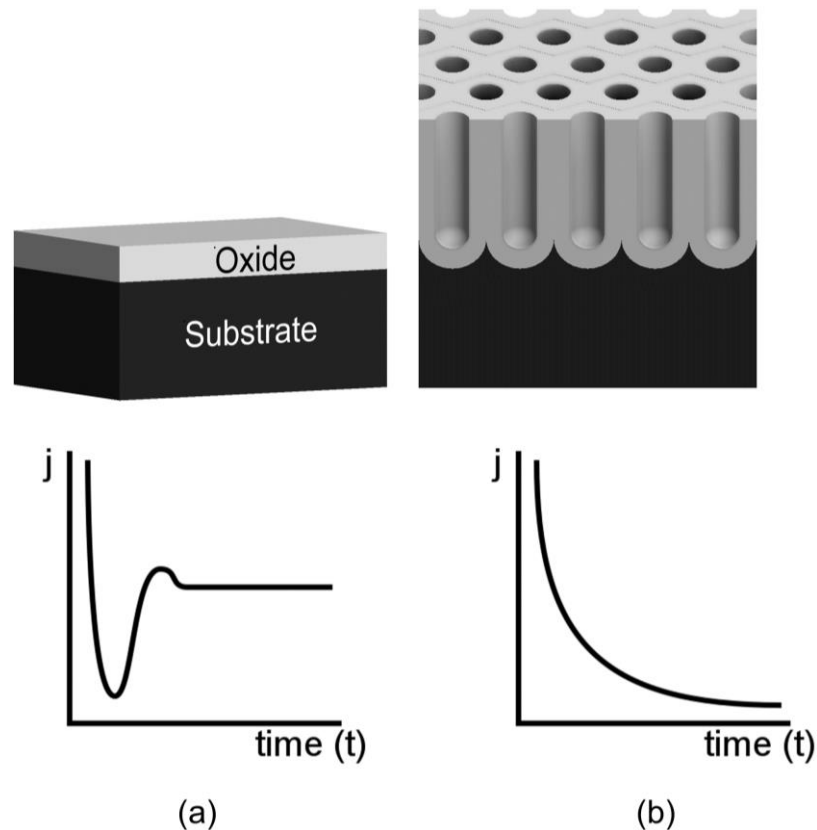
Fig. 5 *Two different types of anodic aluminium oxide coatings: (a) compact barrier type, and (b) porous type, along with the respective current (j) vs time (t) transients under potentiostatic conditions [14].*

1.6.1.   Compact barrier coating

A compact non-porous, barrier type, anodic aluminium oxide coating can be formed in electrolytes (pH 5-7) such as borate, oxalate, citrate, and phosphate solutions, in which the oxide is practically insoluble. These coatings are thin (< 700 nm) and dielectrically compact. The commercial use of barrier type coatings is in the field of dielectric capacitors, which cannot be achieved by using porous type coatings [45-47]. The high dielectric constant and the stability of amorphous Al_2O_3, even at high temperatures, make this compound a good candidate for gate insulator materials [7, 14, 46]. Compact barrier type coatings, which support high electric fields, can also be formed on Mg in a glycerol/fluoride electrolyte with water [48]. The resulting thickness of the compact barrier coating is mainly determined by the applied voltage and the type and concentration of the electrolyte [46, 49, 50].

1.6.2. Porous coating

By contrast, the porous type of anodic aluminium oxide can be formed in strongly acidic electrolytes (pH < 4) such as sulfuric acid (H_2SO_4), oxalic acid ($C_2H_2O_4$) or phosphoric acid (H_3PO_4), in which the resulting coating can be only sparingly soluble in electrolyte [7, 34]. The porous type of anodic magnesium coating can be formed in the NaOH electrolyte [2, 44], alkaline borate electrolyte [51], etc. Porous ZnO coatings can be formed in H_2O [40], $C_2H_2O_4$ [52] or NaOH [21] electrolytes. The resulting thickness of the porous coating is controlled by the applied current density/voltage, anodizing time and the temperature of electrolyte [53]. Such type of coating is more widespread in the industry, nanoscience, and nanotechnology. Especially the development of electron microscopy led to a deeper understanding of the porous aluminium oxide structures. In 1953, Keller et al. [50] described the porous anodic aluminium oxide coating model as a close-packed array of hexagonally arranged cells containing pores in each cell centre (Fig. 6) [7]. The porous type anodic coating consists of a compact barrier coating on the bottom and a relatively regular porous structure on top of the coating. The porous anodic coating can be characterized by parameters such as pore diameter, wall thickness, interpore distance (cell diameter), thickness of the compact barrier coating and the porous coating. The pore diameter increases with applied voltage, concentration and temperature of the electrolyte and with decreasing pH of the electrolyte. The high porosity of porous coatings results in a decrease in corrosion resistance, abrasion resistance and hardness of the coating. Such anodic coatings are, on the other hand, more convenient for easy dyeing for decorative purposes.
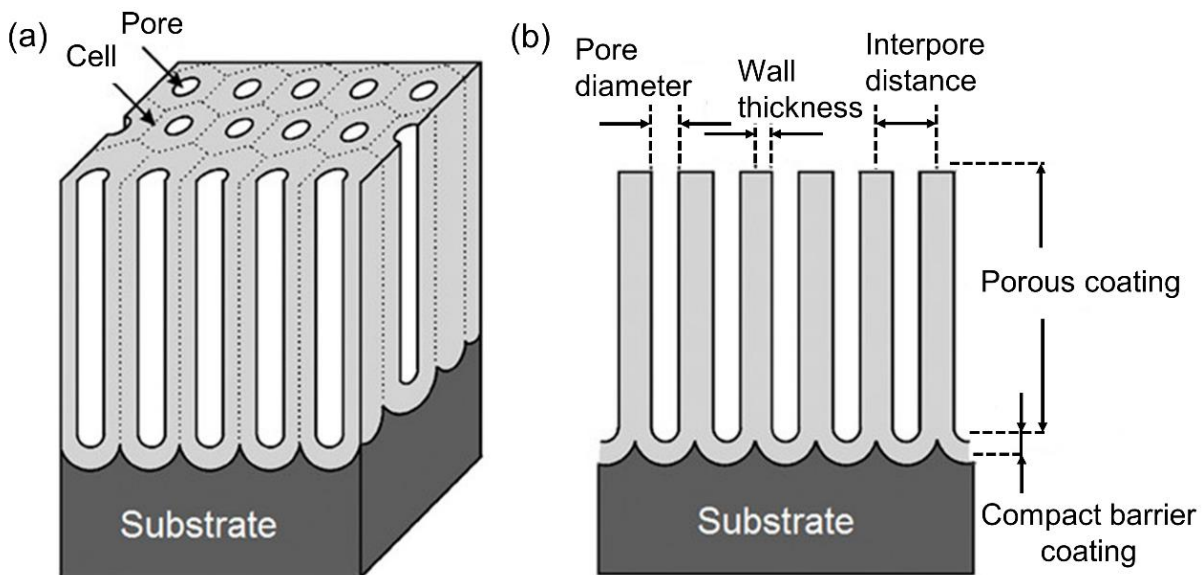
Fig. 6 *Idealized structure of the porous type (a), and (b) a cross-sectional view of the anodic oxide coating on aluminium [7].*

The mechanism of the pore growth of anodic aluminium oxide coating has been continuously investigated for decades, and currently, it is still studied and discussed [7, 54-56]. Typical voltage-time (V-t) or current-time (I-t) curves that are recorded during the galvanostatic

16

or potentiostatic anodizing process of high purity aluminium are shown in Fig. 7. The growth process of the porous anodic aluminium oxide coating can be divided into four stages [56] as illustrated in Fig. 7. During the beginning of the process, a thin and compact barrier coating (stage I in Fig. 7 [8]) is formed on the aluminium surface. Initial pores are developed in the barrier coating during stage II, while the conventional porous coating morphology starts to form during stage III and stage IV.
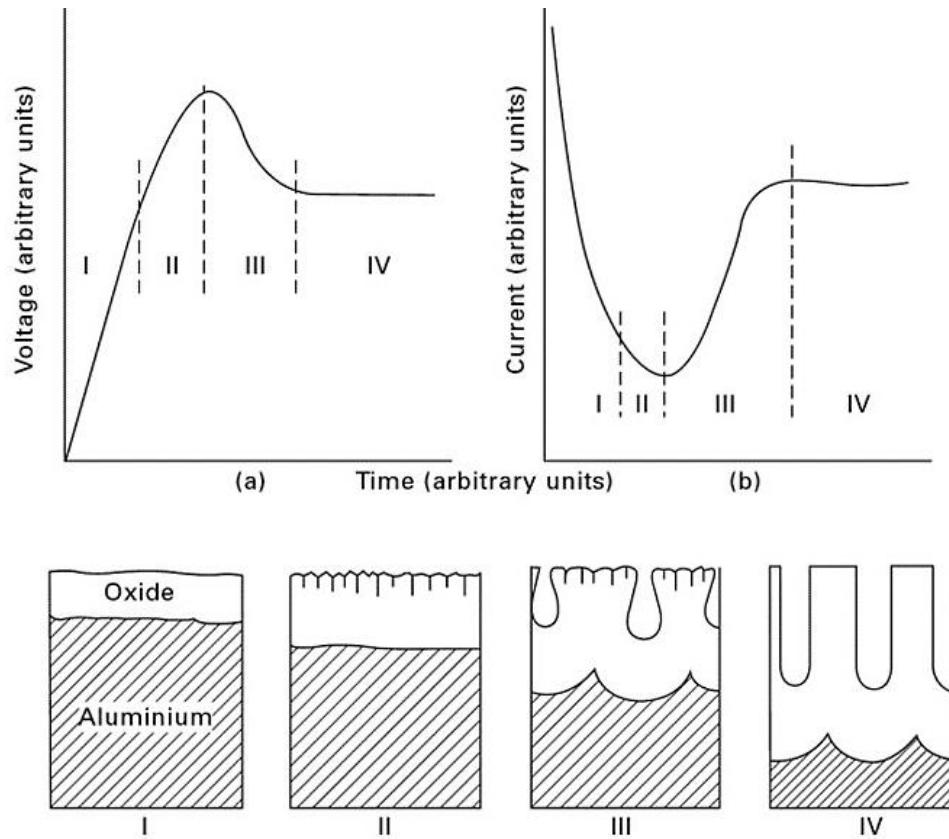
Fig. 7 *Schematic diagrams showing the development of porous anodic aluminium oxide coating growth on aluminium substrate during (a) the galvanostatic, and (b) the potentiostatic anodizing process [8].*

1.7. Common properties and parameters of anodic coatings

Appearance

In general, it is known that the anodizing process increases the resulting surface roughness. The increase in roughness is influenced by the type of substrate material, pre-treatment, anodizing conditions such as voltage/current density, anodizing time, temperature and type of the electrolyte [57]. The pre-treatment creating a smoother surface and removing all impurities from the substrate and therefore, is used before anodizing, which reduces the risk of undesirable appearance [58]. Alloying elements in the substrate material which dissolve during the anodizing process have no effect on the final appearance of the coatings but can contribute to the formation of defects such as cavities and pores, and deteriorate corrosion resistance of produced anodic coatings [59, 60]. Elements that are soluble in the electrolyte have a negative influence on the final coating appearance and can lead to a local change in the coating colour [61].

Coating thickness

The thickness of the coatings produced by standard anodizing methods is one of the most important criteria defining the corrosion resistance of anodic coatings. A thick anodized coating is usually more corrosion-resistant than a thin one [2]. Furthermore, fatigue strength decreases with increasing thickness of the anodized coating [62]. The coating thickness is determined by calculation using Faraday's law equation (21) [63]:

$$h = 0.4 \times \eta \times I \times S^{-1}, \tag{21}$$

where h is the thickness of the anodic coating (μm), η is the degree of electrolyte efficiency (0.6-0.7), t is the anodizing time (min), I is the current (A), and S is the anodized area (dm^{-2}).

For anodizing of Al and its alloys in the sulfuric acid electrolyte (Type II, Type III), a very simple calculation (see Eq. 22) can also be used to predict the thickness of the anodic coating. In most cases, Eq. 22 applies to anodizing conditions 12-20% H_2SO_4 at 4-27 ℃ [64]:

$$h = (I \times t)/3.12, \tag{22}$$

where h is the thickness of the anodic coating (μm), I is the current (A), and t is the anodizing time (min).

Generally, the thickness of an anodic coating depends on the type, concentration, and temperature of the electrolyte, the voltage/current density, anodizing time and chemical composition of the substrate. For example, Theohari et al. [65] studied the effect of temperature on the anodizing process of pure aluminium and AA5050 alloys. The porous anodic aluminium oxide coatings formed on the aluminium alloy after 40 min of anodizing exhibited a higher thickness than the coating formed on pure aluminium under the same anodizing conditions (15 V, 10 and 20 ℃). Oliveira et al. [66] studied anodizing of AZ91D magnesium alloy

at different voltages (3, 5, 8, 10 V) at room temperature in the 3 M NaOH electrolyte with an Na_2SiO_3 addition. The anodic coatings obtained at 3 and 5 V were thicker than coatings obtained at 8 and 10 V. The corrosion resistance of the samples was higher for coatings produced at a lower voltage (3 and 5 V), and the resulting porosity was also lower.

The anodic coating formed usually has a larger elementary cell volume than the substrate has. Therefore, the anodic coating grows above the original size of the component (substrate). Typical for Type II, or decorative anodizing, of aluminium is a growth ratio of 2/3 of the coating under and 1/3 above the original surface of the substrate (Fig. 8a). For Type III, or hard anodizing, a typical growth ratio is 1:1 (Fig. 8b) [58].
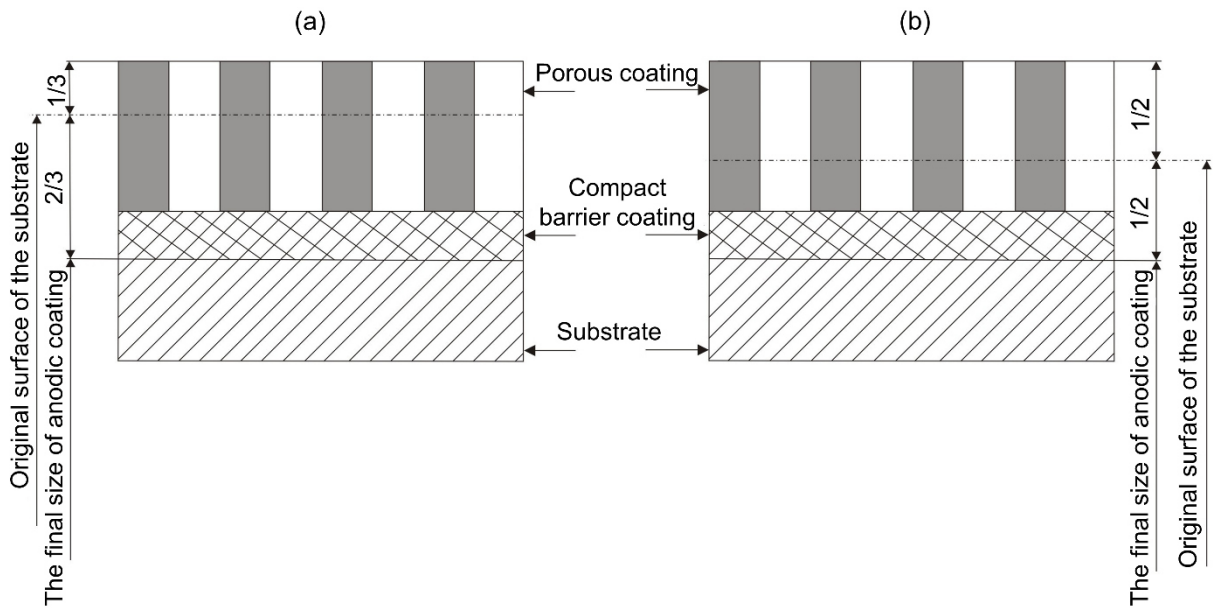
Fig. 8 *Schematic diagram of porous anodic aluminium oxide coating growth for (a) decorative anodizing (Type II), and (b) hard anodizing (Type III) [58].*

Porosity of the coating

The coating porosity depends on the conditions of the anodizing process. It is not to be seen as a negative property because it allows filling the pores with dyes or with various particles (PTFE, SiC, etc.), which improves the appearance of the anodic coating or its adhesion, corrosion and wear resistance. Generally, increasing the electrolyte temperature and anodizing time leads to an increase in porosity, but a decrease in hardness [67, 68].

Corrosion resistance

The corrosion resistance depends on the pH of the corrosive environment, the thickness of the anodic coating and its homogeneity [34]. It is well known that Mg and its alloys are not corrosion-resistant unlike Al, Zn and its alloys. Many authors studied the corrosion behaviour of Al, Zn and Mg before and after the anodizing process. In all of the studies [1, 2, 8, 23], the anodizing technique increased the corrosion resistance of the sample in comparison with the uncoated sample. As mentioned before, anodic coatings produced at a low voltage or current

density are thinner and less porous than coatings produced at a high voltage or current density, which leads to a lower corrosion resistance [2, 7]. Sealing of anodic coating or addition of SiC, TiO_2, and Al_2O_3 particles to the electrolyte improve the corrosion resistance. These particles could be adsorbed on the surface of the coating, embedded in the coating and stored into micropores during anodizing [67, 70].

Hardness of anodic coating

An anodic coating is relatively brittle and very sensitive to cracking. Variables such as the chemical composition of the substrate and the conditions of the anodizing process influence the hardness of the anodic coating [68, 71]. Guezmil et al. [72] reported that the Vickers microhardness values of anodized Al 1050A and Al 5756 alloys decrease with the increase in current density and electrolyte temperature. Porous anodic aluminium oxide coatings produced on Al 1050A showed higher Vickers microhardness values than coatings on Al 5754 did.

Porous anodic aluminium oxide coatings produced in the sulfuric-oxalic acid electrolyte have a higher microhardness compared with coatings produced in the sulfuric acid electrolyte. The particles of Al_2O_3 contained in the electrolyte have a positive influence on hardness [67].

1.8. Influence of substrate chemical compositions on the growth of anodic coatings

The presence of alloying elements or additives in the form of chemical compounds (intermetallic phase within the substrate) has a strong effect on the non-uniform growth of the anodic coating. It also has a considerable influence on the resulting corrosion resistance, mechanical properties, and appearance of the produced coating. As shown in Table 5, it is well known that some components of the aluminium alloy can influence the final colour of the anodic coating produced in the conventional sulfuric acid electrolyte [58].

Table 5 Effect of the alloying elements on the appearance and properties of the produced porous anodic aluminium oxide coatings [58].

Elements	Effect
Silicon (Si)	> 5 %, dark grey to black coatings are produced
Magnesium (Mg)	≤ 3%, clear, colourless coatings are produced > 3%, nonstandard colouring of oxide coatings is produced (not suitable for further dyeing)
Copper (Cu)	< 2%, colourless coatings are produced higher amounts of Cu will result in discolouration, and the anodizing process becomes more difficult
Zinc (Zn)	good and protective coatings are produced with contents of up to 5%, colourless when the microstructure is homogeneous, quite brown when second phase precipitates are present

The behaviour of second phase particles during anodizing of Al and Mg alloys was studied [73, 74]. During the anodizing process in the sulfuric acid, intermetallic phases in the aluminium substrate, namely MgZn2, AlCuMg, and Al2CuMg can be dissolved or oxidized, which leads to the formation of nanocavities and cracks in the coatings [59, 74, 75]. The behaviour of intermetallic phases during the anodizing process and their influence on the process also depend on the process conditions such as pH electrolyte, voltage/current density.

The formation and growth of the porous anodic aluminium oxide coating on cast Al-Si alloys were studied by Zhu et al. [76], Forn et al. [77], Li et al. [78], and Fratila-Apachitei et al. [79, 80]. The influence of Si particles on the growth of anodic oxide coatings is shown in Fig. 9 [80]. During the anodizing process, the Si particle is anodized, but at a lower rate than the Al phase. The oxidation of the Si particle stops when it becomes isolated from the initial material. The growth of the anodic coating also relates to the microstructure of the initial material. The eutectic phase plays a significant role in the growth of the anodic aluminium oxide

coating (Fig. 10 [76]). The change of Si particle morphology from flakes to fibres reduces the amount of the unanodized Al phase and also the number of cracks and cavities in the coating [76].
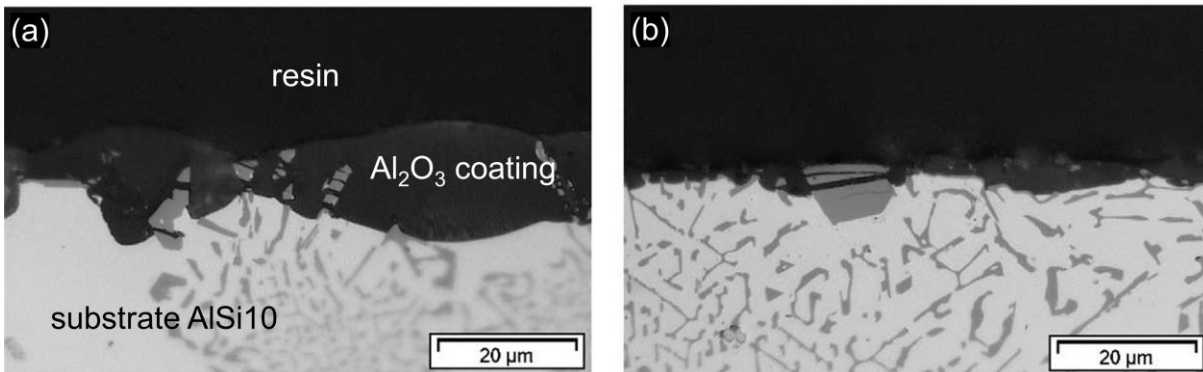
Fig. 9 Influence of Si particles on the growth of porous anodic aluminium oxide coating produced in the 2.25M H$_2$SO$_4$ at 4.2 A/dm^2, 0 °C for 10 min [80].
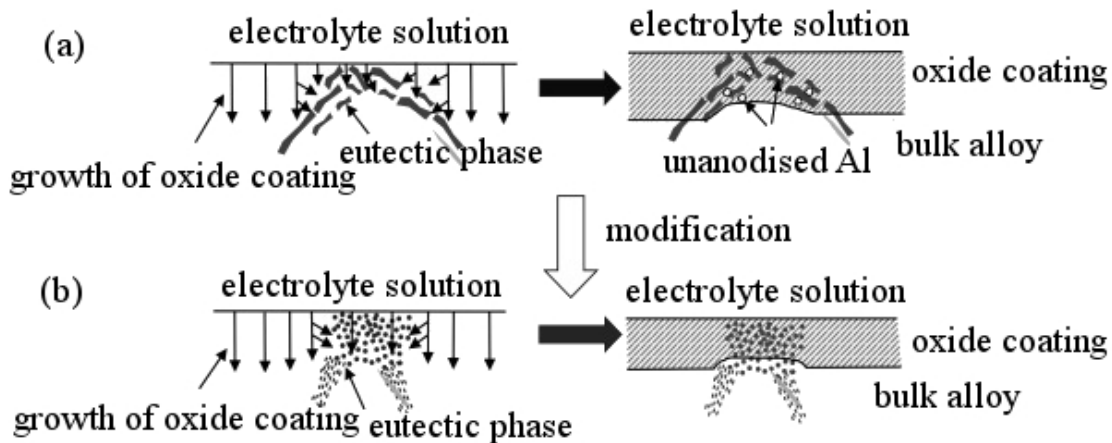
Fig. 10 Influence of the eutectic phase and of the modification process on the growth of porous anodic aluminium oxide coating (a) unmodified condition, and (b) modified condition [76].

Heat treatment (solid solution annealing) prior to the anodizing process may be used to increase the uniformity and thickness of the produced anodic coating. The heat treatment process changes the shape, distribution, and size of the particles of intermetallic phase within the substrate.

1.9. Technological process

The technological process of anodizing is a multiple-step process that includes pre-treatment, anodizing process and post-treatment, as shown in the diagram in Fig. 11. It is necessary to consider the fact that anodization will highlight the texture of the substrate. Therefore, it is necessary to select a suitable pre-treatment method for surface preparation. Also, it is essential to consider if the individual substrates can fulfil the requirements, i.e. enhancement of surface properties and/or decorative finish.
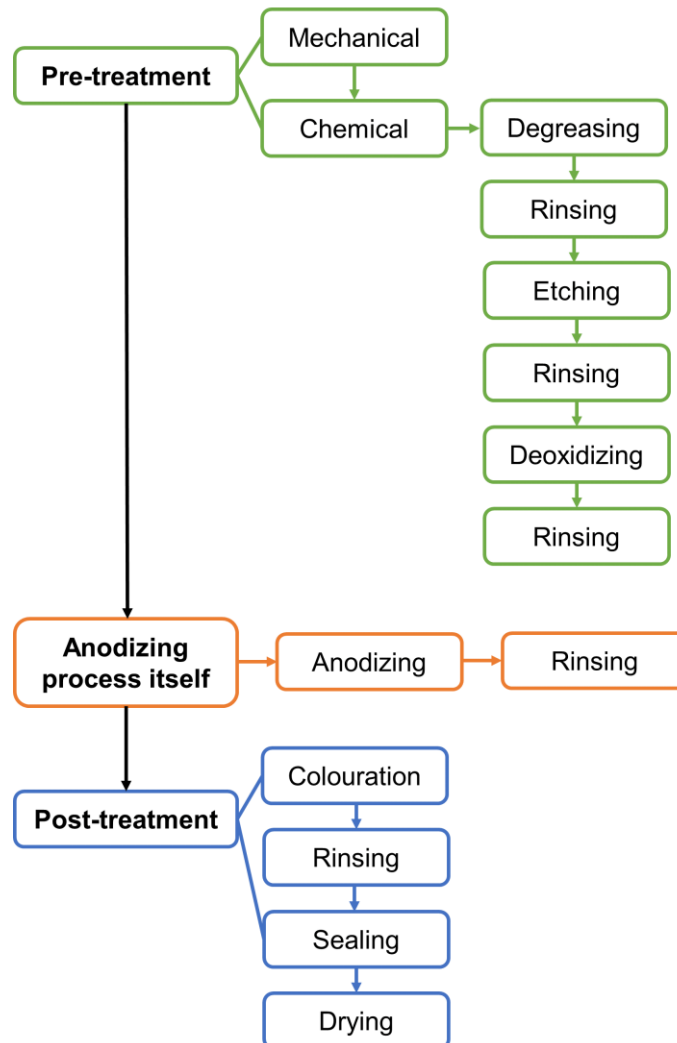
Fig. 11 Technological process of anodizing.

1.9.1. Pre-treatment

Surface pre-treatment has a significant effect on the final appearance and properties of anodic coatings (homogeneity and thickness of the coating, fatigue life, corrosion resistance, etc.). Several authors [81, 82, 87] investigated the influence of pre-treatment on fatigue life. Results obtained from fatigue testing showed that etching and high surface roughness resulted in a significant decrease in fatigue life.

1.9.1.1. Mechanical pre-treatment

Mechanical pre-treatment (blasting, sanding, polishing, ultrasonic cleaning, etc.) removes the surface defects of components (e.g. burrs in the dividing plane of the castings, the surface texture after forming, the corrosion products on the surface of the component, etc.) and produces the required quality of the surface.

1.9.1.2. Chemical pre-treatment

Chemical or electrochemical pre-treatments of the surface are intended to remove polishing agents, oils, greases and general dirt from the surface of components in order to leave a clean surface ready for a subsequent process. Chemical treatments include degreasing, etching, activation, and other steps [64].

Degreasing

Degreasing is used to remove impurities (oils and greases, solid particles from abrasive grits and metal chips, polishing agents, etc.) from the surface. Degreasing methods are (i) alkaline degreasing, (ii) emulsion degreasing, (iii) solvent degreasing and (iv) ultrasonic degreasing. During the process, there is no change in the chemical composition or structure of the substrate. An alkaline degreasing solution consists of low-cost, water-soluble salts such as NaOH, KOH, and Na_2CO_3 combined with dispersants and surfactants in water. The degreasing is commonly carried out by immersion or spraying, usually at a temperature of 50-95 °C [32, 83]. The operating temperature is very important. Complete removal of impurities from the surface does not occur at lower temperatures. During the process, it is important to eliminate impurities that float on the surface of the degreasing solution.

Chemical etching

During etching, a natural oxide layer, corrosion products, and old chemical coating are removed, and the surface is made slightly rougher. Besides the surface impurities, the substrate is dissolved too, which leads to undesirable penetration of hydrogen into the substrate. Dilute acids (H_2SO_4, HCl, and H_3PO_4), or alkali (NaOH, KOH) are used for etching. Nitric and hydrofluoric acids are used in mixtures with other acids. Inhibitors are added into the etching bath in order to minimize hydrogen entry into the metal, and their use should also bring economic and environmental benefits [84]. Prolonged etching can cause pitting and have a negative effect on fatigue life.

Deoxidizing

When alloying elements (Cu, Ni, Mg, Si, etc.) and inorganic salts are not dissolved during the etching process, a dark-spotted coating is formed on the component surface. Previously used HNO_3 is nowadays replaced by H_2SO_4 and HF acids. The deoxidizing operation takes place for

several minutes at a moderate temperature. After the deoxidizing process, the surface of the component must be clean, bright and wettable [64, 83].

Rinsing

Rinsing is a significant step after immersion in each chemical tank. Tap water is contaminated with salts, usually based on Ca, Mg, Na, Cl, which can cause spots on the surface of cleaned parts, and these spots can interfere with the anodizing surface quality. Therefore, only deionized water or sequential rinsing in tap and then deionized water is used. The purpose of the rinsing is to remove undesirable residues of chemicals that remained on the surface or in the cavities of components after the previous operations. Unwanted residues could contaminate the solution in the next step and influence the appearance and properties of the produced coating. Extended rinsing time after the anodizing procedure is recommended [64, 83].

1.9.2. Anodizing process itself

Anodizing tank is commonly made of reinforced PVC, PP, HDPE or stainless steel. The tank is usually equipped with cooling, heating, stirring, temperature sensor and sensor of electrolyte level, pH meter, power source, and cathode.

Power supply

Although DC anodizing provides many of the desirable features required for optimized bonding, alternating current (AC), pulse current (PC) or mixed current offer some further advantages [45]. Bononi et al. [85] studied the effect of electrical parameters (DC, PC and combination DC/PC) on AA2024-T3 anodic coating growth mechanisms. The pulse current anodizing process reduces the coating defectiveness, and a combined DC/PC process leads to optimized microhardness. Saijo et al. [86] studied anodizing of AZ91D alloy in an environmentally friendly electrolyte using AC and DC. The results showed that using AC resulted in a lower porosity and a higher corrosion resistance of anodic coating in comparison with the coating produced by DC anodizing.

Cathodes

Stainless steel, carbon, aluminium, lead or platinum are used as the cathodes. The cathode can be used in the shape of sheet, plate or rod. The anode-to-cathode surface area ratio for hard anodizing of aluminium is 2:1 or 3:1. Regarding the anode-cathode ratios for anodizing of Zn, Mg and their alloys, scientific publications recommend an anode-to-cathode ratio of 1:1. The position of the cathode in the tank is also significant. The cathode is often placed inside the tank, along its sides at a certain distance from the anodizing component (i.e. the anode). The recommended working depth of the cathodes is slightly larger than the working depth of the components [64].

Temperature of electrolyte

The electrolyte temperature is an important parameter affecting the properties of anodic coating (thickness, porosity, microhardness, etc.) and must be controlled [65, 68]. Aerts et al. [68] investigated the influence of electrolyte temperature on the porosity and the mechanical properties of porous anodic aluminium oxide coating on AA1050. With increasing electrolyte temperature, microhardness and porosity decreased.

It is recommended to keep the bath temperature homogeneous with an accuracy of ±1 °C. The electrolyte may be agitated by means of compressed air. Recently, acid sprayers located on the bottom of the tanks have been used, which provides better circulation of the acid and temperature control [31].

1.9.3. Post-treatment

Dyeing of anodized coating

Porous anodic aluminium oxide coatings produced by Type II method can be dyed for decorative purposes (architecture, sports equipment, pens, etc.). The colour appearance of the porous anodic aluminium oxide coatings obtained can be achieved either directly, during the process of anodizing (integral colouring, self-colouring), or during post-treatment processes such as dyeing (adsorption) or electrolytic colouring (Fig. 12) [34].
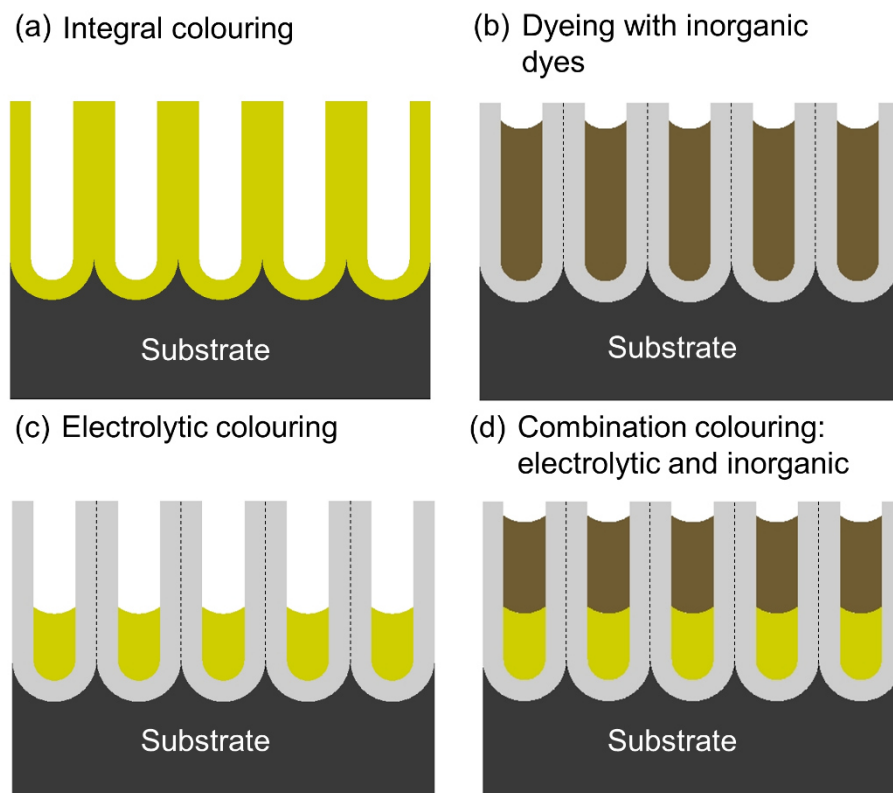
Fig. 12 Colouring of porous type anodic aluminium oxide coating [34].

Sealing

The sealing of anodic coatings is the final operation of the technological process, which leads to the closing of the pores and cracks present in the coating, in order to achieve the desired corrosion resistance and mechanical properties. For coloured coatings, the sealing process is essential to retain pigments and also to increase the UV resistance of dyes in coatings [87, 88]. Typically, sealing methods for aluminium and its alloys used in the industrial practice are implemented in hot deionized water (≥97 °C) (so-called hot DI sealing or hydrothermal sealing). Other options are cold or hot nickel acetate sealing and sodium silicate sealing [89, 90]. In past decades, various sealing techniques have been developed, and new environment-friendly and low energy consumption processes are continually being developed, and the existing ones are improved [87, 91]. Cold sealing, or cold impregnation, (25-30 °C) often utilizes nickel fluoride solution. The fluoride in the solution dissolves the porous anodic aluminium oxide coating and then is deposited as fluoro-aluminate [92]. The advantage of the cold seal is low energy consumption, on the other hand, there is a high demand for chemicals, and there are special rules for environmentally friendly disposal of nickel from wastewater. Kim et al. [87] investigated a non-toxic sealing method based on the use of $NaAlO_2$ solution for porous anodic aluminium oxide coating. When the $NaAlO_2$ solution (85 °C, pH 7, and sealing time 5 min) was neutralized with H_2SO_4, precipitates that act as nuclei for the growth of boehmite (AlOOH) were produced. Porous anodic aluminium oxide coating sealed by this method showed high Vickers hardness, corrosion resistance, and low mass loss of the oxide in a sealing quality test. This method could be a potential non-toxic low-cost and rapid sealing procedure that can replace the commonly used Ni-based sealing method in the future.

For each method of Al, Mg and Zn anodizing, it is preferable to use a different type of sealing process, depending on the desired final properties. Anodic coatings produced on Mg substrate are usually sealed in phosphate, silicate or borate containing solutions [2, 93].

1.10. Future trends

Plasma electrolytic oxidation (PEO), also known as micro-arc oxidation (MAO), is a relatively novel and attractive surface treatment technology similar to the anodizing process but it requires high voltage (over 200 V) and current density, see Fig. 13 [8, 94].
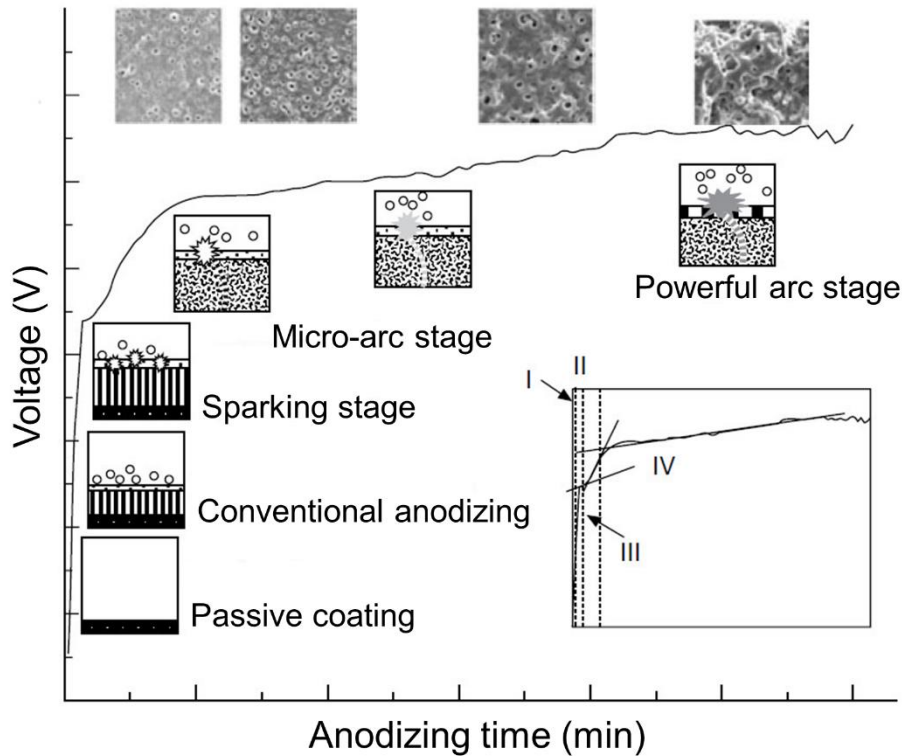
Fig. 13 *Schematic illustration of discharge phenomena and the coating microstructure developed during the plasma electrolytic oxidation process [8].*

A higher voltage applied in combination with a suitable electrolyte creates plasma discharges at the anode substrate interface. These discharges are short, often in the range of nanoseconds to milliseconds. The mechanism of the PEO coatings is complicated because it requires an understanding of several electrochemical, chemical and chemical-thermal reactions [2, 9, 95]. Compared to the conventional anodizing, the PEO process produces crystalline ceramic oxide coatings on various metal surfaces such as Al, Mg, Ti and their alloys with higher microhardness, wear resistance, corrosion resistance, dielectric properties and better thermal stability [2, 96]. PEO is a unique and irreplaceable technique for the fabrication of functional coatings for specific applications. The equipment for the PEO process includes a special power supply generating positive and negative pulses, and a cooled electrolyte tank. This process is more expensive in terms of equipment than conventional anodizing.

2. Aims of the thesis

The thesis is focused on (i) the development of technological process conditions for 99.5% aluminium alloy (AA1050), zinc alloy (ZnTi2) and pure magnesium (99.9% Mg) substrates, and (ii) the characterization and evaluation of the produced anodic coatings. The main aim is focused on the production of anodic coatings doped with particles, namely aluminium oxide (Al_2O_3) and polytetrafluoroethylene (PTFE) particles, in order to improve the hardness and tribological properties of the anodic coatings when compared to the substrate. The partial aims of this work are the following:

- Optimization of (i) the mechanical and chemical pre-treatment of the substrates prior to the anodizing process and (ii) anodizing conditions in terms of temperature, concentration and type of electrolyte, current density/voltage and anodizing time.

- Detailed characterization of the produced anodic coatings via SEM with EDX, TEM, XRD, Raman spectroscopy and Vickers hardness test as well as the measurement of the thickness of the anodic coatings.

- Evaluation of the effect of the anodizing process conditions on the formation and properties of the anodic coatings.

- Preparation of stable electrolytes which contain Al_2O_3 and Al_2O_3/PTFE particles in order to utilize them for the production of composite anodic coatings.

- Characterization of produced composite anodic coatings via SEM with EDX, Vickers hardness test and measurement of their thickness.

- Evaluation of the effect of Al_2O_3 and Al_2O_3/PTFE particles on the anodizing process and properties of composite anodic coatings.

- Evaluation of the effect of Al_2O_3 and PTFE particles on tribological properties of the anodic oxide coatings produced on aluminium alloys.

3. Experimental part

3.1. Experimental apparatus

Experiments were performed on the galvanic apparatus (Fig. 14a) developed for this purpose. This device was equipped with ten tanks. The first three tanks were used for the chemical pre-treatment (degreasing, etching, neutralizing), and the fourth was used for the anodizing process. The rest of the tanks were used for rinsing. All rinsing tanks were equipped with overflow pipes to avoid potential surface contamination. A PVC pipe with holes for compressed air distribution was placed at the bottom of all tanks. The etching tank was equipped with a controlled heating system. Finally, the anodizing tank was equipped with an external cooling system (EuroCold, Italy), a thermocouple (as shown in Fig. 14b) and the direct current (DC) power supply unit QPX 1200 (Aim-TTi, United Kingdom) operating between 0-60 V and 0-50 A.
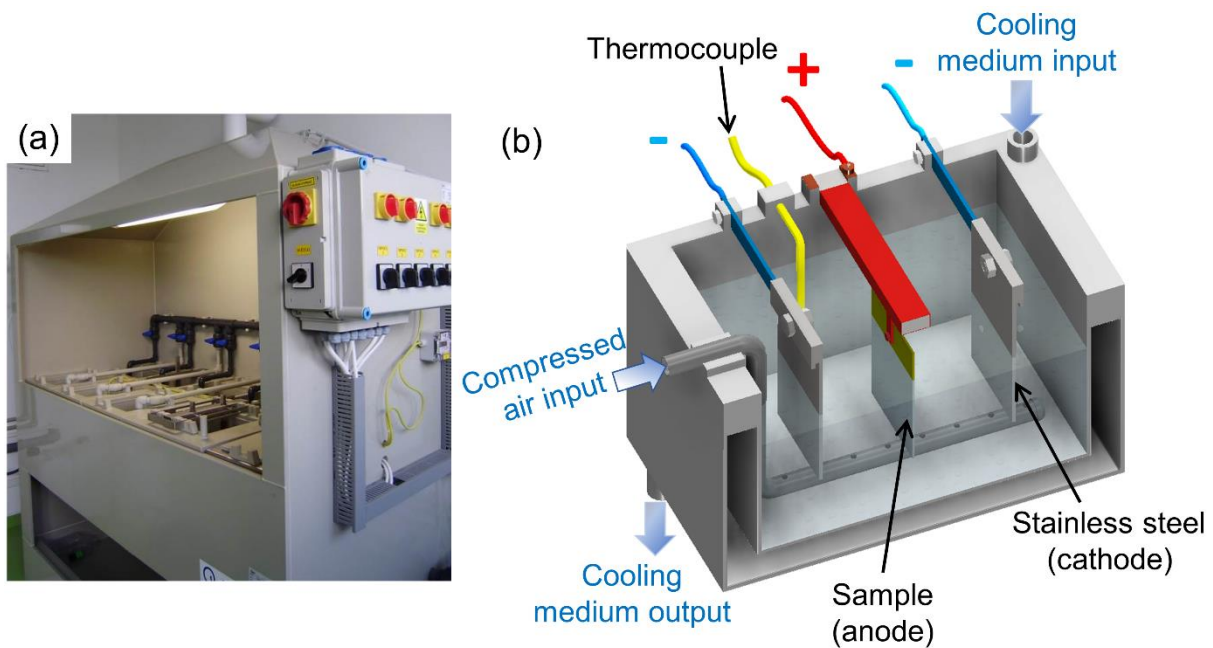
Fig. 14 *Experimental apparatus used for all experiments: (a) overall view of the apparatus, and (b) schematic illustration of the anodizing tank set up.*

3.2. Materials and mechanical pre-treatment

3.2.1. Aluminium alloy - AA1050

A commercially pure aluminium alloy sheet (Vy-Tech, Czech Republic, AA1050) was cut into 80 mm × 60 mm × 6 mm samples which were used as the working electrodes (anodes). The chemical composition of the alloy was determined using the optical spectrometer Q4 Tasman (Bruker, Germany). The measurement revealed the presence of 0.1 Si, 0.3 Fe, 0.004 Cu, 0.005 Zn, 0.008 Mg, 0.01 Ti, and Al balance (wt.%). Two series of the samples with different mechanical pre-treatment were prepared. The first series of samples was ground with #800 and #1200 grit silicon carbide (SiC) papers (Struers) and the second one was ground with SiC papers from #800 up to #4000 grit, and further mechanically polished with 3 and 1 μm diamond pastes (Urdiamant, Šumperk) using ethanol as a lubricant to obtain a mirror-like surface. The samples were masked with a polyester "acid-resistant" tape, so the resulting working electrode size was 50 mm × 60 mm × 6 mm (Fig. 15a).

3.2.2. Pure magnesium - 99.9% Mg

A commercially cold extruded pure Mg rod (12.7 mm in diameter, MG007924, Goodfellow, United Kingdom, 99.9% Mg) was cut into cylinders of 80 mm in length and then cut in half along the axis, as shown in Fig. 15b. Two series of the samples with different mechanical pre-treatment were prepared. The first series of samples was ground with #800 and #1200 grit SiC papers, and the second series of samples was ground with SiC papers from #800 up to #4000 grit, and further mechanically polished with 3 and 1 μm diamond pastes using ethanol as a lubricant to obtain a mirror-like surface. The samples surface was masked with a polyester "acid-resistant" tape to obtain the resulting working electrode area 0.19 dm^2.

3.2.3. Zinc alloy - ZnTi2

A commercially rolled ZnTi2 sheet (AlmioPlus s.r.o., Czech Republic, ZnTi2) was cut into 86 mm × 18 mm × 1 mm samples, masked with a polyester "acid-resistant" tape and used as the working electrodes (anodes) in the experiments. The resulting working electrode size was 56 mm × 18 mm × 1 mm, as shown in Fig. 15c. The chemical composition of the zinc alloy, according to the supplier, was 2% Ti and 98% Zn (wt.%).

31
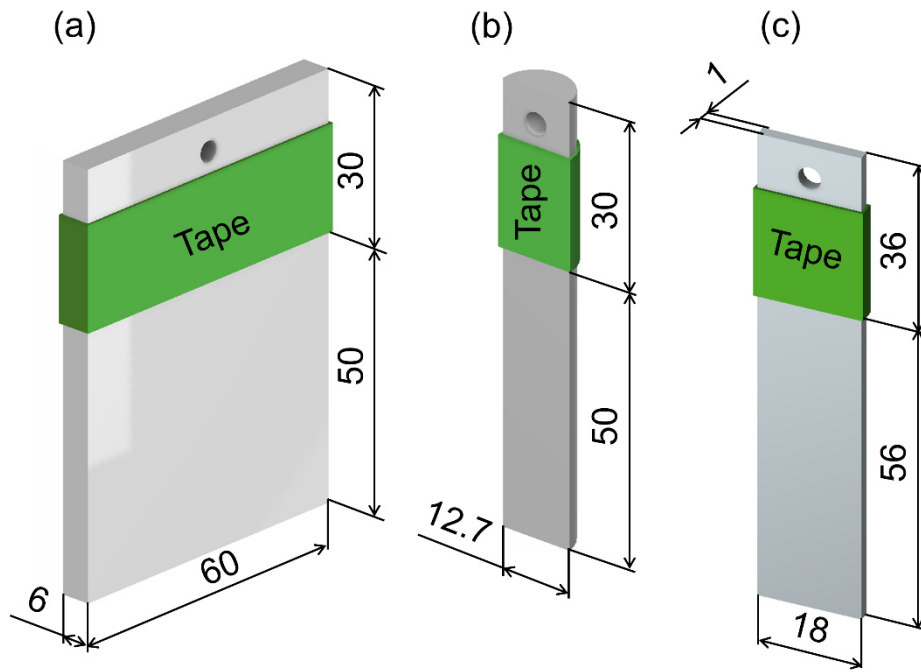
Fig. 15 *Schematic representation of the initial samples: (a) AA1050 sheet, (b) 99.9% Mg rod, and (c) ZnTi2 sheet.*

3.3. Chemical pre-treatment

Prior to the anodizing process, all samples were chemically pre-treated, and the chemicals used were mostly of analytical grade.

3.3.1. Aluminium alloy - AA1050

First, the samples were ultrasonically degreased in acetone (min. 99.5%, p.a., Penta), ethanol (96%, p.a., Lach-Ner) and isopropyl alcohol (min. 99.7%, p.a., Lach-Ner) for 120 s in each solution. In the second step, alkaline etching in 10% NaOH (min. 98%, p.a., Lach-Ner) solution at 35 °C for 30 s was used. Subsequently, all samples were neutralized in 1:1 mixture of concentrated HNO_3 (min. 65%, p.a., Lach-Ner) and deionized water at room temperature for 60 s. After the alkaline etching and neutralizing steps, all samples were rinsed two times in deionized water, in separate tanks.

3.3.2. Pure magnesium - 99.9% Mg

First, the samples were degreased in ethanol and isopropyl alcohol in an ultrasonic bath for 120 s in each solution. In the second pre-treatment step, the samples were etched in 0.5% HF (min. 38%, p.a., Lach-Ner) for 30 s. Finally, the samples were rinsed two times in ethanol and dried with cold air.

3.3.3. Zinc alloy - ZnTi2

The samples were degreased in ethanol and isopropyl alcohol in an ultrasonic bath for 120 s in each solution, etched in 0.25% HNO_3 (65%, p.a., Lach-Ner) for 6 s, rinsed two times in deionized water and dried with cold air.

3.4. Anodizing process

3.4.1. Preparation of a stable electrolyte containing Al_2O_3/PTFE particles

For the initial experiments, in which Al_2O_3 and PTFE particles were used for doping the produced anodic coatings, the particles were just added to the 15% H_2SO_4 electrolyte. After the anodizing process, the particles were observed on the bottom of the anodizing tank. SEM observation and EDX analysis did not reveal the presence of secondary particles in the produced anodic coating. Based on the available data in the literature [70, 97, 98] an anionic surfactant (98.5%, sodium dodecylbenzenesulfonate, SDBS, Sigma Aldrich) was chosen for the preparation of a stable electrolyte for further experiments. After the anodizing process under the same conditions, only Al_2O_3 particles were observed by SEM, while EDX analyses confirmed their presence on the surface of the anodic coating. Due to the PTFE particles sedimentation on the bottom of the anodizing tank, the PTFE particles were replaced with a commercial PTFE suspension for the next experiments [70]. A detailed description of the procedure with the individual stable electrolytes with PTFE and/or Al_2O_3 particles is provided in individual subchapters. The preparation of a stable electrolyte containing the particles was based on the conclusions reported by Chen et al. [70] and Li et al. [98]. Electrolytes containing the particles were stable for more than five hours after the solution preparation.

3.4.2. Anodizing of AA1050

The anodizing process was performed in the 15% H_2SO_4 (98%, p.a., Lach-Ner) electrolyte with or without varying the composition (by adding oxalic acid ($C_2H_2O_4$, 99%, p.a., Lach-Ner) and Al_2O_3 and PTFE particles) at temperatures of (i) 24 ºC, (ii) 18 ºC or (iii) 10 ºC under a constant voltage (16-20 V) or constant current density (1-3 A/dm^2). In all experiments, where a lower electrolyte temperature of 10 ºC was used, glycerol ($C_3H_8O_3$) was added to the electrolyte to reduce the heat produced during the reactions at the oxide-substrate interface and to keep the process temperature constant. Anodizing was performed using DC power supply with two stainless steel plates AISI 316L of 50 mm × 60 mm × 2 mm in dimension, which were used as cathodes. The distance between the anode and the cathode was 65 mm. During the anodizing process, current density/voltage *vs* anodizing time was recorded at intervals of 5 and 1 s. The electrolyte was agitated with compressed air to improve the temperature distribution on the sample surface and in the electrolyte bath. The temperature of the electrolyte bath was controlled using a digital thermometer and cooled with a water-glycol chiller. After the anodizing process, the samples were rinsed in deionized water and dried with cold air.

The stable dispersion electrolyte solution was prepared following the protocol below:

- Solution 1: 0.6 g/L of sodium dodecylbenzenesulfonate ($CH_3(CH_2)_{11}C_6H_4SO_3Na$, 98.5%, SDBS, Sigma Aldrich) was added to 5 mL of deionized water and stirred for 30 min;
- Solution 2: 6 g/L of Al_2O_3 particles (diameter < 500 nm) were added to Solution 1, and the dispersion was stirred for 60 min in an ultrasonic bath;
- Solution 3: Solution 2 was subsequently added to 1000 mL of 15% H_2SO_4 containing 20 g/L $C_2H_2O_4$ and 10 mL/L $C_3H_8O_3$, and stirred for 30 min;
- Final electrolyte: 15 mL/L of 60 wt.% PTFE (Sigma Aldrich), a commercially available suspension, was added to Solution 3 and kept under stirring for 12 hours.

3.4.3. Anodizing of 99.9% Mg

The anodizing process was performed in the 1 M NaOH (min. 98%, p.a., Lach-Ner) electrolyte with or without Al_2O_3 and PTFE particles at 24 °C under a constant voltage of 4-50 V using DC power supply. Two stainless steel plates with of 50 mm × 18 mm × 1 mm in dimension were used as the cathodes in the experiment. The distance between the anode and the cathode was 64 mm. During the anodizing process, current density *vs* anodizing time was recorded at 1 s intervals, and the electrolyte was agitated with compressed air. After the anodizing process, the samples were rinsed in ethanol and dried with cold air.

The stable dispersion electrolyte solution was prepared following the protocol below:

- Solution 1: 0.6 g/L of sodium dodecylbenzenesulfonate ($CH_3(CH_2)_{11}C_6H_4SO_3Na$, 98.5%, SDBS, Sigma Aldrich) was added to 5 mL of deionized water and stirred for 30 min;
- Solution 2: 10 g/L of Al_2O_3 particles (diameter < 500 nm) were added to Solution 1, and the dispersion was stirred for 60 min in an ultrasonic bath;
- Solution 3: Solution 2 was subsequently added to 1000 mL 1 M NaOH and stirred for 30 min;
- Final electrolyte: 15 mL/L of 60 wt.% PTFE, a commercially available suspension, was added to Solution 3 and kept under stirring for 12 hours.

3.4.4. Anodizing of ZnTi2

The anodizing process was carried out under varying concentration of individual electrolytes (i) NaOH (min. 98%, p.a., Lach-Ner), (ii) KOH (min. 85%, p.a., Lach-Ner) and (iii) $C_2H_2O_4$ (99%, p.a., Lach-Ner). Also, the stable 0.5 M NaOH electrolyte solution containing 6 g/L Al_2O_3 particles was produced. Anodizing was carried out at 21 °C and in the potentiostatic regime ranging from 4 to 50 V using DC power supply. The ZnTi2 samples and two stainless steel

plates with of 56 mm × 18 mm × 1 mm in dimension were used as the anode and the cathode in the experiment, respectively. The distance between the anode and the cathode was 70 mm for experiments utilized agitation with compressed air, and 40 mm for experiments in which magnetic stirring was used. During the anodizing process, the current density vs anodizing time was recorded at time intervals of 5 s. After the anodizing process, the samples were rinsed in deionized water and dried with cold air.

The stable dispersion electrolyte solution was prepared following the protocol below:

- Solution 1: 0.6 g/L of sodium dodecylbenzenesulfonate (98.5%, SDBS, Sigma Aldrich) was added to 5 mL of deionized water and stirred for 30 min;
- Solution 2: 6 g/L of Al_2O_3 particles (diameter < 500 nm) were added to Solution 1, and the dispersion was stirred for 60 min in an ultrasonic bath;
- Final electrolyte: Solution 2 was subsequently added to 1000 mL 0.5 M NaOH and stirred for 12 hours.

3.5. Characterization techniques

X-Ray diffraction

The phase composition was identified by means of X-ray diffraction (XRD, SmartLab 3 kW, Rigaku, Japan) using Cu Kα radiation (λ = 1.54059 Å generated at 30 mA and 40 keV). The assessment of the peaks was performed utilizing the software HighScore Plus (PANalytical).

Scanning electron microscopy

Prior to the scanning electron microscopy (SEM) examination, the samples were cut into smaller samples on a precise cut-off machine Secotom (Struers, Denmark) using (i) intensive water cooling for AA1050 and ZnTi2, and (ii) without cooling for 99.9% Mg. After cutting, all samples were rinsed in an ethanol ultrasonic bath for 300 s. The surface morphology and cross-section of the produced anodic coatings were investigated by SEM Lyra3 (Tescan, Czech Republic) equipped with energy-dispersive X-ray spectroscopy (EDX, XFlash 5010, Bruker AXS Microanalysis, Germany) for area/point chemical analyses.

Before the microstructural observations, all samples were coated with a 10 nm carbon layer using a Leica EM ACE600 (Leica, Germany) evaporation coating unit. The surface morphology evaluation was carried out using the secondary electrons (SE) mode and the backscattered electrons (BSE) mode with an electron beam acceleration voltage of (i) 10 keV (AA1050 samples), and (ii) 15 keV (99.9% Mg and ZnTi2 samples).

Samples for cross-sectional microstructural observation were produced using the cold mounting technique followed by conventional metallographic procedures - wet grinding with SiC papers from #800 up to #4000 grit and polishing with 3 and 1 μm diamond pastes with ethanol as a lubricant. The AA1050 samples were finally chemical-mechanical polished with OPS suspension (Struers). As-coated cross-sectional samples were observed using the BSE mode. The metallographic preparation of ZnO samples using different mounting techniques was investigated in detail and published by the author of the thesis in Scientific Reports [99].

Transmission electron microscopy

Transmission electron microscopy (TEM) was used for the detailed analysis of the produced anodic ZnO coatings. TEM lamellas were prepared by focused ion beam and field emission scanning electron microscope (FIB-FESEM, FEI Helios NanoLab 660, ThermoFisher Scientific, Czech Republic) from each region of interest with an approximate dimension of 12 μm × 2 μm ×10 μm. A 500 nm platinum layer was deposited on the top of each lamella in order to prevent subsequent damage from sputtering. To prevent Ga^+ implantation, coarse and fine sputtering was performed with a maximum current of 430 V and 41 pA with a subsequent cleaning process at 5 keV on each side of the lamella. The estimated thickness of the final lamellae was 50-100 nm. The analyses were carried out

using a high-resolution transmission electron microscope (HRTEM, FEI Titan Themis 60-300, ThermoFisher Scientific, Netherlands) operated at 300 keV, equipped with (i) a high angle annular dark-field (HAADF) detector (Fischione) and with a Cs-image corrector for TEM imaging, (ii) a Super-X detector (ThermoFisher Scientific, Netherlands) for EDX spectroscopy, and (iii) a Gatan GIF Quantum 966 ERS for electron energy loss spectroscopy (EELS).

Thickness of anodic coatings

The average thickness of anodic coatings was measured on cross-sectional SEM micrographs at twenty randomly selected positions on each sample, using the Olympus Stream Image Analyses Software.

Hardness of anodic coatings

The microhardness of non-treated AA1050 substrate and porous anodic oxide coatings was measured on cross-sectional samples using the Vickers hardness tester Duramin 100 (Struers, Denmark) under constant loads of 0.49 N (HV0.05) and 0.0245 N (HV0.025), with a testing time of 10 s. The reported hardness values data are the average value of 10 individual measurements.

Ball-on-disc wear test

The tribological behaviour of the anodic coatings produced on AA1050 was evaluated using the reciprocal ball-on-disc wear test using a standard UMT TriboLab (Bruker Corporation, USA) tribometer at room temperature. The wear test counterparts (AISI G133 alumina balls, 6 mm in diameter) were stationary fixed in the holder and pressed to the moving anodized sample by a normal load of 3 N. Alumina was chosen as the counterpart material since it is very hard and chemically inert [100]. The sample was moving back-and-forth along a stroke of 10 mm with a frequency of 3 Hz. The duration of each test was 2000 cycles. After the test, the cross-sectional profiles of wear tracks were measured using a Contour GT X8 (Bruker Corporation, USA) optical profiler, and the total wear loss of the samples was calculated as a resulting cross-sectional area of the wear track multiplied by its length.

Raman spectroscopy

The Raman spectra of ZnO coatings were measured at room temperature by an In Via Reflex Raman spectrometer (Renishaw, United Kingdom) containing grating with 2400 g/mm. A CCD camera was used as the detector, and for the excitation the 442 nm line of a He-Cd laser was used. For each recorded spectrum, the background was subtracted.

4. Results and discussion

4.1. Anodizing of AA1050 sheet

Prior to the anodizing process, samples were mechanically and chemically pre-treated, and the effect of the pre-treatment was studied. The effects of mechanical pre-treatment and anodizing conditions on the quality and properties (morphology, thickness, hardness, etc.) of the produced anodic aluminium oxide (AAO) coatings were systematically studied. Utilizing the sulfuric acid electrolyte results in the formation of the porous type of AAO coatings, and sulfuric acid was therefore chosen as the primary electrolyte. This experimental part was aimed at designing and optimising the process conditions of anodizing AA1050 and at the producing a homogenous porous anodic aluminium oxide (PAAO) coating doped with Al_2O_3 and PTFE particles of better mechanical and tribological properties when compared to the substrate.

4.1.1. Effect of pre-treatment on surface morphology

Figures 16 to 18 show the scanning electron micrographs of the substrate surface morphology of the initial sample and after the mechanical and chemical pre-treatment. As can be observed in Fig. 16a-c, the initial substrate surface is relatively smooth with apparent scratches and rolling lines. The mechanically ground samples consisted of rough, parallel lines from the final manual grinding oriented in one direction, as shown in Fig. 17. The surface of the polished samples was nearly smooth and contained only a small number of scratches, which were produced during mechanical polishing, as shown in Fig. 18. Tiny featureless white spots, which indicate the presence of intermetallic phase particles, were also observed on the surface of the initial material [101-103]. Specifically, two types of intermetallic phase particles were observed: (i) irregular-shaped and (ii) round-shaped particles. The number of irregular-shaped particles was higher than that of the round-shaped ones. An EDX analysis revealed that intermetallic phase particles present in AA1050 were most often based on binary Al-Fe or ternary Al-Fe-Si phases, as shown in Table 6. The EDX analysis also confirmed that the round-shaped particles contained more Si, compared to the irregular-shaped ones. After the chemical pre-treatment, the intermetallic phase particles were more visible with scalloped surface appearance (Figs. 16d-f, 17d-f, 18d-i), because of the lower rate of its dissolution within the aluminium matrix in the NaOH solution. The aluminium matrix dissolution rate was higher than the dissolution rate of Fe and Si, as was also confirmed in the works [104, 105]. After chemical pre-treatment, the initial samples contained rolling lines and a higher number of scallops (Fig. 16d-f) when compared to the polished and chemically pre-treated samples (Fig. 18d-i). In the cross-section of the initial material, intermetallic particles were observed, especially in the rolling direction, see Fig. 19.

Initial

SEM-SE | SEM-BSE | SEM-BSE
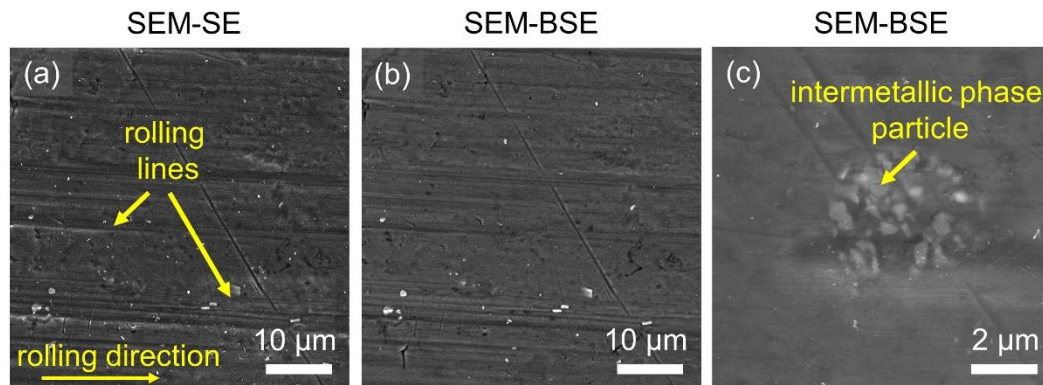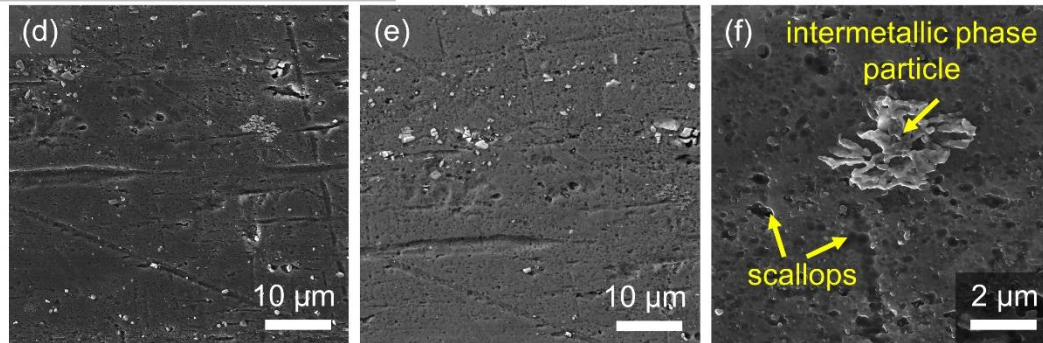
Fig. 16 *Micrographs of the AA1050 surface: (a-c) in the initial state,
and (d-f) after the chemical pre-treatment process.*
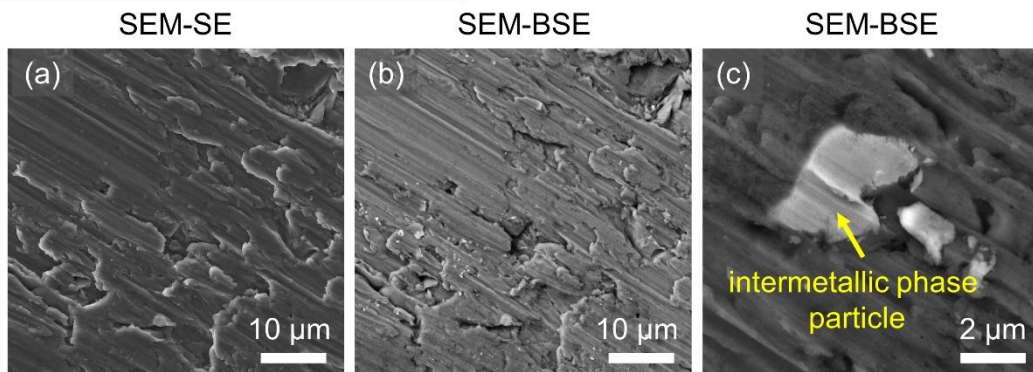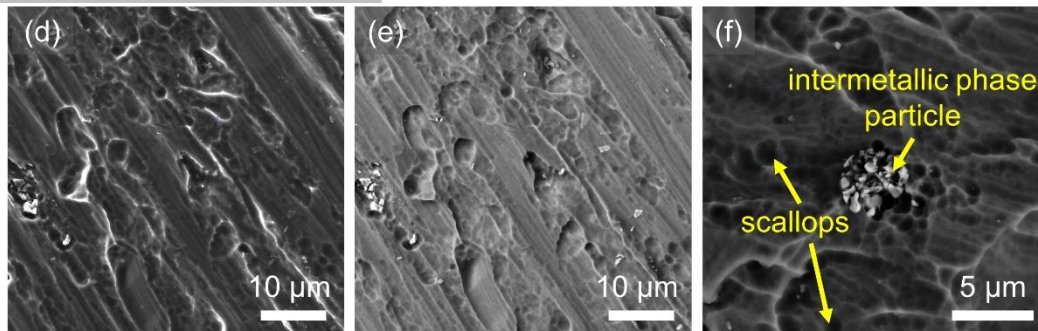
Fig. 17 *Micrographs of the AA1050 surface after mechanical grinding with #1200 SiC paper:
(a-c) before, and (d-f) after the chemical pre-treatment process.*

40
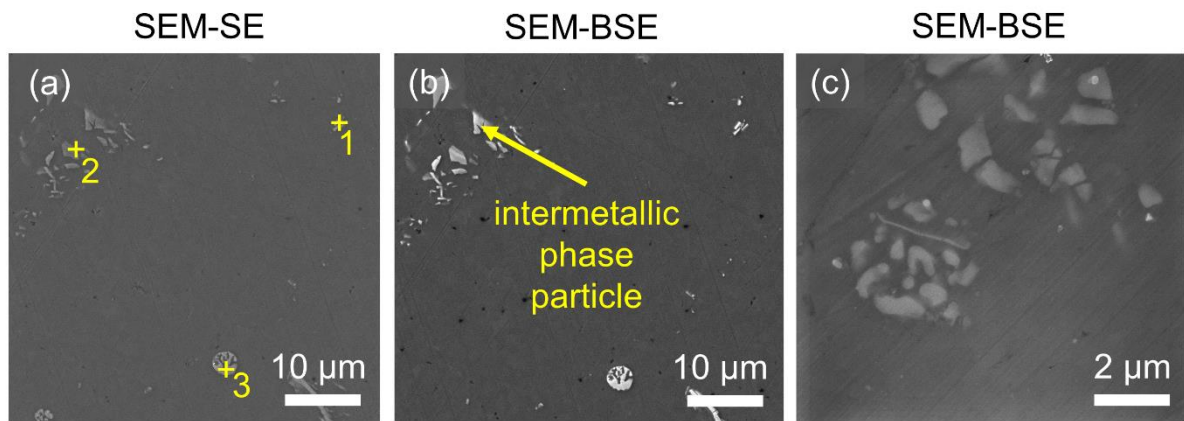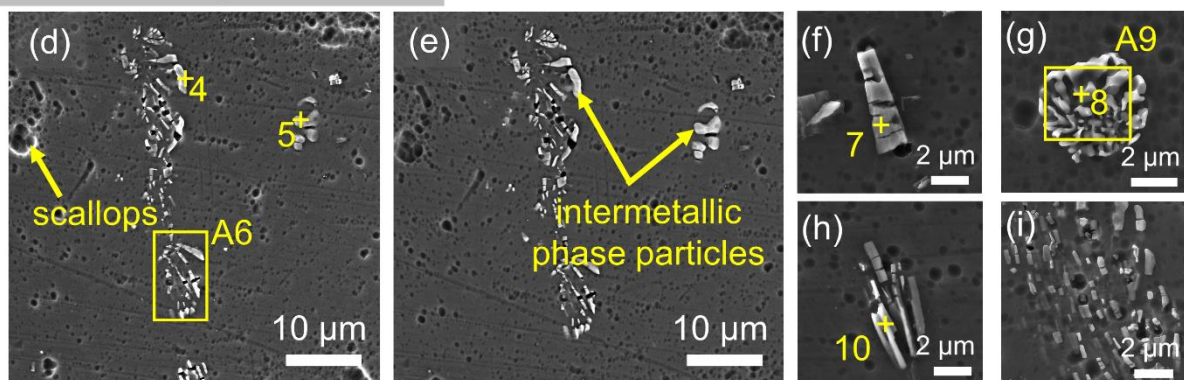
Fig. 18 *Micrographs of the AA1050 surface: (a-c) after mechanical polishing, (d-i) after chemical pre-treatment process, and (f-i) detail of intermetallic phase particles morphology.*

Table 6 *EDX analysis of selected spots (1-10) and areas (A6 and A9) before (1-3) and after (4-10) the chemical pre-treatment process. The locations of the EDX analysis are clearly indicated in Fig. 18.*

Position	Element (wt.%)				
	O	Al	Fe	Si	Fe/Si
1	1.2	97.4	1.4	-	-
2	0.9	89.5	8.9	0.7	12.7
3	1.6	83.5	9.8	5.1	1.9
4	1.1	67.5	28.7	2.7	10.6
5	0.9	80.4	17.3	1.4	12.4
A6	1.2	95.7	2.4	0.7	3.4
7	1.0	64.3	33.6	1.1	32.4
8	2.2	64.1	24.2	9.5	2.5
A9	1.7	72.8	19.6	5.9	3.3
10	1.3	79.6	17.6	1.5	11.7
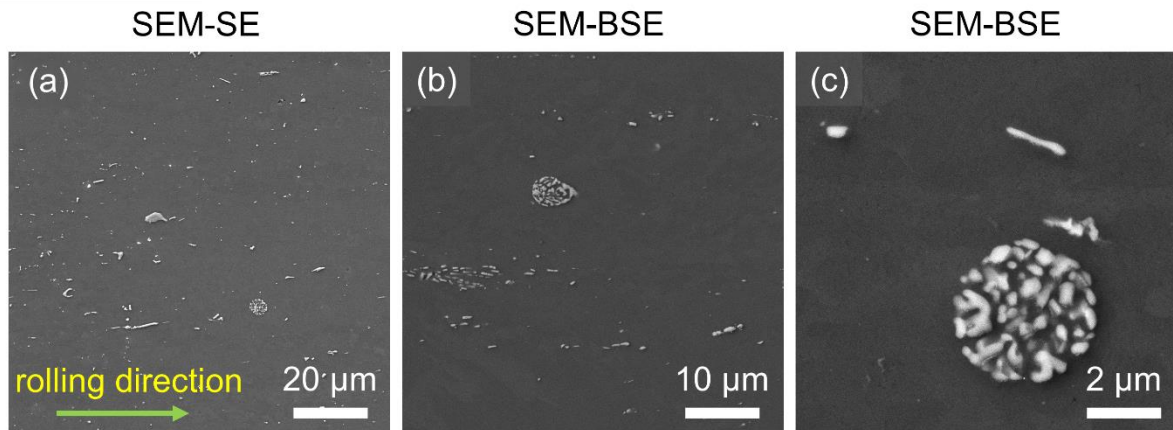
Fig. 19 *Cross-section micrographs of experimental material AA1050: (a) overview, (b, c) higher magnification, and (c) detail of intermetallic phase particles.*

4.1.2. Effect of mechanical pre-treatment, voltage and current density on anodizing at 24 ºC

The conditions under which the first set-up of experiments was carried out are summarized in Table 7, where the effect of pre-treatment, voltage and current density on the morphology, thickness and Vickers microhardness of the produced PAAO coatings were studied.

Table 7 Conditions for experimental set-up to study the effect of mechanical pre-treatment, anodizing voltage and current density.

Sample	Mechanical pre-treatment	Electrolyte (% H_2SO_4[x])	Bath temperature (ºC)	Voltage (V)	Current density (A/dm^2)	Anodizing time (s)
Al 1	as-received	15	24	16	-	1800
Al 2	as-received	15	24	17	-	1800
Al 3	as-received	15	24	18	-	1800
Al 4	as-received	15	24	20	-	1800
Al 5	as-received	15	24	-	3	1800
Al 6	grinding #1200	15	24	-	3	1800
Al 7	polishing	15	24	-	3	1800

[x]H_2SO_4 - sulfuric acid

Anodizing process of AA1050 sheet at 24 ºC

Constant voltage - AA1050 sheet

Figure 20 shows current density *vs* anodizing time curves, obtained during the potentiostatic anodizing process of AA1050 in the 15% H_2SO_4 electrolyte at 24 ºC and different voltages, namely 16, 17, 18 and 20 V. As shown in Fig. 20a, increasing the voltage leads to an increase in the current density. Such similar progress of current density *vs* anodizing time curves in the sulfuric, oxalic acid electrolytes and their mixture was also observed by other authors [106-108] during the potentiostatic anodizing process. Since the current density was recorded every 5 s, the beginning of the anodizing process, i.e. information about the formation of the compact barrier type of coating, was not recorded in detail. Therefore, the further experiments were set to record second by second to obtain a detailed record of the shape of voltage curves. When 20 V was applied, the experiment was manually stopped after 600 s because the current density increased rapidly with anodizing time. In addition, the reaction was intense, more gas bubbles were observed when compared to the previous experiments, and the electrolyte temperature increased by 4 ºC during the anodizing process.
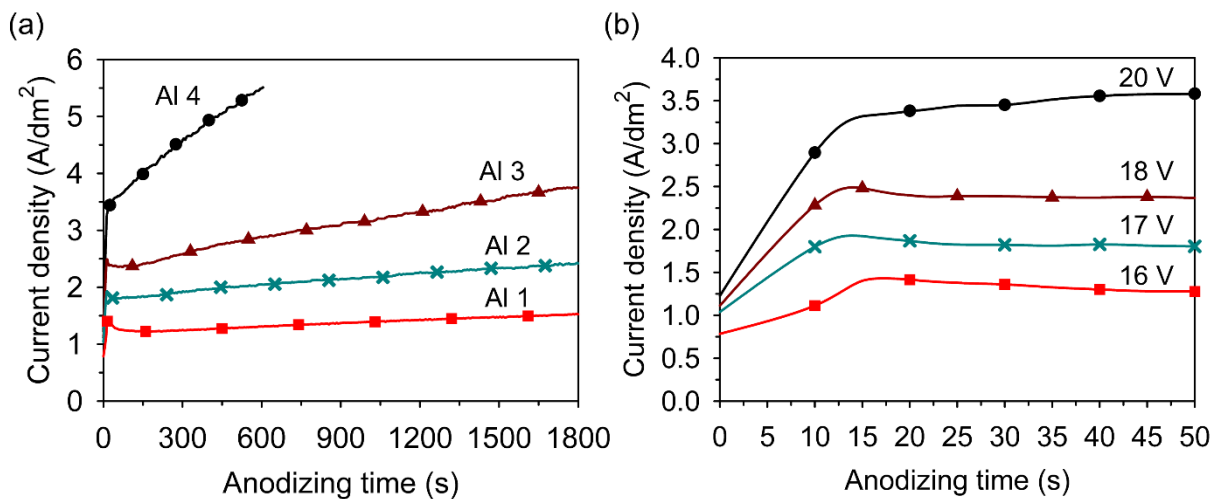
Fig. 20 *Current density vs anodizing time curves recorded during anodizing of AA1050 in the 15% H_2SO_4 electrolyte at 24 ºC, and different applied voltages (a) after 1800 s, and (b) detail of the record up to 50 s.*

Constant current density - AA1050 sheet

Figure 21 shows the voltage *vs* anodizing time curves for AA1050 recorded during the galvanostatic anodizing process in the 15% H_2SO_4 electrolyte at 24 ºC and 3 A/dm^2 provided on the different mechanically pre-treated sample surface. The voltage during the anodizing process was recorded every 1 s. From this curve, an important piece of information about PAAO coating formation was obtained. Generally, the anodizing process can be divided into four stages [7]. All four main stages, which correspond to the mechanism of PAAO coating formation and growth, were recorded. At the beginning of the anodizing process, the voltage increased almost linearly with anodizing time, and compact barrier type of AAO coating was

produced (first stage). With the anodizing process continuing, the nucleation of pores began to form (second stage). After reaching the maximum voltage, the voltage decreased gradually with time and the porous type of AAO coating was formed (third stage). Finally, the voltage plateau was reached and indicated a steady-state growth of the PAAO coating thickness (fourth stage). A similar type of behaviour in the sulfuric, oxalic and chromic acid electrolytes confirms the preliminary studies of Sulka et al. [7] and Rehim et al. [109].
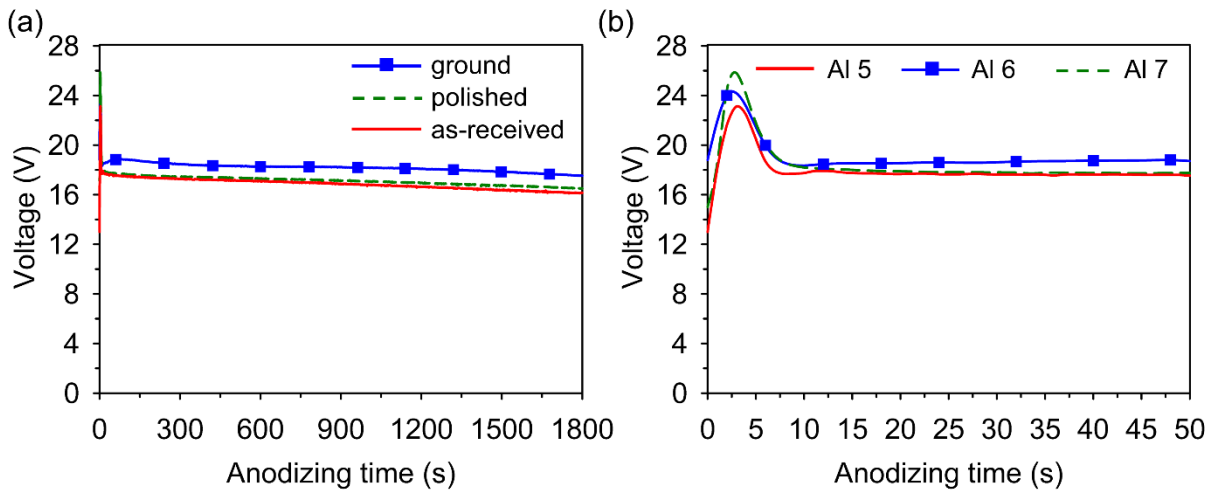
Fig. 21 *Voltage vs anodizing time curves recorded during galvanostatic anodizing in the 15% H$_2$SO$_4$ electrolyte at 24 °C and 3 A/dm^2 on different mechanically pre-treated substrates (a) after 1800 s, and (b) detail of the record up to 50 s.*

Effect of voltage/current density and pre-treatment on the morphology, thickness, and hardness of the produced porous AAO coating at 24 °C

Constant voltage - AA1050 sheet

The surface morphology of produced PAAO coatings at different voltages was almost similar in appearance to each other, but with different pore diameters. The pore diameter of PAAO coatings produced at the lowest voltage of 16 V and the highest voltage of 20 V was larger compared to the pore diameter of PAAO coatings produced at 17 and 18 V. The formed PAAO coatings copied the topography of the initial substrate state as can be seen in Fig. 22 and Fig. 16. The morphology of porous structure was more homogenous in areas where the initial surface was smoother before the anodizing process (Fig. 22c). In the cross-section, an irregular pore structure was found (Fig. 22d). The most regular porous structure could be achieved by mechanical polishing or electropolishing pre-treatment of the initial substrate and two-step anodizing process. Sulka et al. [110] found that the two-step anodizing process in the 20% H$_2$SO$_4$ electrolyte at 15-25 V had a significant effect on the improved the formation of a more regular porous structure (with the ideal, hexagonal pore arrangement and high uniformity of pore sizes). Thus, the three-step anodizing process did not have such a positive effect on regular porous structure formation as the two-step anodizing process had.

15% H₂SO₄ / 1800 s / 24 °C / 16 V (sample Al 1)

SEM-SE   SEM-BSE   SEM-BSE   SEM-BSE

(a) ... 10 µm   (b) A ... 2 µm   (c) B ... 500 nm   (d) PAAO coating ... substrate ... 500 nm
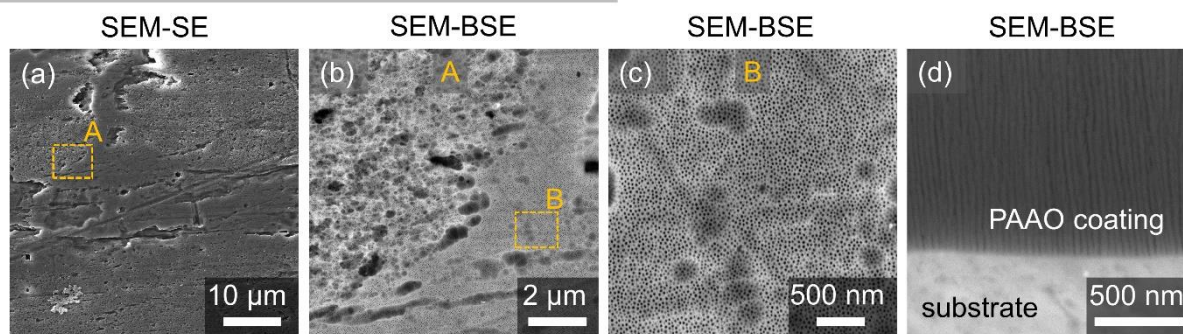
Fig. 22 *Micrographs of the coating surface (a-c) and (d) detail of PAAO coating structures in cross-section of AA1050 after anodizing in the 15% H₂SO₄ electrolyte for 1800 s at 24 °C and 16 V.*

With increasing voltage, the growth of PAAO coating thickness was expected. As can be seen in Fig. 23 and in Table 8, when the lowest voltage of 16 V was applied, a thicker PAAO coating of 29.5 µm was formed compared to the higher voltages of 17 and 18 V, in which the thickness of PAAO coating was 21.5 and 13.2 µm, respectively. When 20 V was applied, and almost three times shorter anodizing time was used, the thicker PAAO coating (19.5 µm) was formed. In the PAAO coating cross-section, partially oxidized intermetallic particles were found (Fig. 23a,b). The EDX analysis of PAAO coatings confirmed the presence of aluminium, oxygen and sulfur. The presence of sulfur in the PAAO coating is the result of the incorporation of sulfur ions from the sulfuric acid electrolyte into the formed PAAO coating during the anodizing process. As has been reported [108, 111, 112], the negatively charged ions (i.e. O^{2-}, OH^- and SO_4^{2-}) of the electrolyte are attracted to the positively polarized anode (experimental material AA1050). On the surface of the anodized material, these ions interact with Al^{3+} cations and form the PAAO coating. The PAAO coating produced at 20 V contained more sulfur compared to PAAO coatings produced at lower voltages (see Table 8). This result indicates that using higher voltage leads to higher ionic mobility of sulfur during the anodizing process, i.e. more sulfur ions are incorporated into the formed coatings.

Figure 24 shows the XRD patterns obtained from the initial AA1050 material and anodized samples Al 1, Al 3 and Al 4. The results show three peaks related to the aluminium substrate and two peaks related to intermetallic phase particles. The type of intermetallic phase particles cannot be determined from XRD measurements because the phases in the alloy are small, and their distribution is low. The identification of these intermetallic phase particles is below the detection limit of the device. Amorphous Al_2O_3 phase formation was confirmed after anodizing and observed at 2theta angles between 20 and 35 degrees. Microhardness measurements revealed that the anodic coating Al 1 was about ten times harder than the initial material. Measuring the HV0.05 hardness for the Al 2-Al 4 coatings was not possible due to the very thin PAAO coatings.
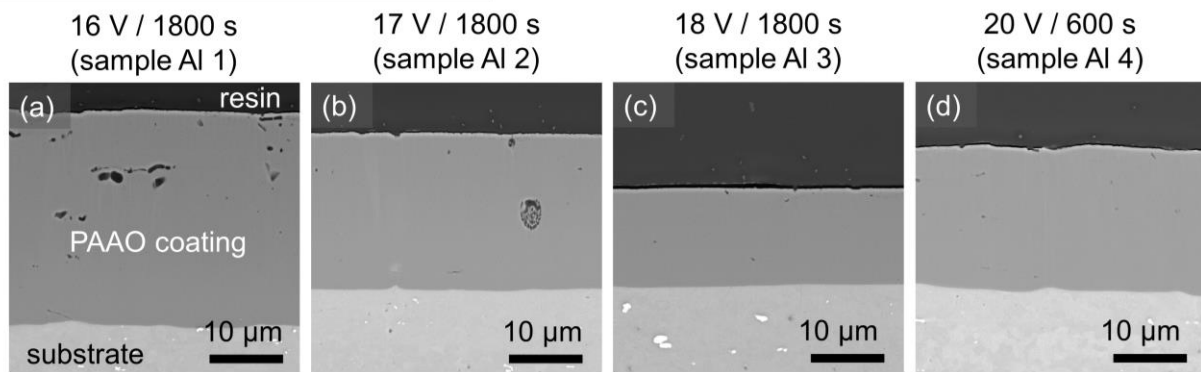
Fig. 23 *Micrographs (SEM-BSE) of the cross-section of AA1050 after anodizing in the 15% H₂SO₄ at 24 ºC and at different voltages and times: (a) 16 V, 1800 s, (b) 17 V, 1800 s, (c) 18 V, 1800 s, and (d) 20 V, 600 s.*
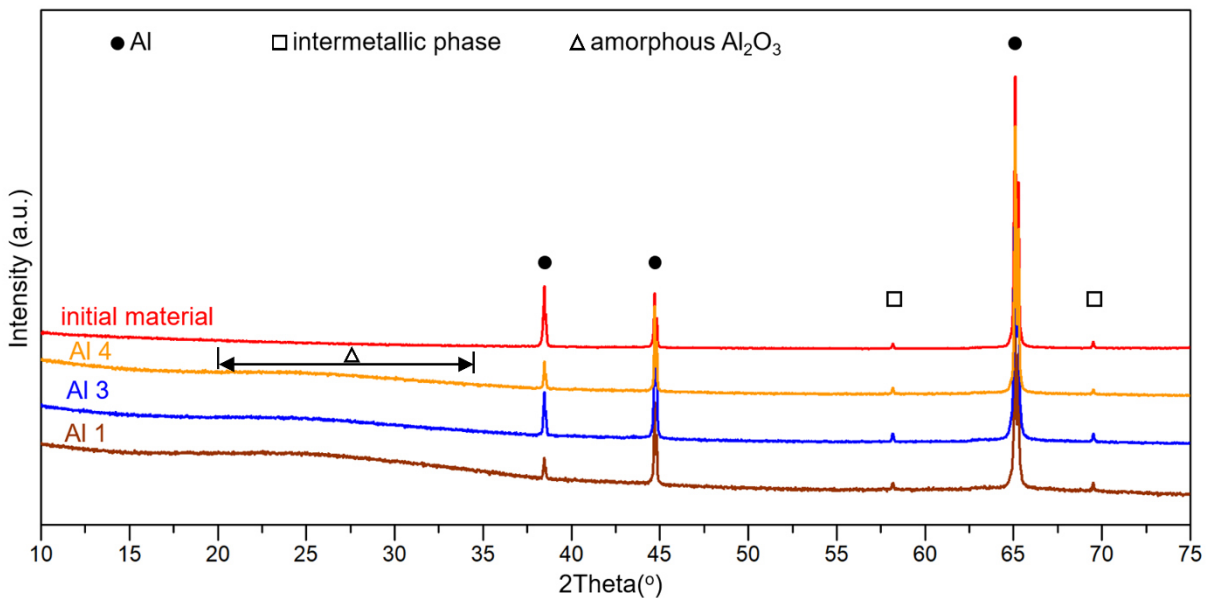
Fig. 24 *X-ray diffraction patterns of the initial material (AA1050) and the anodized samples in the 15% H₂SO₄ electrolyte and at 24 ºC in the potentiostatic regime: sample Al 1 (16 V), sample Al 3 (18 V), and sample Al 4 (20 V).*

Constant current density - AA1050 sheet

Figure 25 shows the effect of mechanical pre-treatment on the morphology and thickness of the produced PAAO coatings in the 15% H₂SO₄ at 24 ºC and at a constant current density of 3 A/dm². On the surface of the Al 7 coating produced on a mechanically polished substrate, some cavities were found (see Fig. 25g) whose shape and dimension were similar to the intermetallic particles observed on the chemically pre-treated initial surface. These cavities were also found on the Al 6 and Al 5 PAAO coating surfaces, but in this case, the cavities were not as clearly recognized as on the Al 7 coating produced on the mechanically polished substrate. The presence of cavities on the surface can be explained by the preferred dissolution of intermetallic phase particles during the anodizing process, as observed by other

46

authors [102, 113]. Intermetallic phase particles based on Al-Fe and Al-Fe-Si are of lower oxidation rates than the aluminium matrix, and therefore they can be trapped in the coating during the anodizing process and thus reduce the local growth of the PAAO coating [80]. This phenomenon was also apparent in the cross-section of the produced PAAO coating (Fig. 25i, arrow), where the coating thickness dropped in the near vicinity of the round-shaped intermetallic phase particle. The local chemical composition analyses (Fig. 35 and Table 15) revealed a significantly lower Fe content within the intermetallic phase, and also confirmed the higher dissolution rate of Fe compared to Si during the anodizing process. The oxygen was also detected in the coating cross-section at the site of intermetallic phase particles, which indicated its partial oxidation. The behaviour of the intermetallic phase particles contained in AA1050 is studied in more detail in section 4.1.7. After anodizing, the sample Al 5 was of a lower PAAO coating thickness (28.5 μm) than the mechanically pre-treated sample Al 6 or Al 7 (30.7 or 30.4 μm). As apparent, the grinding pre-treatment of the initial substrate surface had a negative effect on the decrease in coating microhardness, see Table 8. Results of EDX analysis shown in Table 8 confirmed the presence of aluminium, oxygen and sulfur.
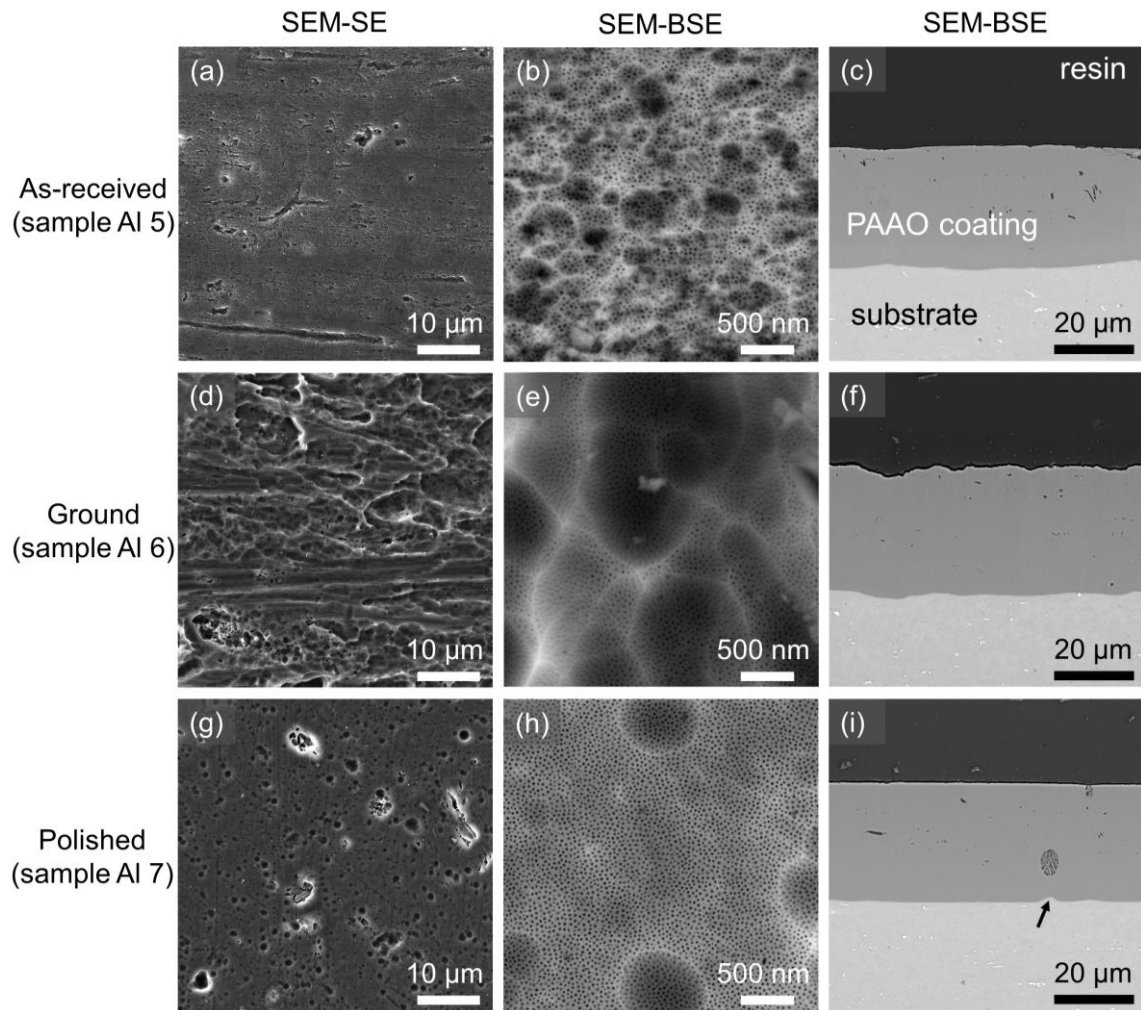
Fig. 25 *Micrographs of the coating surface (left and middle) and its cross-section (right) after the mechanical pre-treatment (a-c) as-received state, (d-f) ground, (g-i) polished and anodized in the 15% H_2SO_4 for 1800 s at 24 °C and 3 A/dm².*

Table 8 *EDX analysis of the initial substrate surface and PAAO coatings estimated from an area of 0.21 mm², and the thickness and microhardness of PAAO coatings.*

Sample	Element (wt.%)			Thickness of PAAO coating (μm)	Microhardness HV0.05
	Al	O	S		
Substrate	97.5	2.5	-	-	40.2±0.2
Al 1	50.0	44.6	5.4	29.5	402±9.8
Al 2	50.8	44.0	5.2	21.5	-
Al 3	50.9	43.8	5.3	13.2	-
Al 4	51.3	43.0	5.7	19.5	-
Al 5	50.2	43.8	6.0	28.5	407±8.1
Al 6	49.8	44.4	5.8	30.7	398±9.6
Al 7	50.2	44.1	5.7	30.4	405±6.3

Figure 26 shows the XRD patterns obtained from the initial material and anodized samples Al 5-Al 7. The results show three peaks related to the aluminium substrate and two peaks related to intermetallic phase particles. Amorphous Al_2O_3 phase formation was confirmed after anodizing and observed at 2theta angles between 20 and 35 degrees.
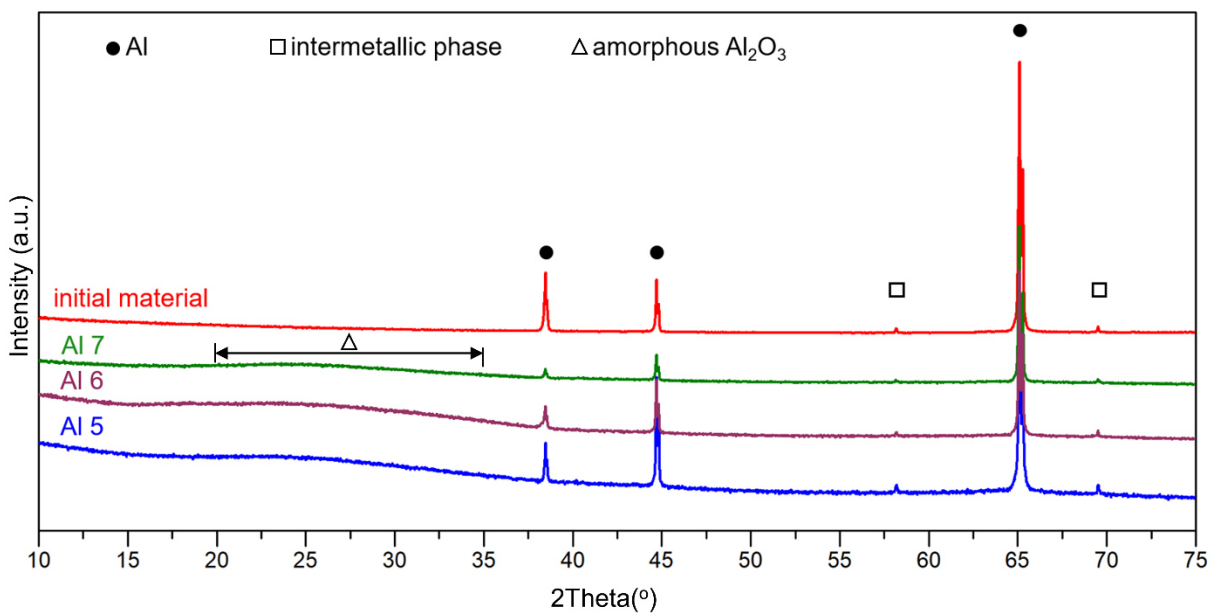
Fig. 26 *X-ray diffraction patterns of the initial material (AA1050) and anodized samples (Al 5-Al 7) in the 15% H_2SO_4 electrolyte at 3 A/dm² and at 24 °C for 1800 s with different mechanical pre-treatment (Al 5) as-received, (Al 6) ground, (Al 7) polished.*

4.1.3. Effect of temperature on the produced PAAO coating

For this experimental set-up, the temperature of the electrolyte was reduced and kept constant at 18 °C and then at 10 °C. The conditions for this experimental set-up are summarized in Table 9. This subchapter is focused on the study of the influence of anodizing temperature on the thickness, hardness and morphology of the produced PAAO coatings.

Table 9 Conditions for the experimental set-up to study the effect of the electrolyte temperature.

Sample	Mechanical pre-treatment	Electrolyte (% $H_2SO_4^x$)	Bath temperature (°C)	Voltage (V)	Current density (A/dm²)	Anodizing time (s)
Al 8	grinding #1200	15	18	16	-	1800
Al 9	polishing	15	18	16	-	1800
Al 10	polishing	15	18	-	3	1800
Al 11	polishing	15	10	-	3	1800

^{x}H_2SO_4 - sulfuric acid

Porous AAO coatings produced at a constant voltage of 16 V and electrolyte temperature of 18 °C on the AA1050 with different mechanical pre-treatments, (i) grinding (Fig. 27a, sample Al 8) and (ii) polishing (Fig. 27b, sample Al 9), were of a lower thickness (9.5 μm and 12.8 μm, Table 10) than the PAAO coatings formed at 24 °C (29.5 μm). With increasing temperature, the current density increases, and the oxidation rate is higher; therefore, the produced PAAO coatings become thicker [65]. The PAAO coatings formed at a constant current density of 3 A/dm² and at lower temperatures (18 and 10 °C) were found to have a coating thickness of 29.8 and 33.5 μm (Fig. 27c,d and Table 10), respectively.

Porous AAO coatings produced at a constant current density of 3 A/dm² and different temperatures 18 and 10 °C are shown in Fig. 27c,d. Decreasing the electrolyte temperature from 24 °C to 18 °C had no significant effect on the hardness and thickness of the produced coating as in the case of lowering the temperature to 10 °C. Decreasing the electrolyte temperature from 18 °C to 10 °C increases the PAAO coating (i) thickness from 29.8 to 33.5 μm, and (ii) hardness from 417 to 451 HV0.05. The increase in coating thickness with decreasing electrolyte temperature can be explained by the increase in voltage, see Fig. 28b. A higher temperature of the electrolyte caused a higher dissolution of PAAO coating, which means that the rate of dissolution is faster than the rate of PAAO coating formation. Most scientists [7, 65, 68, 72] studied the influence of electrolyte temperature on the thickness, porosity and hardness of the produced PAAO coatings. Aerts et al. [68] found that the PAAO coating formed at a temperature of 5 °C had a dense structure with small pores which were separated by thick walls while increasing the electrolyte temperature (10-50 °C) led to increased pore diameters,

decreased wall thickness and increased porosity of the formed PAAO coating. For this reason, while the electrolyte temperature is decreasing, the hardness and wear volume is increasing [68, 72].

The PAAO coating formed at a constant current density contained a higher amount of sulfur than the coating produced at a constant voltage. On the surface and in the cross-section of the coating Al 11, produced at a lower temperature, hillocks were found, as can be seen in Fig. 27d and Fig. 28.
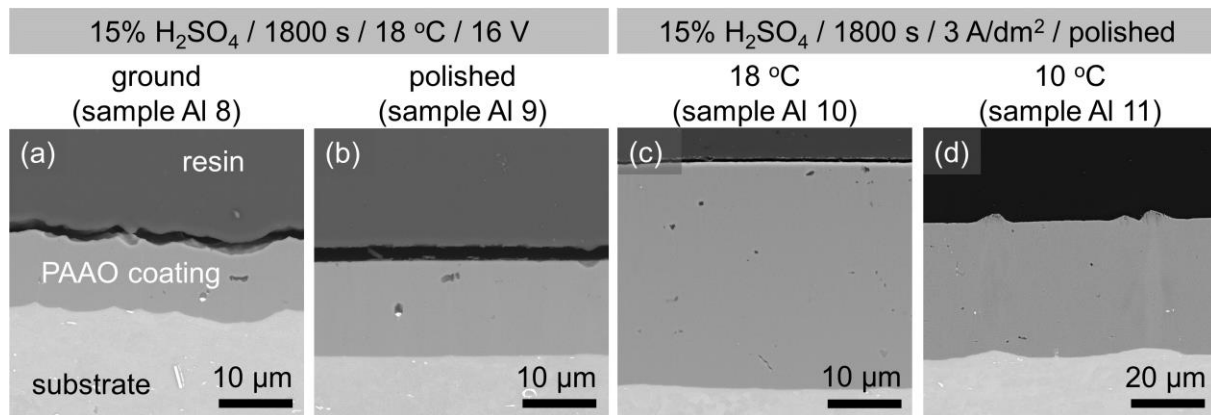
Fig. 27 *Micrographs (SEM-BSE) of the cross-section of AA1050 after the mechanical pre-treatment (a) grinding, (b-d) polishing and anodized in the 15% H_2SO_4 electrolyte for 1800 s at (a-b) 16 V, 18 °C, (c, d) 3 A/dm², and at (c) 18 °C, (d) 10 °C.*

Table 10 *EDX analysis of anodized samples estimated from a surface area of 0.21 mm², and the thickness and microhardness of PAAO coatings.*

Sample	Element (wt.%)			Thickness of anodic coating (μm)	Microhardness HV0.05
	Al	O	S		
Al 8	50.5	44.2	5.3	9.5	-
Al 9	50.7	43.9	5.4	12.8	-
Al 10	50.1	44.0	5.9	29.8	417±5.4
Al 11	49.9	43.8	6.3	33.5	451±15.4

The formation of hillocks during the anodizing process of aluminium and its alloys in the sulfuric acid electrolyte was also observed by other research groups [101, 114, 115]. Hillocks indicate a local burning during the anodizing process, and this local phenomenon was observed under different anodizing conditions during both the laboratory-scale experiments and the industrial processing [54]. Generally, the local burning is caused by very high local current densities, which lead to a significant increase in the local temperature. But an exact connection between the generated heat and the origin of the hillocks is still unknown [115].

Gastón-García et al. [101] suggested that the presence of Fe- and Si-based intermetallic phase particles in the aluminium alloy initiate the local burning, which causes the hillocks formation. Michalska-Domanska et al. [108] also observed hillocks on the surface of PAAO coatings formed on both low and high purity aluminium substrates. They proposed that the formation of hillocks is caused by the incorporation of sulfate ions rather than by the presence of intermetallic phase impurities present in anodized aluminium alloys. Detailed SEM and EDX investigations into the appearance of hillocks on the surface and in the cross-section (Fig. 35e,g and Table 15) confirmed that the hillocks contained more sulfur and oxygen than the hillock-free PAAO coating did. Figure 28d-f shows details of the structure of the PAAO coating in cross-section near the hillock area. Roa et al. [116] investigated the mechanical properties of the PAAO coating, which contained hillocks, using the nanoindentation technique. The results showed that in the areas where excessive current density was concentrated highly degraded PAAO hillocks were formed. These hillocks were found be to of lower hardness than the surrounding PAAO coating [116]. Cracks were predominantly observed on the hillock surfaces (Fig. 28b-c), and the depth of the cracks was only up to 0.5 µm below the anodized surface coating, i.e. in the vicinity of the hillocks and intermetallic particles. The cracks observed in the hillocks can be attributed to high internal stress accompanied by the concentration of high local current density. The result is a fast growth of PAAO coating on the site of the hillocks [115].
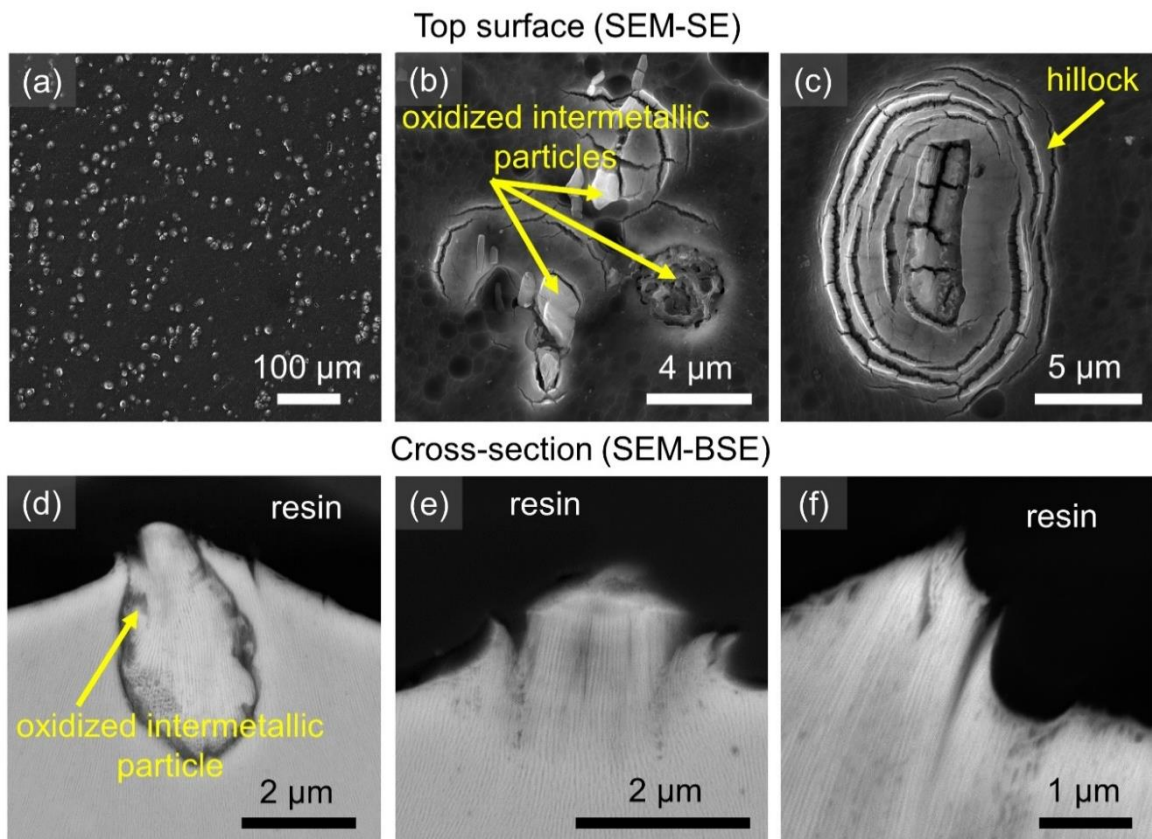
Fig. 28 *Micrographs of (a-c) the coating surface and (d-f) a detail of hillocks in cross-section sample Al 7 produced in the 15% H_2SO_4 electrolyte for 1800 s at 10 °C and 3 A/dm².*

51

4.1.4. Effect of current density, electrolyte composition and concentration on anodizing process, morphology, hardness and thickness of the produced PAAO coating

Based on the previous experiments, the mechanical pre-treatment polishing, constant current density and electrolyte temperature of 10 °C were selected. The conditions for this experimental set-up are summarized in Table 11. In this subchapter the effect of sulfuric acid and oxalic acid concentration, the value of current density and the anodizing time was studied in order to understand better their influence on morphology, thickness and hardness of the produced PAAO coatings. Part of these results was published by the author of the thesis in Applied Surface Science journal [117].

Table 11 Experimental conditions for the evaluation of the effect of current density, electrolyte composition and concentration on the anodizing process.

Sample	Mechanical pre-treatment	Electrolyte	Temperature (°C)	Current density (A/dm^2)	Anodizing time (s)
Al 12	polishing	15% H$_2$SO$_4$$^\times$ + 10 mL/L C$_3$H$_8$O$_3$*	10	3	1800
Al 13	polishing	15% H$_2$SO$_4$ + 20 g/L C$_2$H$_2$O$_4$$^\circ$ + 10 mL/L C$_3$H$_8$O$_3$	10	3	1800
Al 14	polishing	15% H$_2$SO$_4$ + 40 g/L C$_2$H$_2$O$_4$ + 10 mL/L C$_3$H$_8$O$_3$	10	3	1800
Al 15	polishing	15% H$_2$SO$_4$ + 20 g/L C$_2$H$_2$O$_4$ + 10 mL/L C$_3$H$_8$O$_3$	10	2	1800
Al 16	polishing	15% H$_2$SO$_4$ + 20 g/L C$_2$H$_2$O$_4$ + 10 mL/L C$_3$H$_8$O$_3$	10	1	1800
Al 17	polishing	15% H$_2$SO$_4$ + 20 g/L C$_2$H$_2$O$_4$ + 10 mL/L C$_3$H$_8$O$_3$	10	1	3600
Al 18	polishing	18% H$_2$SO$_4$ + 20 g/L C$_2$H$_2$O$_4$ + 10 mL/L C$_3$H$_8$O$_3$	10	3	1800
Al 19	polishing	10% H$_2$SO$_4$ + 20 g/L C$_2$H$_2$O$_4$ + 10 mL/L C$_3$H$_8$O$_3$	10	3	1800

$^\times$H$_2$SO$_4$ - sulfuric acid; *C$_3$H$_8$O$_3$ - glycerol; $^\circ$C$_2$H$_2$O$_4$ - oxalic acid

Anodizing process

Figure 29 shows the effect of anodizing conditions (electrolyte composition and current density) on the shape of the voltage *vs* anodizing time curves for AA1050, recorded during the galvanostatic anodizing process. A change in anodizing conditions and also in the type of aluminium alloys strongly influences the slope appearance in the voltage *vs* anodizing time curves, which is related to the formation rate and thickness of compact barrier and porous anodic aluminium oxide (PAAO) coatings.

The use of the lower electrolyte temperature of 10 ^{o}C and the constant current density of 3 A/dm^2 (curve Al 12) led to an increase in the voltage and resulted in the formation of thicker PAAO coatings containing smaller pores when compared to the coating Al 7 (see Fig. 29a), i.e. that one produced at 24 ^{o}C (curve Al 7) [72].

Addition of 20 g/L of $C_2H_2O_4$ (oxalic acid) to the 15% H_2SO_4 electrolyte (curve Al 13) led to a slight increase in voltage when compared to the same process without $C_2H_2O_4$ addition (curve Al 12). Abdel Rehim et al. [109] studied the effect of anodizing conditions on the shape of the current density *vs* time curve and found that adding oxalic acid to the sulfuric acid electrolyte reduced oxide dissolution and produced less porous and more compact PAAO coatings.

When the lower current density of 2 A/dm^2 was applied, only a small drop in the voltage (curve Al 15) was recorded. A further decrease in current density down to 1 A/dm^2 (curve Al 17) led to a significant voltage drop in comparison with anodizing at higher current densities (2 and 3 A/dm^2, curves Al 15 and Al 13, respectively). From a comparison of the voltage *vs* anodizing time curves (Fig. 29b), it follows that anodization at higher current densities (curves Al 13 and Al 15) took less time in the linear part (first stage), in which the compact barrier type of coating is formed when compared to those at 1 A/dm^2 (curve 17). This means that the compact barrier coating formed at a higher current density (3 or 2 A/dm^2) is less dense than the compact barrier coating formed at 1 A/dm^2. With increasing current density in the linear part, an increase in voltage was recorded. This behaviour can be explained by the increase in the growth rate of the compact barrier coating. Chung et al. [118] studied the influence of current density and electrolyte concentration on the growth of PAAO coatings. Results showed that the decreasing current density led to a decrease in ionic mobility in the electrolyte, confirming the presence of the O^{2-} and OH^- ions at the electrolyte/AAO coating interface and Al^{3+} ions from the oxidation process of substrate AA1050. Higher current densities led to higher O^{2-}, OH^- and Al^{3+} mobility for the formation of thicker PAAO coatings. The electrolyte concentration (1-5 M H_2SO_4) did not influence the coating growth rate as the applied current density (0.3-3 A/dm^2) did.

Addition of 40 g/L $C_2H_2O_4$ to the 15% H_2SO_4 electrolyte at a current density of 3 A/dm^2 led to a slight increase in the local voltage maximum (curve Al 14) when compared to the curve of sample Al 13. The voltage value in the stage of steady-state growth was found to be the same as for the sample Al 13, where only half the amount was added, i.e. 20 g/L of $C_2H_2O_4$.

The use of a higher electrolyte concentration, i.e. 18% H_2SO_4 with 20 g/L of $C_2H_2O_4$, led to a voltage decrease (curve Al 18). Opposite behaviour was observed at a lower electrolyte

concentration, i.e. 10% H_2SO_4, where the voltage significantly increased (curve Al 19) in comparison with the curve Al 13. Due to the increase in voltage (curve Al 19), higher ion mobility can be expected, and thicker PAAO coating can be produced.

Also, it was found that during the anodizing processes with higher current densities (3 and 2 A/dm^2) and a lower electrolyte temperature of 10 ^{o}C, see curves Al 12-15, Al 18 and Al 19, when the maximum voltage was reached, there was some deflection in the continuous descent slope when compared to curves Al 7 and Al 17. This type of deflection in the voltage *vs* anodizing time curves was also observed by Aerts et al. [115], where they proposed that the deflection indicated a local burning on the interface of electrolyte; as a result, PAAO coatings with the hillocks are formed.
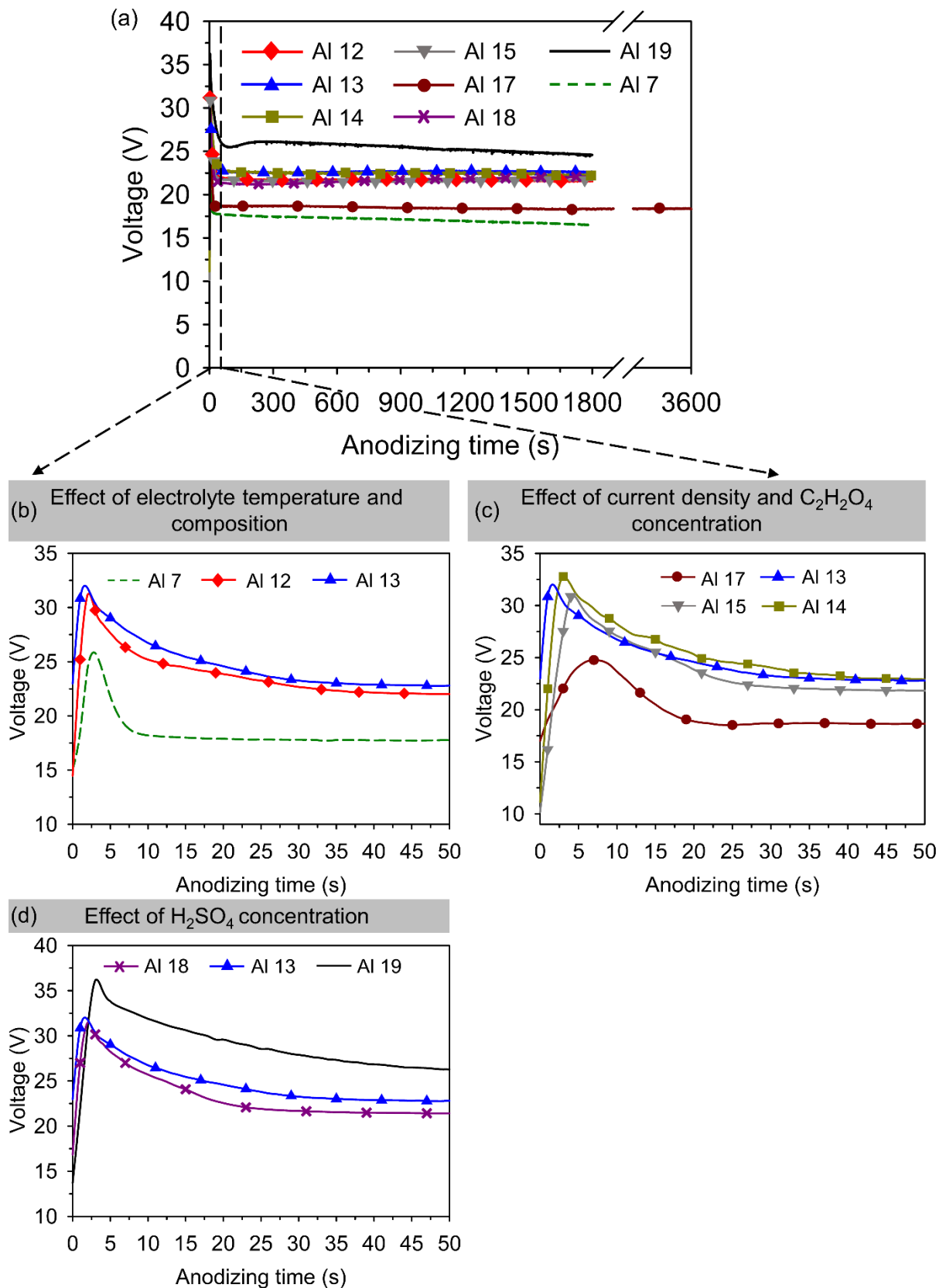
Fig. 29 *Voltage vs anodizing time curves for samples Al 7, Al 12-Al 15, Al 18 and Al 19 recorded during galvanostatic anodizing of AA1050 in different process conditions (a) after 3600 s, and (b-d) detail of the record up to 50 s.*

Effect of anodizing conditions on the PAAO coating microstructure, thickness and hardness

Figures 30 and 31, as well as Table 12, show the effect of different anodizing conditions such as electrolyte composition and current density on the morphology and thickness of the produced PAAO coatings at lower temperatures.

The surface morphology of PAAO coating Al 12 prepared at electrolyte temperature of 10 °C in the 15% H_2SO_4 electrolyte with 10 mL/L $C_3H_8O_3$ (glycerol) under a constant current density of 3 A/dm^2 (Fig. 30a-c) revealed the presence of some hillocks. The number of these hillocks was lower than the number of those observed on the coating Al 11, where $C_3H_8O_3$ addition was not used.

Addition of 10 mL/L of $C_3H_8O_3$ to the 15% H_2SO_4 electrolyte led to an increase in coating hardness from 451 to 472 HV0.05 and a decrease in coating thickness from 33.5 to 32.8 µm.

Addition of 20 g/L $C_2H_2O_4$ to the 15% H_2SO_4 electrolyte led to the formation of a harder (489 HV0.05) and thicker (34.4 µm) PAAO coating Al 13 with the typical surface morphology and with hillocks (Fig. 30d-f, Table 12). Some researchers [72, 119, 120] observed the effect of oxalic acid on the decrease of coating porosity, which led to a higher hardness of the produced PAAO coatings. Guezmil et al. [72] showed that the alloying element influenced the microhardness of the PAAO coatings. The microhardness values obtained for AA1050 were higher than those obtained for AA5754. Fratila-Apachitei et al. [121] found that for anodized multiphase cast aluminium alloys the copper and magnesium particles had a significant effect on the decrease in coating microhardness than silicon particles had. It is well known that Cu and Mg particles can cause macroscopic defects in the produced coating in the form of cavities.

Addition 40 g/L of $C_2H_2O_4$ had a negative effect, namely a lower coating thickness and hardness. Also, a higher number of hillocks were formed on the surface and in the cross-section of coating Al 14, as shown in Fig. 30g-i.

When the lower current density of 2 A/dm^2 was applied, the thinner (22.4 µm) and softer (456 HV0.05) PAAO coating Al 15 with a lower number of hillocks was formed, see Table 12. A further decrease in current density down to 1 A/dm^2 resulted in the formation of a thinner PAAO coating Al 16 without hillocks, as depicted in Fig. 30j-l. With the anodizing time increasing from 1800 to 3600 s, the thickness of the porous AAO coating increased from 9.9 to 18.9 µm, as could be expected.

An important finding was that the PAAO coatings Al 12-Al 15 exhibited a high microhardness data scatter, which was due to the presence of a high number of hillocks on the coating surface. Roa et al. [116] studied in detail the mechanical properties of porous AAO coatings containing hillocks and confirmed by nanohardness measurements that the hillocks exhibited locally lower hardness due to higher porosity and the presence of cracks. Guezmil et al. [72] demonstrated that with an increase in current density in the range of 1-3 A/dm^2 at a fixed PAAO coating thickness of 30 µm led to an increase in PAAO coating microhardness. Fratila-Apachitei et al. [121] anodized AlSi(Cu) alloy in the range from 3 to 6 A/dm^2 at a fixed anodizing time and studied microhardness across the increased

coating thickness. Results showed that the microhardness decreased with decreasing distance from the substrate while increasing the current density resulted in no beneficial effects for average PAAO coating microhardness. Increasing the anodizing time resulted in the formation of a thicker PAAO coating with lower average microhardness.

Higher microstructural homogeneity was obtained by lowering the current density from 3 to 1 A/dm^2, which also provided a more uniform hardness distribution across the coating Al 17, see Fig. 30 and Table 12. With decreasing current density, the coating thickness decreased, which confirmed the lower mobility of O^{2-}, OH^-, SO_4^{2-} and Al^{3+} ions.

Increasing the concentration of the sulfuric acid from 15 (sample Al 13) up to 18% (sample Al 18) led to the formation of a thinner (32.3 μm) but also less hard coating (459 HV0.05) with fewer hillocks. It was expected that by increasing the electrolyte concentration, a thinner and less hard PAAO coating without hillocks would be formed. As can be seen from the results, it would be desirable to increase the electrolyte concentration even more, but then a less hard coating would be produced. On the other hand, the decreasing concentration of sulfuric acid from 15 to 10% led to the formation of a thicker (34.8 μm) and less hard (460 HV0.05) PAAO coating which consisted of a higher number of hillocks, see Fig. 31 and Table 12. With decreasing concentration of the electrolyte, the production of the hard coating was expected. Zhang et al. [122] studied the influence of the concentration of electrolyte (100-400 g/L) on pore parameters and microhardness on the performance of PAAO coating on AA2024. The results showed that with increasing electrolyte concentration, the dissolution effect of the electrolyte on the formed PAAO coating decreased, resulting in higher coating porosity and lower microhardness. The decrease in hardness can be explained by the higher number of hillocks, which have a negative effect on hardness. The electrolyte concentration did not affect the coating thickness significantly as the current density did. These results are consistent with Chung et al. [118].

The EDX analysis pointed out the presence of aluminium, oxygen and sulfur in PAAO coatings; however, small differences were found in the chemical composition of coatings, see Table 12. PAAO coatings with hillocks Al 12-15 and Al 18-19 formed at higher current densities (2 and 3 A/dm^2, respectively) contained a higher amount of sulfur compared to coatings (Al 16 and Al 17) formed at a lower current density of 1 A/dm^2. The increase in sulfur content with increasing anodizing current density or voltage was also observed by other research teams [101, 108, 118]. Chung et al. [118] produced a PAAO coating without hillocks and found that with increasing current density, the sulfur content increased. Their results and the present study show that using a higher current density/voltage leads to higher ionic mobility of sulfur ions during the anodizing process, i.e. more sulfur ions are incorporated into the formed PAAO coatings. The higher content of sulfur ions also contributes to the formation of hillocks, as was described above.

When a lower temperature of the electrolyte was used, the intermetallic phase particles on the surface were preferentially oxidized. Detailed information on this is given in section 4.1.7.

SEM-SE SEM-BSE SEM-BSE

(sample Al 12)

20 g/L C₂H₂O₄
(sample Al 13)

40 g/L C₂H₂O₄
(sample Al 14)
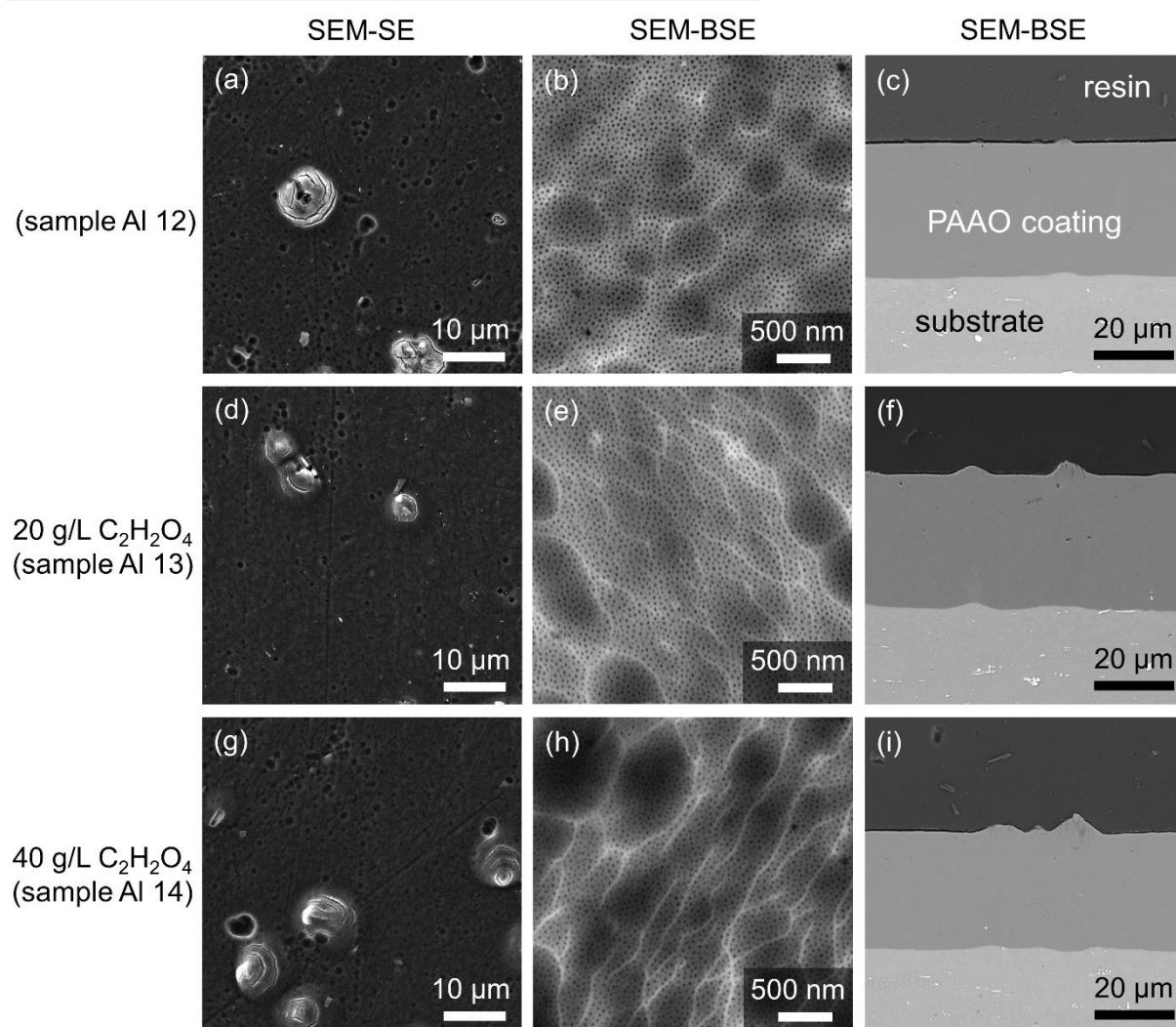
15% H₂SO₄ + 10 mL/L C₃H₈O₃/ 3600 s / 10 °C / 1 A/dm²

20 g/L C₂H₂O₄
(sample Al 17)
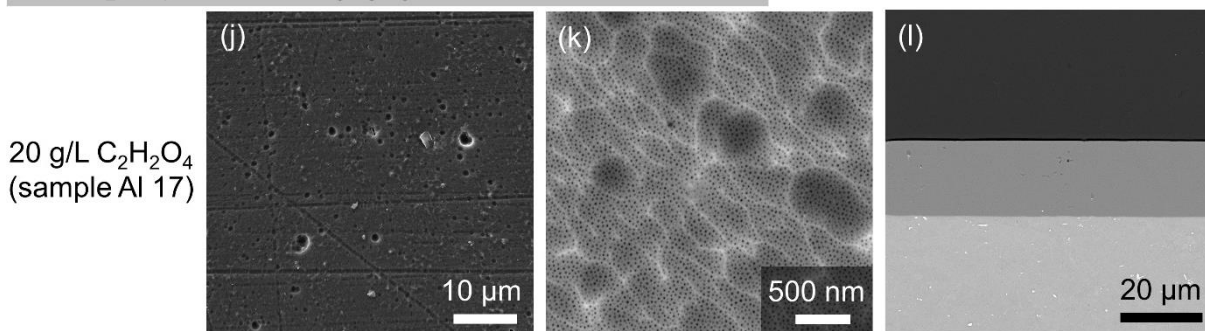
Fig. 30 *Micrographs of the coating surface (left and middle) and its cross-section (right) after anodizing: (i) at a constant current density and anodizing time (a-i) 3 A/dm², 1800 s, (j-l) 1 A/dm², 3600 s, (ii) composition of the electrolyte (a-c) 15% H₂SO₄ + 10 mL/L C₃H₈O₃, (d-f, j-l) 15% H₂SO₄ + 20 g/L C₂H₂O₄ + 10 mL/L C₃H₈O₃, and (g-i) 15% H₂SO₄ + 40 g/L C₂H₂O₄ + 10 mL/L C₃H₈O₃.*

10% H₂SO₄ + 10 mL/L C₃H₈O₃ / 1800 s / 10 ºC / 3 A/dm² (sample Al 18)

SEM-SE · SEM-BSE · SEM-BSE

20 g/L C₂H₂O₄

(a) · (b) · (c) resin / PAAO coating / substrate

10 µm · 500 nm · 20 µm

18% H₂SO₄ + 10 mL/L C₃H₈O₃ / 1800 s / 10 ºC / 3 A/dm² (sample Al 19)

20 g/L C₂H₂O₄

(d) · (e) · (f)

10 µm · 500 nm · 20 µm
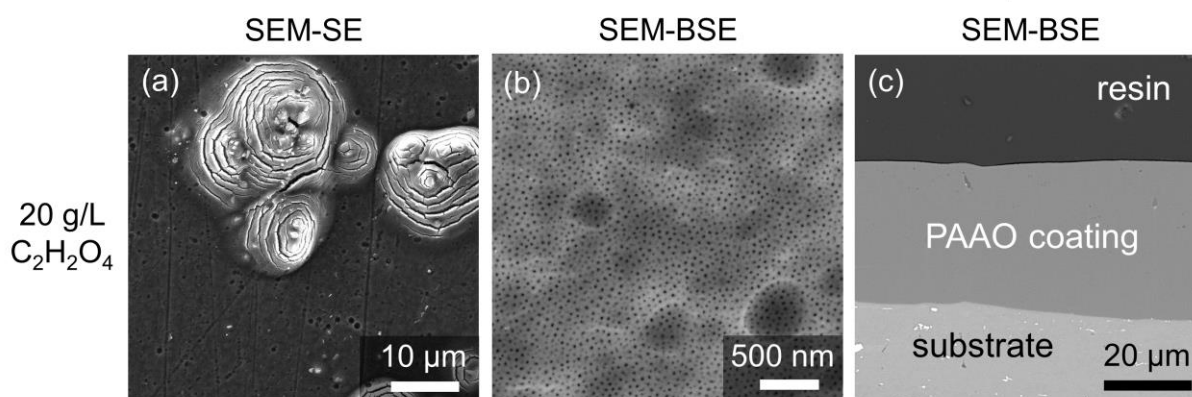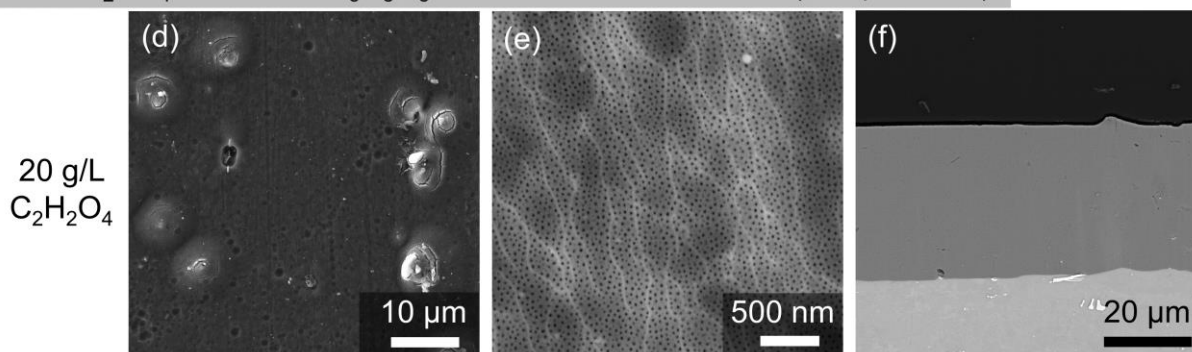
Fig. 31 *Micrographs of the coating surface (left and middle) and its cross-section (right) after anodizing based on the variation of sulfuric acid concentration: (a-c) 10% H₂SO₄, and (d-f) 18% H₂SO₄.*

Table 12 *EDX analysis of PAAO coatings estimated from a surface area of 0.21 mm², and the thickness and microhardness of PAAO coatings.*

Sample	Element (wt.%)			Thickness of PAAO coating (µm)	Microhardness	
	Al	**O**	**S**		**HV0.05**	**HV0.025**
Al 12	49.0	44.7	6.3	32.8	472±13.1	485±10.1
Al 13	49.6	44.0	6.4	34.4	489±12.1	504±10.2
Al 14	49.0	44.5	6.5	29.5	412±13.2	429±9.9
Al 15	49.9	44.1	6.0	22.4	456±10.2	471±10.9
Al 16	50.0	44.8	5.2	9.9	-	-
Al 17	51.0	43.5	5.5	18.9	-	502±5.8
Al 18	49.4	44.1	6.5	32.3	459±10.9	472±6.6
Al 19	49.5	44.4	6.1	34.8	460±13.7	476±12.2

4.1.5. Composite PAAO coatings containing Al$_2$O$_3$ and PTFE particles on AA1050

In this subchapter, the experiments were focused on the doping of the produced PAAO coatings by secondary particles (Al$_2$O$_3$ and PTFE) directly within the anodizing process. Based on previous experiments, these conditions were selected: 15% H$_2$SO$_4$ electrolyte with 10 mL/L C$_3$H$_8$O$_3$ and 20 g/L C$_2$H$_2$O$_4$; current densities 3 and 1 A/dm^2; and temperature 10 °C. All detailed information about the experiment is listed in Table 13. An additional possibility of improving the mechanical and tribological properties of PAAO coatings is the development of composite anodic coatings through the addition of particles such as Al$_2$O$_3$, SiC, polytetrafluoroethylene (PTFE), and TiO$_2$ to the electrolyte [67, 70, 123-125]. Earlier reported studies showed that the addition of SiC, Al$_2$O$_3$, and TiO$_2$ particles led to an increase in the microhardness of produced composite PAAO coatings. In contrast, the addition of PTFE particles improved their friction coefficient and wear resistance. The effect of mechanical pre-treatment on particles deposition during anodizing was also studied in detail.

Table 13 *Summary of the experimental conditions for composite PAAO coating formation.*

Sample	Mechanical pre-treatment	Electrolyte	Addition of particles	Current density (A/dm^2)	Anodizing time (s)
Al 20	polishing	15% H$_2$SO$_4$ [×] + 20 g/L C$_2$H$_2$O$_4$ [°] + 10 mL/L C$_3$H$_8$O$_3$ [*]	0.6 g/L SDBS[#] + 6 g/L Al$_2$O$_3$ [£] + 15 mL/L 60 wt.% PTFE[$]	3	1800
Al 21	grinding	15% H$_2$SO$_4$ + 20 g/L C$_2$H$_2$O$_4$ + 10 mL/L C$_3$H$_8$O$_3$	0.6 g/L SDBS + 6 g/L Al$_2$O$_3$ + 15 mL/L 60 wt.% PTFE	3	1800
Al 22	polishing	15% H$_2$SO$_4$ + 20 g/L C$_2$H$_2$O$_4$ + 10 mL/L C$_3$H$_8$O$_3$	0.6 g/L SDBS + 6 g/L Al$_2$O$_3$ + 15 mL/L 60 wt.% PTFE	1	3600
Al 23	grinding	15% H$_2$SO$_4$ + 20 g/L C$_2$H$_2$O$_4$ + 10 mL/L C$_3$H$_8$O$_3$	0.6 g/L SDBS + 6 g/L Al$_2$O$_3$ + 15 mL/L 60 wt.% PTFE	1	3600

[×]H$_2$SO$_4$ - sulfuric acid; [*]C$_3$H$_8$O$_3$ - glycerol; [°]C$_2$H$_2$O$_4$ - oxalic acid; CH$_3$(CH$_2$)$_{11}$C$_6$H$_4$SO$_3$Na - [#]SDBS - sodium dodecylbenzenesulfonate; [£]Al$_2$O$_3$ - aluminium oxide; [$]PTFE - polytetrafluoroethylene

Anodizing process

As can be seen in Fig. 32, the addition of 6 g/L Al_2O_3 and 15 mL/L 60 wt.% PTFE particles and 0.6 g/L SDBS to the sulfuric-oxalic acid-based electrolyte (curves Al 20 and Al 22) led to a voltage decrease in comparison with the experiments without additional secondary particles (curves Al 13 and Al 17). It is apparent that the voltage evolution in the electrolyte containing Al_2O_3 and PTFE particles was relatively slower (Fig. 32, curves Al 20 and Al 22) in comparison with curves Al 13 and Al 17, which pointed out the reduced rate of the composite PAAO coating formation.
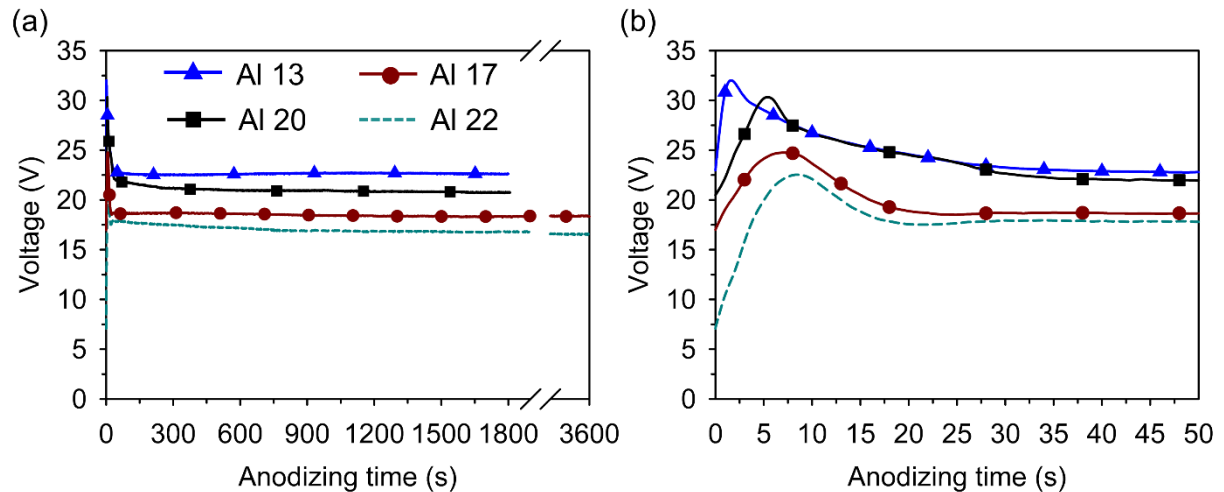
Fig. 32 *Voltage vs anodizing time curves for samples Al 13, Al 17, Al 20 and Al 22 recorded during anodizing of AA1050 in different process conditions after (a) 3600 s and (b) detailed magnification of the record up to 50 s.*

Effect of Al_2O_3/PTFE particles on the PAAO coating microstructure, thickness and hardness

The chemical composition, thickness and microhardness of composite PAAO coatings are listed in Table 14. Figure 32 shows the surface morphologies and cross-sections of the composite PAAO coatings formed directly from the dispersion in the electrolyte at 3 A/dm^2 for 1800 s and at 1 A/dm^2 for 3600 s. The addition of Al_2O_3 and PTFE particles makes no significant difference on the coating surface morphology, see PAAO coatings Al 13 and Al 17 without the secondary particles (Fig. 30d-f and Fig. 30j-l) and composite PAAO coatings Al 20 and Al 22 containing the particles (Fig. 33a-c, Fig. 33g-i). From Fig. 33b,e,h,k it can be seen that the Al_2O_3 and PTFE particles are non-uniformly distributed on the surfaces of the coatings and are in the form of agglomerates. The thickness of composite coatings (Al 20 and Al 22) was found to be thinner (24.2 and 14.1 μm) than that of the PAAO coatings (Al 13 and Al 17) without secondary particles (34.3 and 18.9 μm). This effect is related to the voltage *vs* anodizing time curve (Fig. 32), where the voltage was found to be lower for samples anodized in the electrolyte containing secondary particles. Moreover, composite PAAO coatings formed on the grinding pre-treated samples Al 21 and Al 23 were found to be thinner, with lower

61

hardness and containing a higher amount of Al_2O_3 and PTFE particles on the surface, Fig. 32d-f, 32j-l and Table 14. The coating surfaces Al 20 and Al 21 produced at 3 A/dm^2 also contained hillocks. Addition of secondary particles to the sulfuric-oxalic acid-based electrolyte had a positive effect on the increasing coating hardness, as shown in Table 14. A similar effect was observed by Chen et al. [70] in that Al_2O_3 particles were entrapped in the PAAO coating and improved its hardness, while PTFE particles decreased the number and size of pore defects.

The most uniform coating morphology without hillocks and with uniform hardness distribution was achieved in the composite PAAO coating Al 22, where a combination of the polishing pre-treatment, a low anodizing current density of 1 A/dm^2 and addition of secondary particles was used for the coating formation.

Table 14 *EDX analysis of composite PAAO coatings estimated from a surface area of 0.21 mm^2, and the composite PAAO coatings thickness and microhardness.*

Sample	Element (wt.%)				Thickness of composite PAAO coating (μm)	Microhardness	
	Al	O	S	F		HV0.05	HV0.025
Al 20	50.0	43.6	5.9	0.5	24.2	512±14.3	527±14.9
Al 21	48.8	44.8	5.8	0.6	16.5	-	512±9.6
Al 22	50.5	43.9	5.2	0.4	14.1	-	521±6.3
Al 23	49.1	44.9	5.3	0.7	13.3	-	-
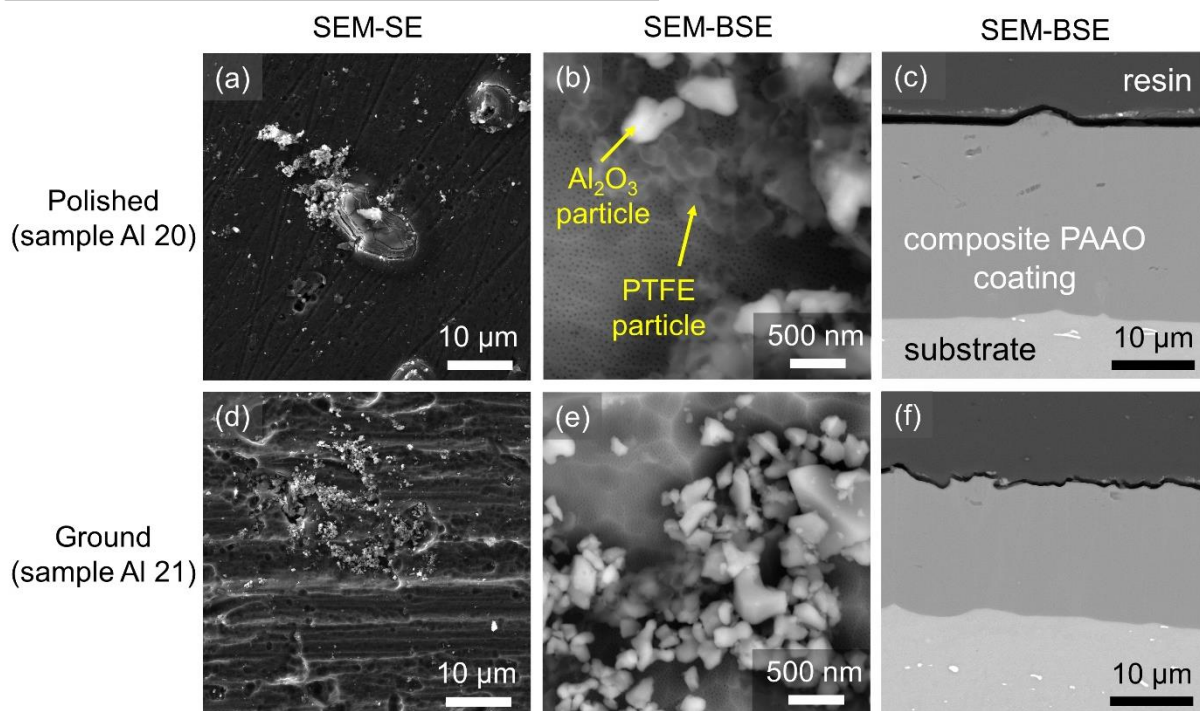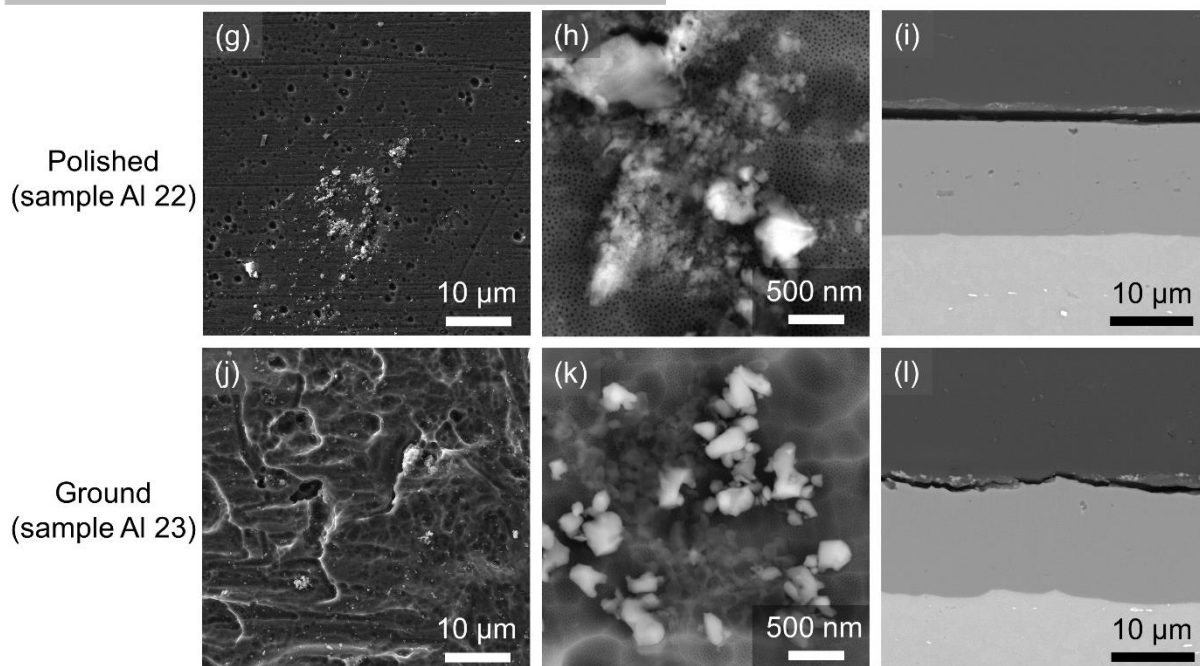
Fig. 33 *Micrographs of surface topography (left and middle) and cross-section (right) of composite anodic coatings formed on from different mechanically pre-treated samples (a-c, g-i) polished, (d-f, j-l) ground, and anodized at (a-f) 3 A/dm² for 1800 s and (g-l) 1 A/dm² for 3600 s.*

4.1.6. Effect of anodizing conditions on the tribological properties of anodic coatings produced on AA1050

Reciprocating sliding ball-on-disk test was used for tribological characterization of the produced anodic coatings. For tribological testing, mechanically pre-treated polished samples were selected: initial substrate, Al 7, Al 12-14, Al 17, Al 20 and Al 22. These samples were selected specifically in order to study of the effect of individual anodizing conditions (such as temperature, current density, and the additions of $C_2H_2O_4$, Al_2O_3 and PTFE particles to the electrolyte) on the coefficient of friction (COF), wear volume and wear trace depth.

Tribological testing results showed that the produced PAAO coatings had a much lower COF in comparison with the initial substrate material (Fig. 34a).No significant effect of any anodizing condition such as reducing the anodizing temperature or the addition of oxalic acid on the COF of the PAAO coatings was observed. Similarly, the addition of Al_2O_3 and PTFE particles to the sulfuric-oxalic acid-based electrolyte did not have a significant effect on changes in the COF for the anodic composite coatings Al 20 and Al 22, when compared to previous studies [70, 126]. Escobar et al. [126] used PTFE aqueous dispersions as the sealing post-treatment for PAAO coatings, and Chen et al. [70] added Al_2O_3 and PTFE particles directly to the electrolyte to produce a composite coating. A small increase in COF was found when compared to these studies, which can be explained by: (i) the relatively low concentration and uneven distribution of PTFE particles on the surface of the composite anodic coating. This amount was probably not high enough for the formation of a stable self-lubricating layer, so the rubbing of the counterface was easier to achieve on the porous AAO coating surface rather than on the PTFE film, and (ii) the different anodizing conditions (concentration, composition, and temperature of the electrolyte, the distance between anode and cathode, etc.) used for the experiment.

Current density reduced from 3 to 1 A/dm^2 led to a decrease in COF in the produced coatings Al 17 and Al 22. The reasons for this behaviour can be related to the difference in pore diameters, coating morphology and lower internal stresses as compared to the rest of the studied coatings. However, a precise explanation of this phenomenon requires more in-depth investigation and is beyond the scope of this thesis.

An analysis of the wear loss revealed a two-orders-of-magnitude difference in the wear resistance of anodic coatings in comparison with the initial substrate. As can be seen from wear trace depth measurements (Fig. 34b), during the wear test the substrate was not exposed in any of the tested samples, so the wear loss occurred only in the coating.

The decrease in the electrolyte temperature from 24 to 10 ºC promoted the reduction in wear loss in the coating Al 12 as compared to the PAAO coating Al 7, see also Fig. 34b. Addition of oxalic acid to the electrolyte and reduction of the current density resulted in slightly lower wear resistance. The improvement in the wear resistance of anodic coatings by way of reducing the electrolyte temperature is in full compliance with the study of Lu et al. [127], and it is assumed that it is primarily associated with the decrease in the AAO coating porosity and in the reduction of defects such as hillocks, local cracks, etc., which enables mechanical properties of the

coating. Contrary to data reported by Guezmil et al. [72], the evidence of a wear loss reduction for harder and less porous coatings with a lower number of hillocks on the surface indicates that the wear resistance of PAAO coatings may be influenced not only by the amount of porosity, surface roughness or hardness but also by other features such as shear strength and crack resistance. This conclusion was demonstrated by adding Al_2O_3 and PTFE particles to the electrolyte, which led to a significant reduction in wear loss; this loss was found to be the lowest for the composite anodic coatings Al 20 and Al 22. Despite the absence of significant effects of the particles on the COF of the PAAO coatings. It is evident that the presence of secondary particles in composite anodic coating results in improved shear strength and elasticity of the coatings, and thus the composite anodic coatings were more resistant to the deformation in the reciprocal sliding test and without any significant coating break up.
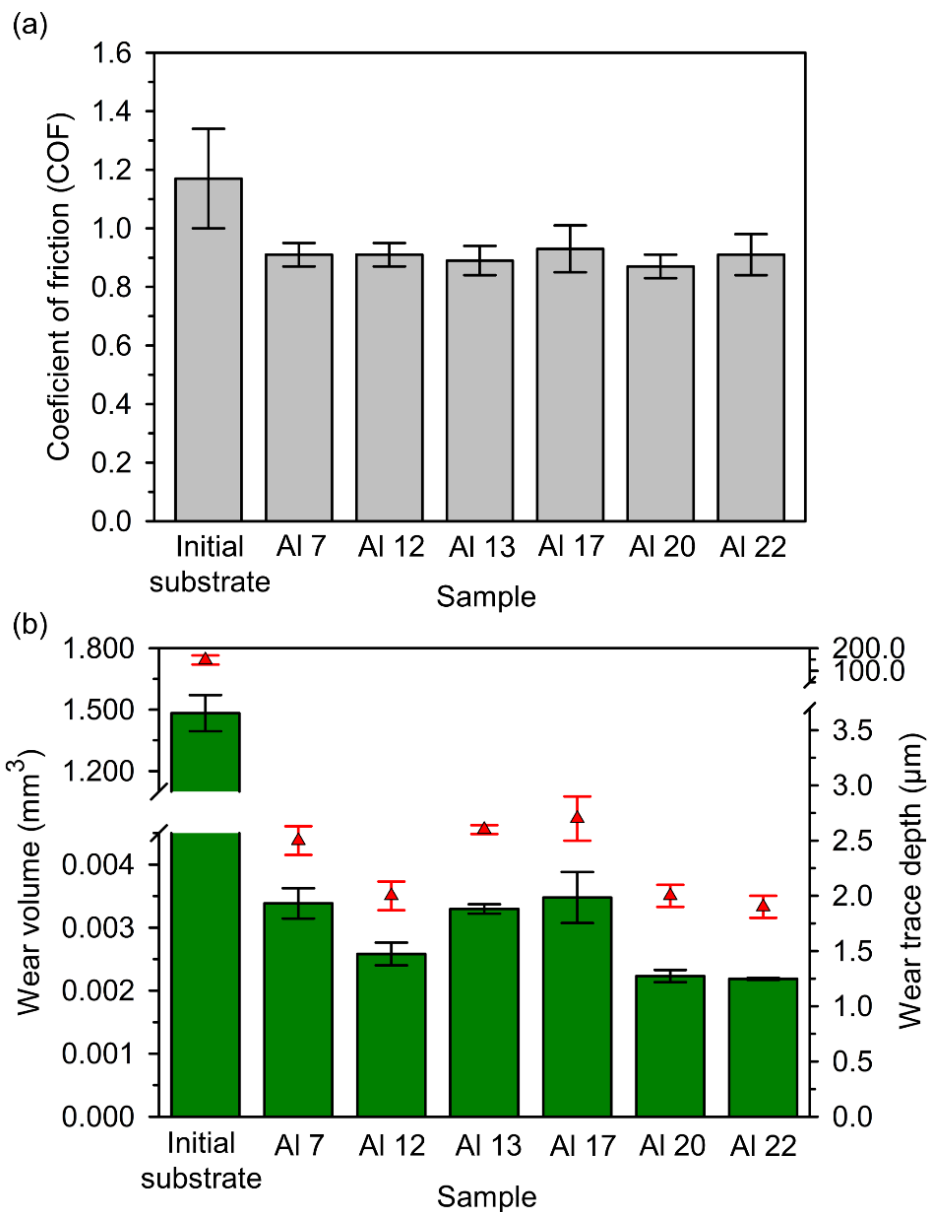
Fig. 34 (a) Friction coefficient, (b) wear volume along with the depth of wear tracks for studied anodic coatings.

4.1.7. Effect of anodizing conditions (electrolyte temperature and current density) on the behaviour of intermetallic particles in AA1050

Experimental material AA1050 contains small intermetallic phase particles based on Al-Fe-Si and Al-Fe with round and irregular shape. The behaviour of these particles after anodizing was studied in detail, as can be seen in Fig. 35 and Table 15. It was observed that these phase particles had during anodizing a significantly different electrochemical behaviour than pure aluminium had.

When the higher electrolyte temperature of 24 °C and current density of 3 A/dm^2 were used, the surface of the coatings after anodizing contained negligible microcavities (see Fig. 35a,b), whose shape and dimension were similar to those of the intermetallic phase particles observed on the surface after the chemical pre-treatment (Fig. 18). The presence of microcavities on the surface of produced coating can be explained by the preferred dissolution of the intermetallic phase particles during the anodizing process in the 15% H$_2$SO$_4$ electrolyte at room temperature and can be supported by the following studies [54, 102, 113, 128].

When the lower electrolyte temperature of 10 °C and current densities of 3 and 2 A/dm^2 were used on the PAOO coating surfaces, oxidized particles and hillocks with cracks were observed, see Fig. 35e-l. Cracks were also observed in the vicinity of oxidized particles, which were caused by an increase in the volume of the oxidized intermetallic phase particles during the anodizing process [103]. On the surface of the PAAO coating produced at a lower current density of 1 A/dm^2 and temperature of 10 °C no hillocks and no cracks were formed near oxidized particles, see Fig. 35i,j. That is why the intermetallic phase particles on the surface of the coating were found to oxidize faster during the anodizing process at higher current densities (3 and 2 A/dm^2).

As can be noticed from the EDX analysis measurements (see Fig. 35 and Table 15), the PAAO coatings produced at a higher temperature of the electrolyte contained lower amounts of Fe and Si in comparison with the coatings produced at a lower electrolyte temperature. An analysis of the chemical composition reveals a significantly lower Fe content within the intermetallic phase particles, which confirms the higher dissolution rate of Fe compared to Si during the anodizing process. Zhu et al. [128] found that Fe-rich intermetallic particles were faster dissolved during the anodizing process at room temperature in contrast to Si particles. Intermetallic phase particles based on Al-Fe and Al-Fe-Si are of lower oxidation rates than the aluminium matrix and therefore, can be occluded while the coating is formed during the anodizing process, see [80]. As can be seen in the cross-section Fig. 35, and from local chemical composition analyses, Table 8, the intermetallic phase particles were trapped in the coating during the anodizing process, and depending on the temperature, were preferably dissolved or oxidized. During anodizing at a higher temperature, intermetallic phase particles were preferably dissolved and partially oxidized. A higher dissolution rate of Fe compared to Si was detected for the anodizing process at the higher electrolyte temperature than anodizing at the lower electrolyte temperature. During anodizing at the lower electrolyte

66

temperature, the intermetallic phase particles were oxidized faster than those oxidizing during anodizing at the higher electrolyte temperature. The results proved that the electrolyte temperature had a significant effect on the oxidation/dissolution rate of intermetallic phase particles.

The effect of current density on oxidation of intermetallic phase particles was observed at a lower temperature. Higher anodizing current density (Fig. 35e-f) led to faster oxidation of intermetallic particles than lower current density (Fig. 35i,j), which is related to faster ion migration/reaction in the electrolyte during the anodizing process.

The incorporation of intermetallic phase particles in the PAAO coating disrupted the local growth direction of the parallel pores (Fig. 35d,h,k,l), locally modified the surrounding porous structure, and produced microcavities (Fig. 35a-c), which have also been reported in earlier researches [103, 129, 130]. For a more detailed and precise study of the behaviour of intermetallic phase particles during anodizing, an analysis by TEM is required.

Montero-Moreno et al. [103] described the incorporation of the intermetallic phase particles into PAAO coating according to the mechanism presented in Fig. 36 [54]. Here is apparent that as soon as the intermetallic particle reached the initial substrate/porous AAO coating interface, the growth of regular parallel pores placed over the particle is terminated. Continuation of the anodizing process leads to the regular parallel pores being substituted by the non-parallel pores, sometimes referred to as branched and deviated neighbouring pores. This deviation is caused by a natural tendency of pores to grow perpendicular to the aluminium surface. With the further continuation of the anodizing process, this local disorder caused by intermetallic phase particles incorporated into the growing coating is finished, and anodic coating with parallel pores arrangement continues above the particle [54].
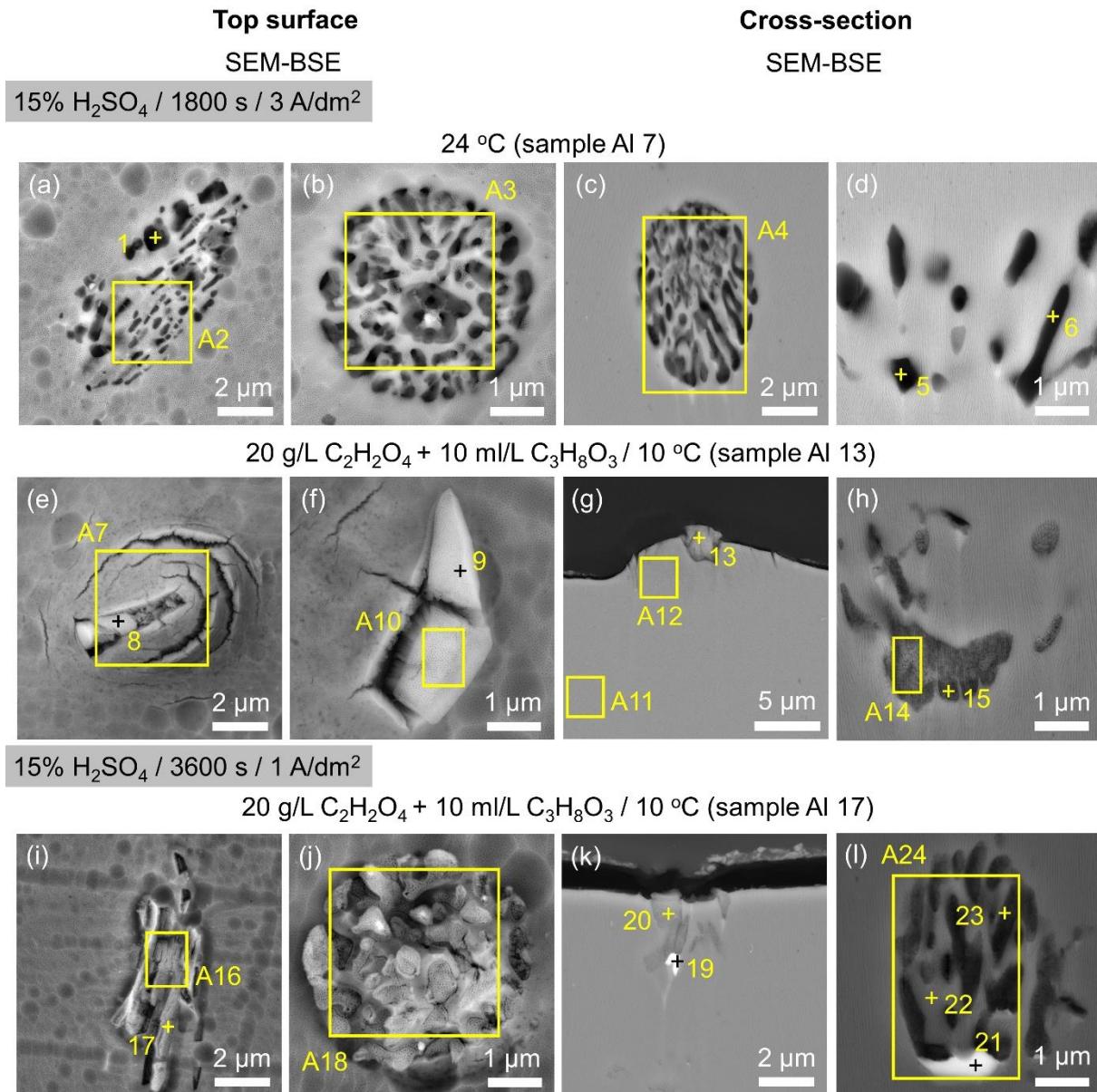
Fig. 35 *Micrographs demonstrating the behaviour of intermetallic phase particles after the anodizing process under different: (i) temperature (a-d) 24 °C, (e-l) 10 °C, (ii) constant current densities (a-h) 3 A/dm², (i-l) 1 A/dm², and (iii) composition of the electrolyte (a-d) 15% H₂SO₄, (e-l) 15% H₂SO₄ + 20 g/L C₂H₂O₄ + 10 mL/L C₃H₈O₃.*
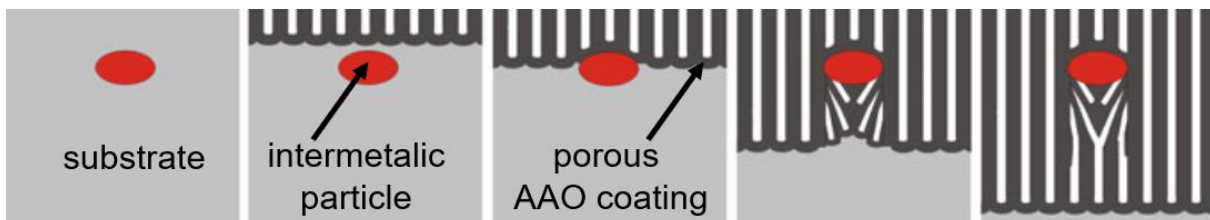
Fig. 36 *Schematic illustration of the incorporation of intermetallic particles during the anodizing process of AA1050 [54].*

Table 15 Point and area (marked as A) EDX analysis of intermetallic phase particles and larger areas after the anodizing process under different conditions. The point of EDX measurement is indicated in Fig. 35.

Position	Element (wt. %)					
	O	**Al**	**S**	**Fe**	**Si**	**Fe/Si**
1	34.5	58.9	4.8	-	1.8	-
A2	41.5	52.2	6.0	-	0.3	-
A3	41.1	51.5	5.9	0.7	0.8	0.9
A4	40.6	51.7	6.0	0.4	1.3	0.3
5	41.0	50.7	5.9	0.3	2.1	0.1
6	33.5	57.4	7.2	0.3	1.6	0.2
A7	46.7	43.1	7.8	2.1	0.3	7.0
8	46.3	34.2	5.9	12.3	1.3	9.5
9	48.8	36.2	4.7	9.7	0.6	16.2
A10	49.6	35.5	4.8	9.4	0.7	13.4
A11	47.7	46.2	6.1	-	-	-
A12	50.3	41.7	8.0	-	-	-
13	42.7	39.9	7.3	9.5	0.6	15.8
A14	43.0	44.1	5.8	4.9	2.2	2.2
15	40.6	44.5	5.9	6.4	2.6	2.5
A16	44.7	38.6	5.3	10.2	1.2	8.5
17	42.4	43.9	4.3	8.7	0.7	12.4
A18	43.0	46.7	5.1	3.9	1.3	3.0
19	12.7	55.2	1.0	29.7	1.4	21.2
20	34.6	44.4	4.9	14.3	1.8	7.9
21	18.0	52.5	1.9	23.5	4.1	5.7
22	38.2	51.6	5.3	3.1	1.8	1.7
23	45.1	47.9	5.4	0.9	0.7	1.3
A24	43.4	47.6	5.4	2.4	1.2	2.0

4.1.8. Closing remarks on anodizing of AA1050

Mechanical and chemical pre-treatment and wide range of anodizing conditions, including voltage, current density, electrolyte temperature and composition, and addition of Al_2O_3 and PTFE particles to the electrolyte, have been applied to aluminium alloy AA1050 substrate to produce porous anodic aluminium oxide coatings. The effect of the conditions mentioned above on the resulting morphology, hardness, and tribological properties of the PAAO coatings was extensively and systematically studied. The main conclusions can be listed as follows:

Effect of pre-treatment on surface morphology

- Polishing is a more suitable pre-treatment technique for aluminium samples than grinding since the surface is more uniform and smooth.
- The intermetallic phase particles contained in AA1050 were based on binary Al-Fe or ternary Al-Fe-Si phases.
- AA1050 contained intermetallic phase particles of irregular- and round-shape. The number of round-shape particles was lower than the number of irregular-shape particles, the latter containing a higher amount of silicon.
- Alkaline etching in the NaOH solution and neutralizing in the HNO_3 solution resulted in the scalloped appearance of sample surfaces, and intermetallic particles were more visible on the surface, due to the higher dissolution rate of the aluminium matrix in the NaOH solution compared to the dissolution rate of Fe and Si.

Effect of mechanical pre-treatment, voltage/current density and temperature on the anodizing process and production of PAAO coatings

- Porous anodic aluminium oxide coatings were produced during potentiostatic anodizing at 16-20 V in 15 % H_2SO_4 at 24 ºC.
- Porous AAO coatings were also produced during a galvanostatic anodizing process at 3 A/dm^2 in the 15 % H_2SO_4 at 24 ºC.
- XRD results showed that the anodized coatings were composed of amorphous aluminium oxide, and EDX analysis confirmed the presence of Al, O and S.
- A coating produced at 16 V and 3 A/dm^2 had similar values of thickness and hardness. The produced PAAO coatings were ten times harder than the initial material.
- Decreasing the electrolyte temperature from 24 to 18 °C led to reducing the thickness of the coatings produced in the potentiostatic regime at 16 V. On the other hand, coatings produced in the galvanostatic regime at 3 A/dm^2 were thicker and harder.
- Reducing the electrolyte temperature from 24 to 10 °C during the galvanostatic anodizing process at 3 A/dm^2 led to increasing the voltage, and the oxidation rate was higher than the dissolution rate. A thicker and harder coating containing hillocks with local cracks was produced.

- With decreasing electrolyte temperature, the sulfur content increased in the PAAO coating, suggesting the incorporation of sulfate ions in the PAAO coating and the formation of hillocks. The hillocks contained more sulfur, and their hardness was lower than that of the surrounding PAAO coating.
- The most regular porous AAO structure was achieved by mechanical polishing of the initial substrate.

Effect of current density, electrolyte composition and concentration on the anodizing process, morphology, hardness and thickness of the produced PAAO coating

- Addition of 10 ml/L glycerol to the 15% H_2SO_4 electrolyte resulted in the formation of a PAAO coating with a lower number of hillocks and increased coating hardness.
- Addition of 20 g/L of oxalic acid to the 15% H_2SO_4 electrolyte also had a possible effect on increasing the thickness and hardness of produced coatings but not such as was observed in the case of a decrease in the temperature of the electrolyte. Further addition of oxalic acid to sulfuric acid had a negative effect on coating hardness.
- The decrease in current density from 3 to 1 A/dm^2 led to a significant voltage drop, which resulted in lower mobility of O^{2-}, OH^-, SO_4^{2-} and Al^{3+} ions. By reducing the current density, a 3.5-times thinner coating without cracks and hillocks was produced at the same time.
- The formation of hillocks is strongly associated with the applied current density and with the incorporation of sulfate ions.
- Increasing or decreasing concentration of the sulfuric acid had a negative effect on hardness.
- A stable electrolyte containing secondary particles was produced using the sodium dodecylbenzenesulfonate anionic surfactant, Al_2O_3 powder and commercial 60 wt.% PTFE suspension.
- Addition of 6 g/L Al_2O_3 and 15 mL/L 60 wt.% PTFE particles and 0.6 g/L sodium dodecylbenzenesulfonate to the sulfuric-oxalic acid-based electrolyte led to a decrease in voltage. The decrease in voltage caused lower incorporation of sulfur into the coating, and thinner and harder coatings were produced. The microstructural examination revealed successive incorporation of Al_2O_3 and PTFE particles in the produced coatings.
- The most uniform coating morphology without hillocks and with uniform distribution of hardness was achieved by the combination of the polishing pre-treatment and the low anodizing electrolyte temperature of 10 ºC, the low anodic current density of 1 A/dm^2, and the addition of Al_2O_3 and PTFE particles to the sulfuric-oxalic acid-based electrolyte.

Effect of anodizing conditions on the tribological properties of the anodic coatings produced on AA1050

- The produced PAAO coatings have a much lower coefficient of friction (COF) and wear resistance in comparison with the initial substrate material.
- No significant effect of any anodizing condition such as reducing the anodizing temperature and current density, adding oxalic acid on the COF of PAAO coatings was observed. Similarly, the addition of Al_2O_3 and PTFE particles to the sulfuric-oxalic acid electrolyte did not have a significant effect on changes in the COF for the anodic composite coating. The friction coefficient was not improved strongly, apparently due to the insufficient concentration of PTFE in the surface tribo-film.
- Significant effect on wear resistance had the anodizing conditions such as lower electrolyte temperature of 10 ^oC and addition of Al_2O_3 and PTFE particles to the sulfuric-oxalic acid electrolyte. A combination of these conditions resulted in 30% higher wear resistance.
- The porous composite AAO coating without structural defects (hillocks and cracks) and with the best combination of mechanical properties was prepared by anodizing at a low temperature of 10 °C and lower current density of 1 A/dm^2 in the sulfuric-oxalic acid electrolyte with a dispersion of Al_2O_3 and PTFE particles.

Effect of anodizing conditions (current density, electrolyte temperature and concentration) on the behaviour of intermetallic particles in AA1050

- Intermetallic phase particles had significantly different electrochemical behaviour during anodizing than pure aluminium had.
- Intermetallic phase particles based on Al-Fe and Al-Fe-Si have lower oxidation rates than the aluminium matrix and therefore, can be occluded in the growing coating during the anodizing process.
- Iron-rich intermetallic particles were dissolved faster during the anodizing process at a higher temperature of 24 ^oC compared to Si particles.
- During the anodizing process at a higher electrolyte temperature, the intermetallic phase particles were preferably dissolved than oxidized. On the surface as well as in the cross-section of the coating, the intermetallic phase caused the formation of microcavities.
- During anodizing at 10 ^oC, the intermetallic phase particles rather oxidized than dissolved.
- Higher anodizing current densities and lower electrolyte temperatures led to faster oxidation of intermetallic phase particles than lower current density did, which is related to the faster ion migration/reaction in the electrolyte during the anodizing process.
- Incorporating intermetallic phase particles into the PAAO coating locally distorted growth direction of parallel pores, locally modified the surrounding porous structure and produced microcavities.

4.2. Anodizing of 99.9% Mg

4.2.1. Optimization of anodizing conditions for 99.9% Mg

The formation of anodic magnesium hydroxide coatings (AMHCs) was performed in the 1 M NaOH electrolyte at 24 °C, utilizing a constant voltage in the range of 4 to 50 V. The effects of mechanical pre-treatment (grinding and polishing) of the initial substrate and voltage on the anodizing process were studied. The experimental conditions are summarized in Table 16 and were chosen based on earlier results [131].

Table 16 *Experimental conditions to study the effect of pre-treatment and utilized voltage.*

Sample	Mechanical pre-treatment	Electrolyte (C_{NaOH}[¶])	Voltage (V)	Anodizing time (s)
Mg 1	grinding (#1200)	1 M	4	1200
Mg 2	polishing (1 μm)	1 M	5	1200
Mg 3	grinding (#1200)	1 M	5	1200
Mg 4	polishing (1 μm)	1 M	10	1200
Mg 5	polishing (1 μm)	1 M	20	1200
Mg 6	grinding (#1200)	1 M	20	1200
Mg 7	polishing (1 μm)	1 M	50	1200

[¶]NaOH - sodium hydroxide

Effect of mechanical and chemical pre-treatment on the surface morphology of the substrate

Scanning electron micrographs of the initial material surface microstructure after different types of mechanical pre-treatment (grinding/polishing) and identical chemical pre-treatment (0.5% HF for 30 s) are depicted in Fig. 37. On the surface of pure Mg sample, after grinding and chemical pre-treatment, parallel lines were observed due to the grinding process. By contrast, the surface of the polished sample was smoother and contained a number of narrow scratches, as shown in Fig. 37b. In both cases, no clear evidence of surface corrosion was observed.
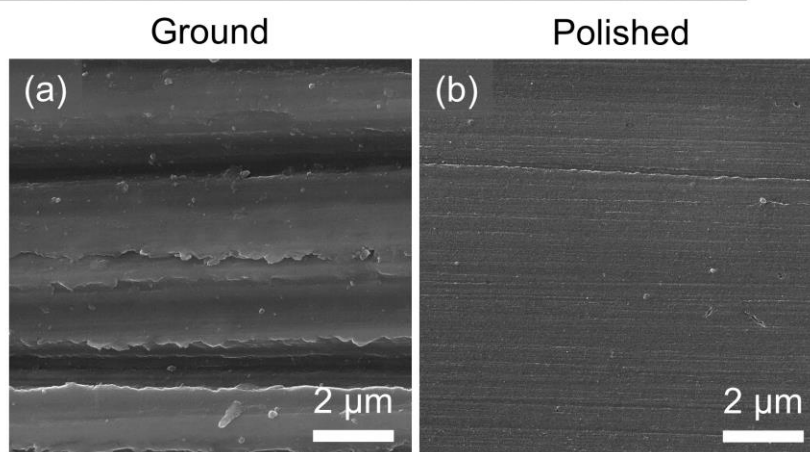
Fig. 37 *Micrographs (SEM-SE) of the pure Mg surface after the mechanical*
and chemical pre-treatment process: (a) ground, and (b) polished.

Anodizing process

Figure 38 shows the current density vs anodizing time curves obtained on 99.9% Mg during the potentiostatic anodizing process. Two different shapes of curves were recorded based on the voltage used. Salaman et al. [44] also recorded two shapes of curves (i) at a low voltage of 3 V and (ii) at a higher voltage of 10-100 V during anodizing AZ31 magnesium alloy in the 1 M NaOH electrolyte.

The first type of the anodizing curve shape appeared when lower voltage values were used, namely 4 and 5 V (curves Mg 1 and Mg 2, Mg 3, Fig. 38). The current density did not increase immediately that the voltage was applied, i.e. the electrical circuit was closed, as in the case of higher voltages. The current density started to increase after 5 s from the beginning of the anodizing process, and this was a result of the dissolution reaction of pure Mg surface substrate (Mg 1-Mg 3) in the electrolyte. Then, magnesium ions reacted with hydroxide ions, and an anodic coating of magnesium hydroxide ($Mg(OH)_2$) started to form. The maximum current density reached the values 3.1 A/dm^2, 9.4 A/dm^2 and 11 A/dm^2 for the curves Mg 1, Mg 2 and Mg 3 at about 40 s (Fig. 38b), respectively; after that, however, the current density grew slowly until the end of the anodizing process, which indicated the growth of the AMHC.

When a voltage of 5 V was applied, a much steeper slope of the current density was recorded (curves Mg 2 and Mg 3) compared to the 4 V (curve Mg 1). This behaviour could be caused by the fact that the dissolution of the magnesium matrix was faster than the formation of the $Mg(OH)_2$ coating.

When higher voltages of 10, 20 and 50 V (curves Mg 4-Mg 7, Fig. 38) were used, the current density immediately increased with anodizing time, which is related to the dissolution reaction of pure Mg substrate. When the local maximum of current density was reached, the current density decreased with anodizing time, and AMHC was produced. Finally, the current density was kept constant with anodizing time due to the stationary dissolution and AMHC formation [132].

The mechanical pre-treatment affected the value of the results of the current density. Lower values of current density were recorded for the polished samples (Mg 2 and Mg 5) when compared to the ground samples (Mg 3 and Mg 6). The reaction during the Mg 1-Mg 3 and Mg 7 experiments was intense, and the evolution of oxygen gas bubbles was more visible during the anodizing process compared to the Mg 4-Mg 6 experiments.
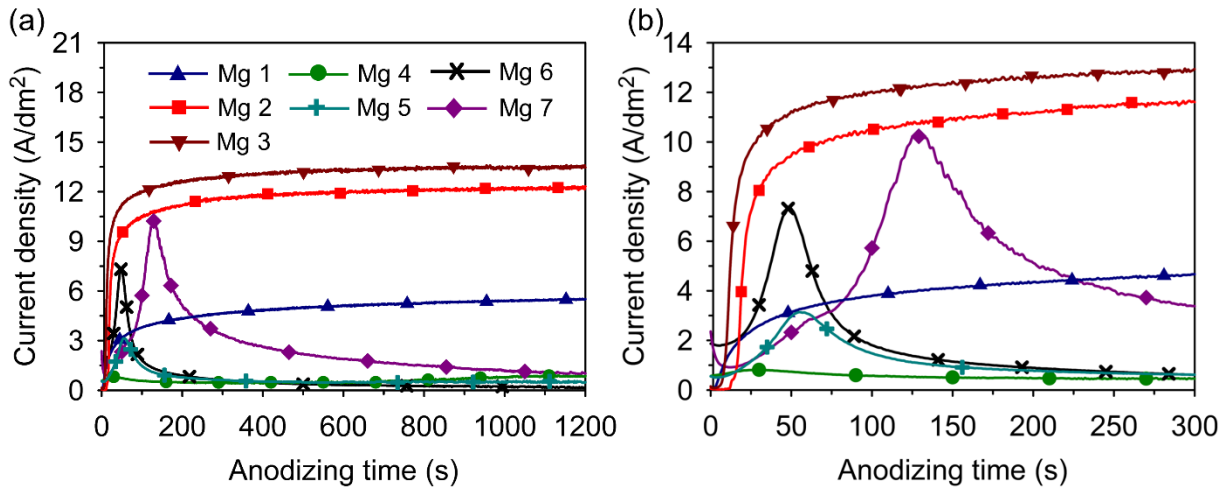
Fig. 38 *Current density vs anodizing time curves recorded during anodizing of pure magnesium in the 1 M NaOH at 24 °C for 1200 s at different voltages (a) after 1200 s, and (b) a detail of the record up to 300 s.*

Microstructure and composition of anodic coatings

Figures 39 and 40 show the effect of different anodizing conditions such as mechanical pre-treatment and anodizing voltage on the microstructure of coatings produced on pure magnesium at 24 °C in the 1 M NaOH electrolyte. Anodic magnesium hydroxide coatings (Mg 1-Mg 3) produced at a low voltage of 4 V (Fig. 39a,b and 40a) and 5 V (Fig. 38c,d), respectively, were found to be of a different morphology than the coatings Mg 5-Mg 7, which were produced at higher voltages (10-50 V, Fig. 39e-l and Fig. 40b,c). The anodic magnesium hydroxide coating Mg 1 produced at 4 V was compact and denser than the coatings Mg 4-Mg 7 produced at higher voltages (10-50 V). The coating had a bulk-like structure with the rough coating surface. On the surface after anodizing, only a few microcracks were observed, while scratches from the mechanical pre-treatment were not found. The thickness of the produced anodic coating was 10.8 µm. In the cross-section (see Fig. 40d), horizontal cracks were observed, and their presence can be explained by the rapid growth of the coating together with the oxygen gas evolution during the anodizing process.

When a higher voltage of 5 V was used, non-uniform coatings (Mg 2 and Mg 3) were produced. On the coating surfaces, two different areas were found, which consisted of (i) hemispherical dimples containing an increased amount of oxygen, and (ii) only a slightly anodized magnesium initial material, as shown in Fig. 41. The AMHC was formed preferably in the dimples area, and the morphology of coatings was similar to the coating Mg 1 (Fig. 38a,b). The presence of dimples can be explained by the local dissolution of pure

magnesium matrix that initiates the formation of separate dimples. The number of dimples increases with anodizing time, and they eventually interlink each other to form a larger area. The process continues until the magnesium surface is completely activated [133]. This mechanism was observed for coating Mg 1 (Fig. 39a,b), and these results are in correlation with the AMHC growth theory proposed by Kim et al. [133]. Mechanically ground pre-treated samples contained deeper dimples as compared to the mechanically polished ones.

When a higher voltage (10-50 V) was applied, thinner and compact anodic coatings with micropores were produced. On the surface of anodic hydroxide coatings (Mg 3 and Mg 6) scratches coming from the mechanical ground pre-treatment process were observed (Fig. 39c,d and 39g,h). With the voltage increasing from 10 to 50 V, more oxygen was detected in AMHC, see Table 17. In the cross-section of the coating Mg 6 (Fig. 40f), a very thin AMHC was found compared to the anodic coating Mg 1 produced at 4 V. Increasing the voltage from 10 to 50 V resulted in the formation of denser and smoother coatings with larger micropores, which can be related to intensive oxygen gas evolution.

As can be seen from the EDX analysis (Table 17), the coatings Mg 1, Mg 2 and Mg 7 contained extra sodium compared to the coatings Mg 4-Mg 6. The presence of sodium in the coatings was the result of also incorporating sodium ions from the sodium hydroxide electrolyte into coatings during the anodizing process at 4, 5 and 50 V.
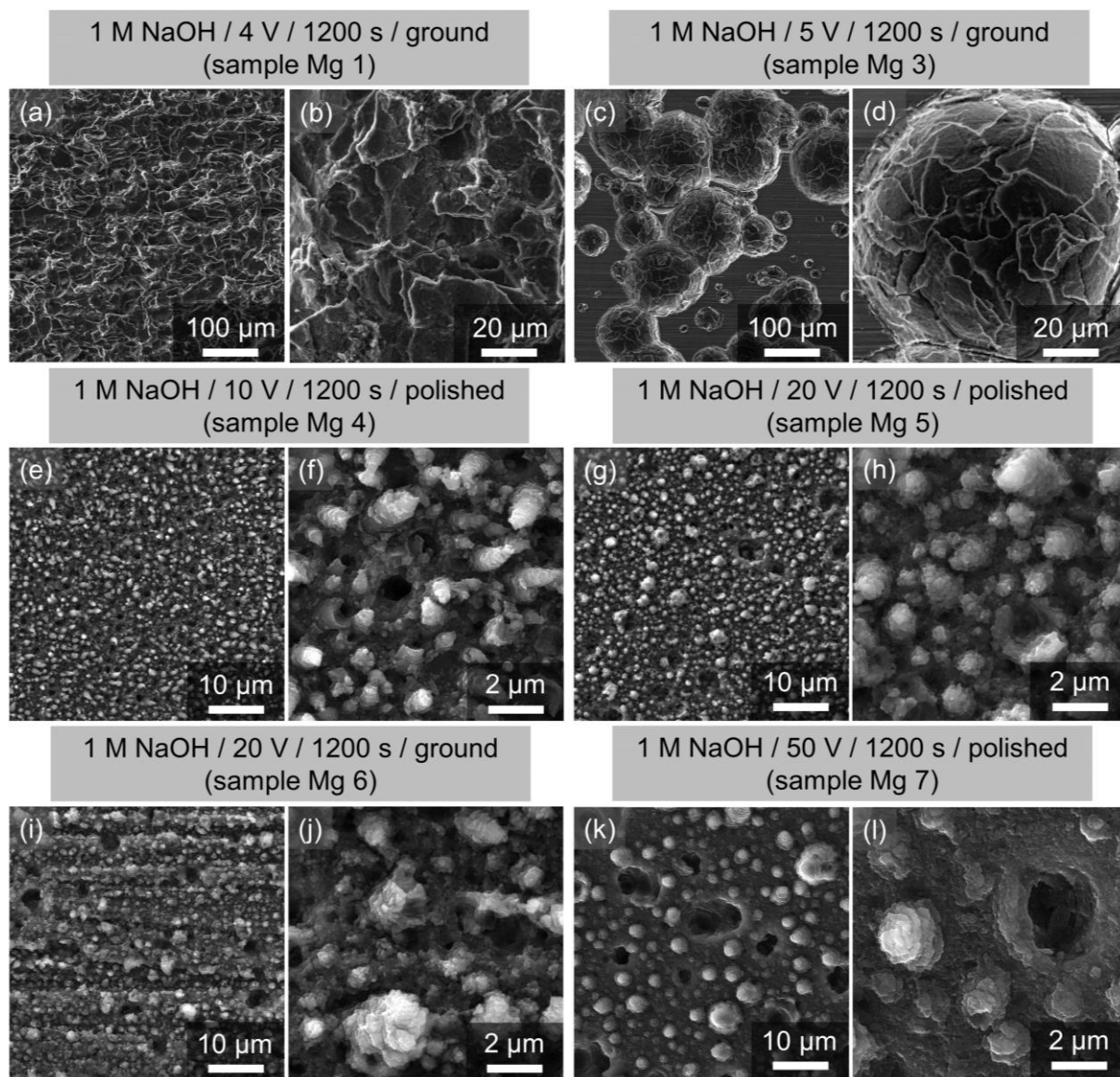
Fig. 39 *Micrographs (SEM-SE) of the free surface after mechanical and chemical pre-treatment (a-d, g, h) ground, (c-f, i, j) polished and anodized in the 1 M NaOH at 24 °C and (a, b) 4 V, (c, d) 5 V, (e, f) 10 V, (g-j) 20 V, (k, l) 50 V.*
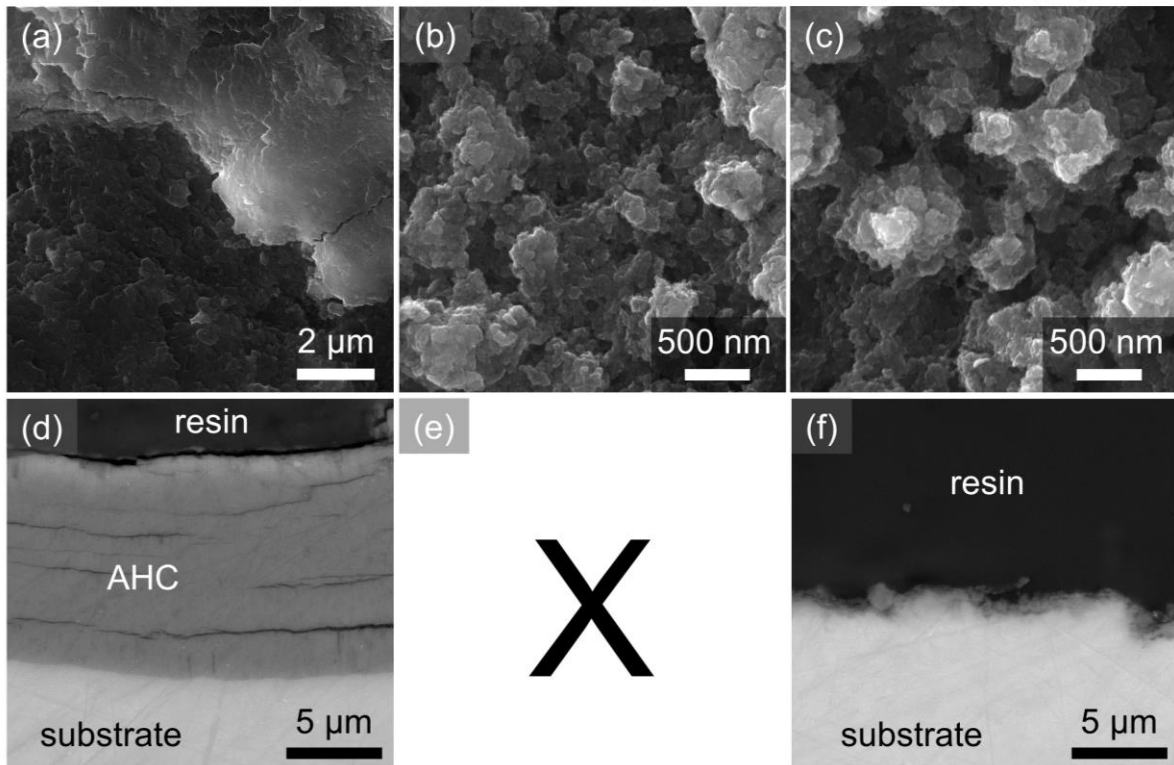
Fig. 40 *Detailed micrographs of the (a-c) free surface, and (d-f) cross-section of anodic hydroxide coatings formed on mechanically and chemically pre-treated samples (a, c, d, f) ground, (b) polished and anodized in the 1 M NaOH at 24 ℃ for 1200 s and different voltages.*
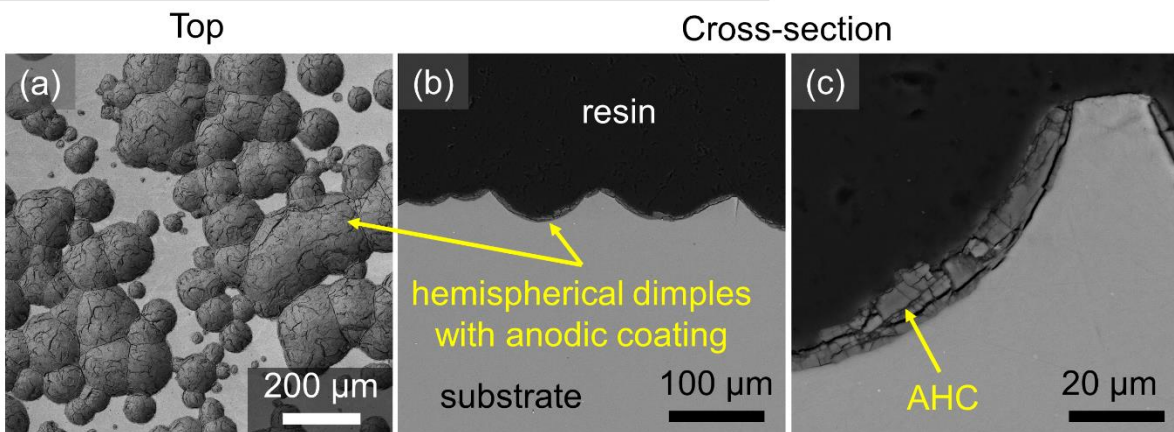
Fig. 41 *Micrographs (SEM-BSE) of the (a) free surface, and (b, c) cross-section of anodic coating Mg 2 formed at 5 V in the 1 M NaOH at 24 ℃ for 1200 s.*

Table 17 *EDX analysis of the anodized samples estimated from a surface area of 0.0016 mm².*

Sample	Element (wt.%)		
	O	Na	Mg
Mg 1	56.6	1.0	42.4
Mg 2 (dimples)	60.7	1.2	38.1
Mg 2 (outside the dimples)	3.0	-	97.0
Mg 4	27.9	-	72.1
Mg 5	29.8	-	70.2
Mg 6	31.6	-	68.4
Mg 7	33.4	0.4	66.2

The phase composition of pure magnesium substrate and anodic magnesium hydroxide coatings produced at different voltages (4, 10 and 20 V) is shown in Fig. 42. The XRD patterns indicate that the anodic coatings produced at different voltages are mainly composed of $Mg(OH)_2$ and Mg phases. The preferential formation of the $Mg(OH)_2$ phase at a lower anodizing voltage (3 V) was found instead of the MgO phase, and our results are in correlation with the published results of Kim et al. [17]. The MgO phase is preferentially formed during plasma electrolytic oxidation at higher voltages (> 80 V) [17].
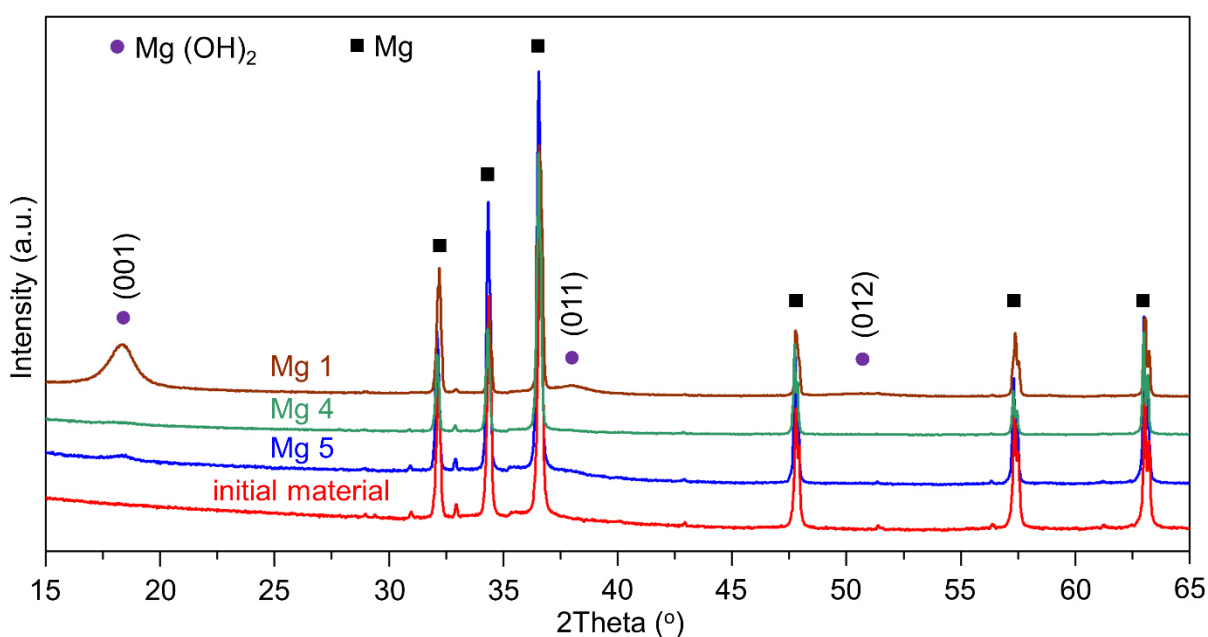
Fig. 42 *XRD patterns of initial material (pure Mg) and AMHCs obtained after anodizing at different voltages, i.e. 4 V (Mg 1), 10 V (Mg 4) and 20 V (Mg 5).*

79

4.2.2. Effect of addition of Al_2O_3 and PTFE particles on the anodizing process and morphology of the produced composite anodic coating

Based on the previous experiments, a constant voltage of 4 and 20 V was used to produce the composite anodic coating (CAC). Added to the 1 M NaOH electrolyte were 10 g/L Al_2O_3, 15 mL/L 60 wt.% PTFE and sodium dodecylbenzenesulfonate surfactant (SDBS). The experimental conditions are summarized in Table 18.

Table 18 Summary of the experimental conditions aimed to form composite anodic coatings.

Sample	Mechanical pre-treatment	Electrolyte (C_{NaOH}[¶])	Particles addition	Voltage (V)	Anodizing time (s)
Mg 1P	grinding (#1200)	1 M	0.6 g/L SDBS[#] + 10 g/L Al_2O_3[£] + 15 mL/L 60 wt.% PTFE[$]	4	1200
Mg 5P	polishing (1 μm)	1 M	0.6 g/L SDBS + 10 g/L Al_2O_3 + 15 mL/L 60 wt.% PTFE	20	1200
Mg 6P	grinding (#1200)	1 M	0.6 g/L SDBS + 10 g/L Al_2O_3 + 15 mL/L 60 wt.% PTFE	20	1200

[¶]NaOH - sodium hydroxide; $CH_3(CH_2)_{11}C_6H_4SO_3Na$ - [#]SDBS - sodium dodecylbenzenesulfonate; [£]Al_2O_3 - aluminium oxide; [$]PTFE - polytetrafluoroethylene

Anodizing process

Adding Al_2O_3 and PTFE particles to the 1 M NaOH electrolyte led to an increase in current density and started the dissolution process of pure Mg substrate, which is apparently based on the current density *vs* anodizing time curves, see Fig. 43. The progress of the curves was found to be the same as in the case of anodizing without additional Al_2O_3 and PTFE particles, see Fig. 38.
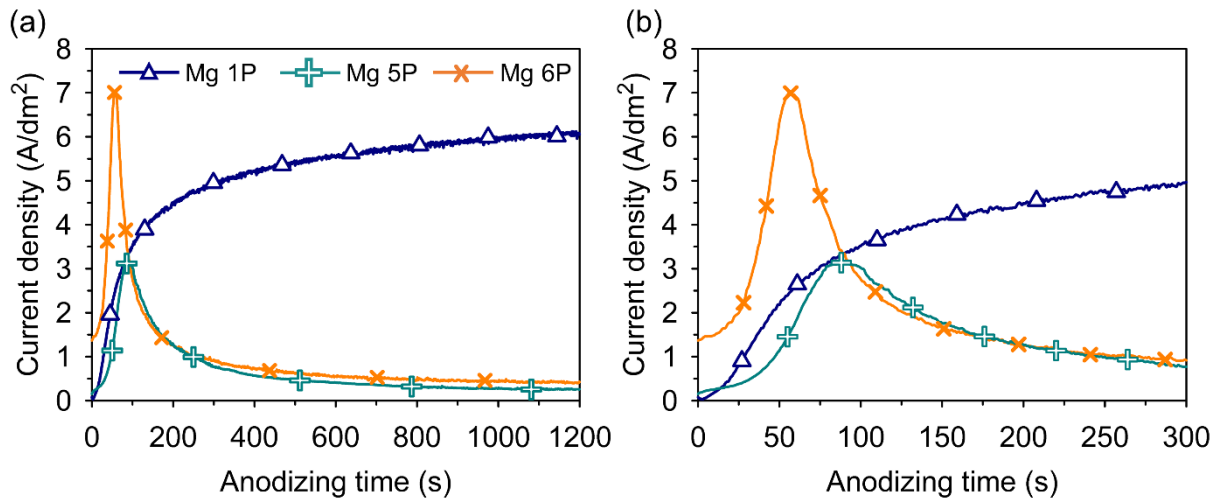
Fig. 43 *Current density vs anodizing time curves recorded during anodizing of pure Mg in the 1 M NaOH electrolyte with Al_2O_3 and PTFE particles at 24 °C for 1200 s (a) after 1200 s, and (b) a detail of the record up to 300 s.*

Microstructure and composition of anodic composite coatings

SEM and EDX results indicated that the Mg surface was rich in Al_2O_3 and PTFE particles after the anodizing process, see Figs. 44, 45 and Table 19. On the free surface of the coating Mg 1P produced at 4 V, two different areas were observed: (i) hemispherical dimples with the composite anodic coating (Fig. 44b,e region D) and (ii) partially oxidized magnesium matrix with Al_2O_3 and PTFE particles (Fig. 44d). The coating microstructure was found to be the same as that of Mg 2 and Mg 3 AMHCs produced at 5 V. The particles were found to be strongly incorporated in the magnesium matrix because after washing in an ultrasonic ethanol bath, the particles remained on the surface of the anodized sample. In the cross-section (i) a local composite anodic coating with horizontal cracks (Fig. 44h) and (ii) a coating containing Al_2O_3 and PTFE particles (Fig. 44i) were observed. Addition of Al_2O_3 and PTFE particles to the electrolyte led to an increase in current density, which resulted in the production of non-compact CAC compared to the Mg 1 coating without the addition of particles to the electrolyte. Reducing the anodizing voltage to less than 4 V (maximum anodizing current density 4 A/dm^2) could lead to the formation of compact CAC.

1 M NaOH + Al₂O₃ and PTFE particles / 4 V / 1200 s / ground (sample Mg 1P)

Top
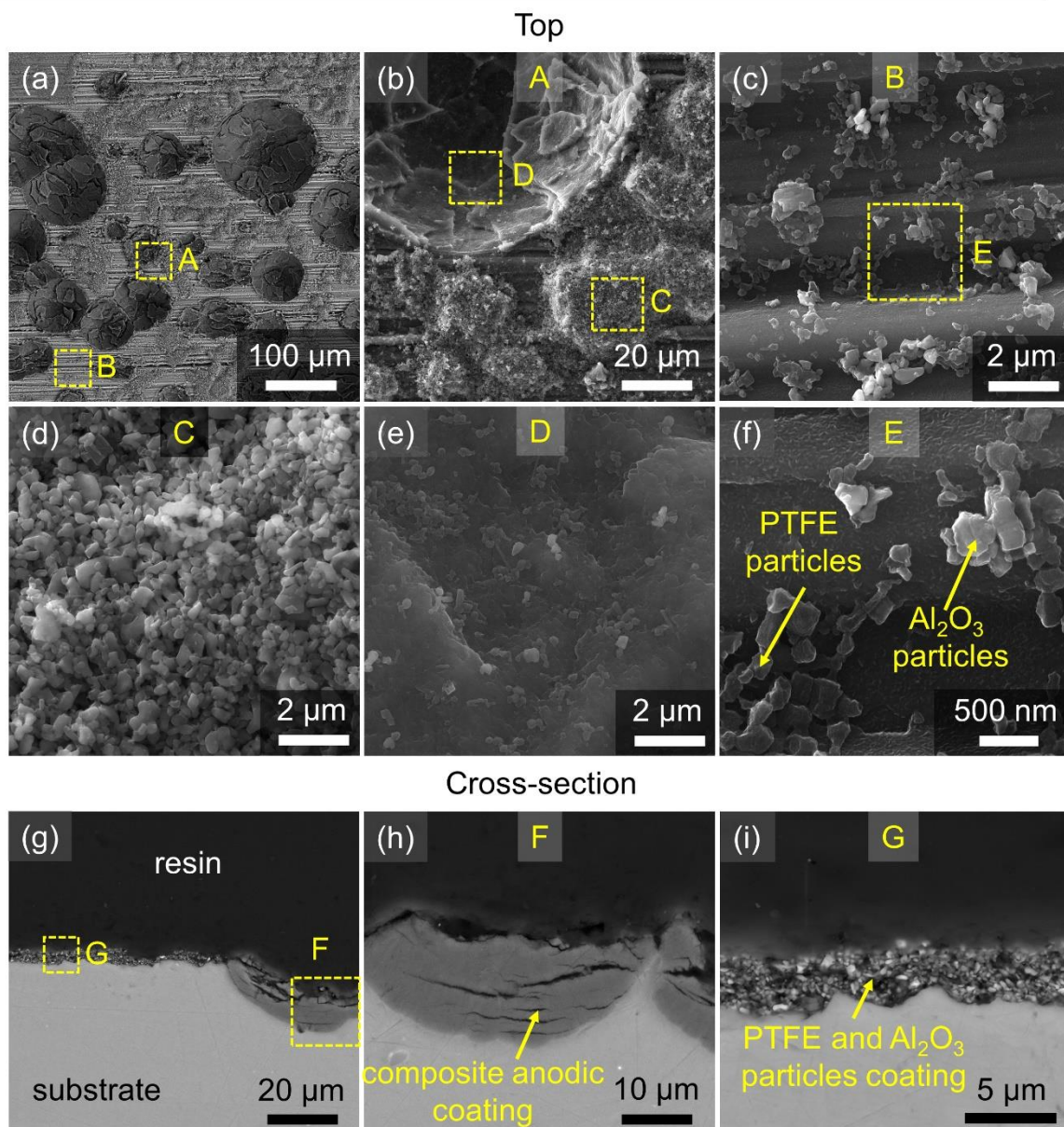
Cross-section

Fig. 44 *Micrographs of the composite anodic coating Mg 1P: (a-f) free surface, and (g-i) cross-section; (a, g-i) SEM-BSE and (b-f) SEM-SE.*

Figure 45 shows the surface morphology of a composite anodic coating with Al_2O_3 and PTFE particles. The surface morphology of both produced coatings without particles (Fig. 39g-j) and with particles (Fig. 45a,b), exhibited some similar features. When comparing high magnification micrographs without (Fig. 40b,c) and with Al_2O_3 and PTFE particles (Fig. 45c,f), a different morphology was observed. An EDX analysis of the composite anodic coating confirmed the presence of Mg, O, Na, Al and F. More Al and F was found on the Mg 6P coating surface, which was of higher roughness before anodizing. The results indicated that the added Al_2O_3 and PTFE particles were incorporated into the coating during the formation of a composite anodic coating.

In the literature, no other similar study was found that would focus on the direct incorporation of Al_2O_3 and PTFE particles from the electrolyte during the anodizing process at lower voltages (≤ 50 V). Further systematic experiments are needed to understand the process of incorporating these secondary particles during the anodizing process.
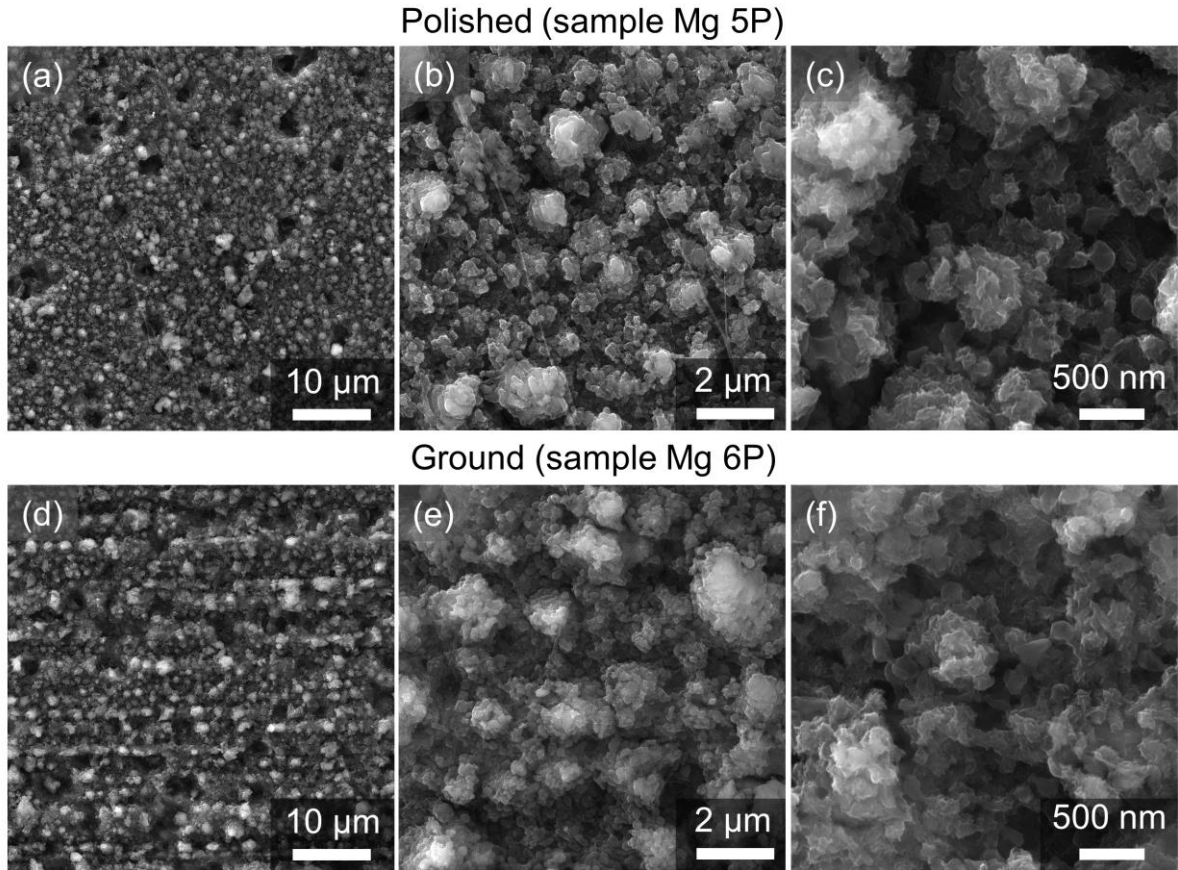
Fig. 45 *Free-surface topography micrographs (SEM-SE) of composite anodic coatings produced on different mechanically pre-treated samples (a-c) polished, (d-f) ground and anodized in the 1 M NaOH with Al_2O_3 and PTFE particles at 20 V, 24 °C for 1200 s.*

Table 19 *EDX analysis of anodized samples estimated from a surface area of 0.0016 mm^2.*

Sample	Element (wt.%)				
	O	Na	Al	F	Mg
Mg 1P (dimples)	56.5	1.3	1.0	4.4	36.8
Mg 1P (outside the dimples)	6.2	0.5	3.5	1.6	88.2
Mg 5P	31.4	0.4	1.1	1.3	65.8
Mg 6P	32.8	0.9	1.6	4.3	60.4

4.2.3. Closing remarks on anodizing of 99.9% Mg

The effects of mechanical pre-treatment (grinding and polishing) of the initial material (pure magnesium) and anodizing conditions such as voltage and addition of Al_2O_3 and PTFE particles to the 1 M NaOH electrolyte on the formation of anodic coatings were examined. The following main conclusions can be drawn:

- Compact anodic magnesium hydroxide coatings (AMHCs) were successfully produced *via* a one-step potentiostatic anodizing process of pure magnesium in the 1 M NaOH electrolyte at 21 ºC, 4 and 10-50 V.

- During the anodizing process, two different shapes of current density *vs* anodizing time curves were recorded, depending on the applied voltage. When a lower voltage of 4 or 5 V was used, the current density increased with anodizing time and more gas oxygen was observed. On the other hand, when a higher voltage was applied, the current density immediately increased and then, after reaching the maximum of current density, decreased with anodizing time.

- Using a lower voltage of 4 V, a thicker (10.8 µm), bulk-like structure coating with horizontal cracks and the rough surface was produced. Increasing the voltage to 5 V led to the formation of non-compact coating with hemispherical dimples containing AMHC with cracks and a slightly anodized magnesium substrate. Vigorous gas evolution during the anodizing process caused the formation of horizontal cracks inside the coatings. When using a higher voltage (10-50 V), a thinner (nm) and smoother coatings with micropores were produced. The coating produced at 50 V was denser, smoother and contained larger micropores, which related to the intensive oxygen gas evolution during the anodizing process.

- Addition of Al_2O_3 and PTFE particles directly to the electrolyte caused an increase in current density during the anodizing process. A non-compact composite coating was produced at 4 V due to the increase in current density. On the coating surface, three different areas were observed: (i) hemispherical dimples containing composite anodic coating, (ii) partially oxidized magnesium substrate with Al_2O_3 and PTFE particles, and (iii) Al_2O_3 and PTFE particles coating. The anodic composite coating produced at 20 V was compact, and the Al_2O_3 and PTFE particles were successively incorporated into the produced coatings. The ground anodized sample contained more Al_2O_3 and PTFE particles.

4.3. Anodizing of ZnTi2

4.3.1. Optimization of anodizing conditions for ZnTi2 sheet

Prior to the process, the samples were chemically pre-treated. The electrolyte for anodizing consisted of sodium hydroxide (NaOH), potassium hydroxide (KOH) or oxalic acid ($C_2H_2O_4$). This synthesis of the electrolyte was inspired by the literature [18, 38, 39, 134]. The electrolyte temperature was 21 °C, and the process conditions were selected based on the previous experiments at work [135] and are summarized in Table 20.

Table 20 *Summary of the initial experimental conditions for anodizing the ZnTi2 alloy, and resulting coatings thickness.*

Sample	Electrolyte	Voltage (V)	Anodizing time (s)	pH	Thickness of anodic coating (µm)
Zn 1	0.04 M NaOH[¶]	50	900	12.6	8.3
Zn 2	0.1 M NaOH	50	900	13.0	11.0
Zn 3	0.1 M NaOH	6	900	13.0	-
Zn 4	0.3 M NaOH	6	900	13.3	1.1
Zn 5	0.3 M NaOH	4	900	13.3	1.4
Zn 6	0.3 M KOH[+]	6	900	13.3	1.4
Zn 7	0.3 M KOH	4	900	13.3	1.5
Zn 8	0.3 M $C_2H_2O_4$[*]	30	600	2.3	2.3
Zn 9	0.025 M $C_2H_2O_4$	10	400	2.0	-

[¶]NaOH - sodium hydroxide; [+]KOH - potassium hydroxide; [*]$C_2H_2O_4$ - oxalic acid

Influence of chemical pre-treatment on the surface morphology of initial material

Scanning electron micrographs (SEM-SE) of the surface morphology of initial material prior to and after the chemical pre-treatment are shown in Fig. 46. On the free surface of the samples before and after the pre-treatment, rolling lines and scratches from the alloy manufacture are present. An analysis of the chemical composition showed that Ti is present in the initial material in the form of the intermetallic phase, which was mostly removed during the chemical pre-treatment (etching). The vicinity of these intermetallic phases was

dissolved, and these phases fell out from the surface, leaving distinctive dimples as shown in the micrograph Fig. 46b.
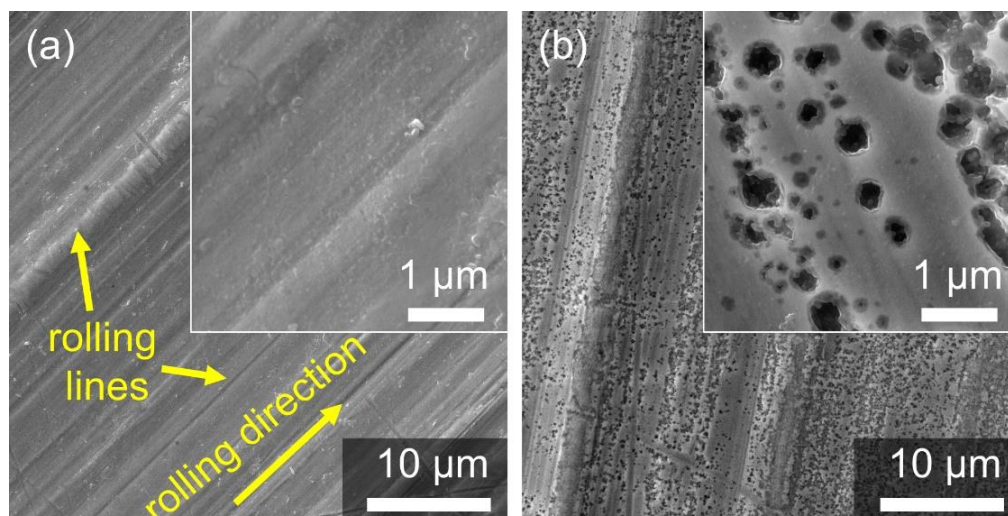
Fig. 46 *Micrographs (SEM-SE) of the free initial material surface (a) prior to, and (b) after the chemical pre-treatment.*

Anodizing process

During the anodizing processes, the current density *vs* anodizing time curves were recorded (see Fig. 47). When the 0.04 and 0.1 M NaOH electrolyte and 50 V were used (Fig. 47a), the current density decreased with anodizing time more rapidly than in the case of lower applied voltages ($\leq$ 6 V), as shown in Fig. 47b. It was found that by increasing the voltage, the current density also significantly increased. Moreover, the intensity of gas bubbling evolution was significantly higher during anodizing at 50 V when compared to lower voltages ($\leq$ 6 V).

When a 0.3 M concentration of the NaOH and KOH electrolytes and 4 V were used (samples Zn 4-Zn 7), a similar electrochemical behaviour was observed (see Fig. 47b). But when a less diluted solution of 0.1 M NaOH was used, the anodizing process did not even start at voltages below 6 V.

In the end, two different types of the anodic coating were produced, referred to as "white" and "black". The white anodic coatings Zn 1 and Zn 2 were produced when a low concentration of the NaOH electrolyte and 50 V were used. The black anodic coatings Zn 3-Zn 7 were produced when lower voltages ($\leq$ 6 V) and a higher concentration of the NaOH and KOH electrolytes were utilized. Dark black anodic coatings were produced at 4 V and 0.3 M in either the NaOH or the KOH electrolyte.

Completely different electrochemical behaviour was recorded for the $C_2H_2O_4$ electrolyte when compared to the NaOH and KOH electrolytes. The current density rapidly decreased with anodizing time (Fig. 47c) and the process finished after 400 s and 600 s (samples Zn 8 and Zn 9, respectively). It occurred due to the faster dissolution of zinc in the electrolyte and the much faster anodic coating growth. It was found that a higher voltage must be applied to start the process when the concentration of $C_2H_2O_4$ in the electrolyte is increased. The resulting coating was of light grey colour.

86
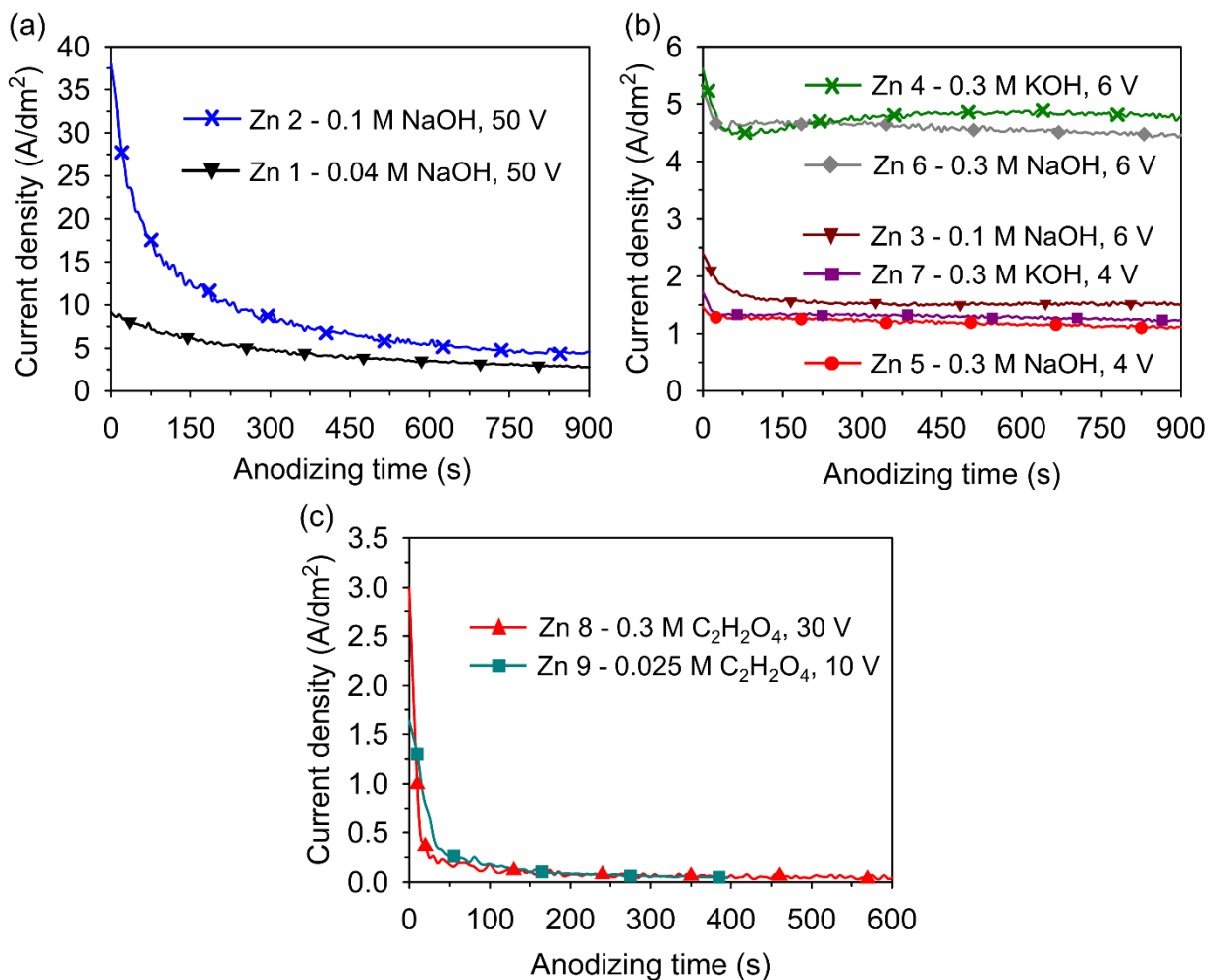
Fig. 47 *Current density vs anodizing time curves of ZnTi2 alloys anodized at 21 °C in the (a) NaOH electrolyte at 50 V (samples Zn 1 and Zn 2), (b) NaOH or KOH electrolyte at 4 and 6 V (samples Zn 3-Zn 7), and (c) $C_2H_2O_4$ electrolyte at 30 and 10 V (samples Zn 8 and Zn 9).*

Morphology, structure and thickness of anodic coatings

Anodic coatings produced under different anodizing conditions (voltage, type and concentration of the electrolyte), were found to have different morphology, microstructure, and thickness (see Figs. 48-50). Anodic coatings Zn 1 and Zn 2 produced at 50 V, in the 0.04 and 0.1 M NaOH electrolyte contained numerous horizontal microcracks, distributed across the whole cross-section of the coating (Fig. 48a-f). The formation of cracks in ZnO anodic coatings produced at high voltages, i.e. 50 V, was also reported by Rocca et al. [38] for the 0.05 M KOH electrolyte, and by Dong et al. [136] for the 0.05-0.2 M NaOH electrolyte and a higher voltage ≥ 20 V. The presence of horizontal cracks and gaps can be caused by the rapid growth of coatings together with vigorous oxygen gas evolution during the anodizing process. The vigorous oxygen evolution caused local stresses in the coating/substrate interface, and therefore the brittle coating cracked in the horizontal direction. In the cross-section, a bulk-like structure with horizontal cracks, gaps and local vertical cracks was observed (Fig. 48c,f).

A detailed analysis of the surface coatings morphology showed a granular appearance (Fig. 48a,e).

Increasing the electrolyte concentration of sodium hydroxide from 0.04 (sample Zn 1) to 1 M (sample Zn 2) led to the formation of a coating with more bulk-like structure appearance and lower number of cracks. The anodic coating thickness increased from 8.3 to 11 μm (Fig. 48c,f). The surface coating morphology showed finer granular appearance.

With the voltage decreased from 50 to 6 V while the electrolyte concentration remained the same, i.e. 0.1 M NaOH, the black, thinner and porous anodic coating Zn 3 was produced (Fig. 48d-i).

Increasing the electrolyte concentration of sodium hydroxide from 0.1 (sample Zn 3) to 0.3 M (Zn 4) resulted in the production of a thicker and porous coating.

Decreasing the voltage from 6 to 4 V (electrolyte concentration was kept constant, i.e. 0.3 M NaOH) resulted in the production of a coating with bigger pores, as shown in cross-section in Figs. 49c and 49f. A small increase in the coating thickness was observed, from 1.1 to 1.4 μm. Hence, the comparison of anodic coatings produced in the NaOH and KOH electrolytes at 4 V showed similar coating morphologies and thicknesses.

Anodic coatings produced at $\leq$ 6 V in the 0.3 M NaOH and KOH electrolytes exhibited a sponge-like structure (Figs. 48g-i and 49), rather than a channel-like porous structure typically observed in porous anodic aluminium oxide coatings [7].

Coatings produced at a higher voltage of 50 V were white, with a bulk-like structure that contained horizontal cracks and gaps (Fig. 48d-f), while coatings produced at lower voltages of $\leq$ 6 V were black and thinner, with sponge-like structure, and without cracks (Fig. 48g-i). The voltage significantly influenced the resulting morphology, thickness and the overall appearance of the produced anodic coatings.

Anodic coatings produced in the $C_2H_2O_4$ electrolyte (see Fig. 50) exhibited a different morphology than the coatings produced in the NaOH and KOH electrolytes. The morphology looks like a nano-rock or nano-flower structure. As can be seen in the cross-section in Fig. 50c, the anodic coating was delaminated during the metallography preparation (cold mounting technique) and exhibited a low adhesion compared to the coatings produced in the NaOH and KOH electrolytes. The anodic coating Zn 9 was found to be very thin, and no metallographic cross-section sample could be prepared by conventional metallographic procedures.
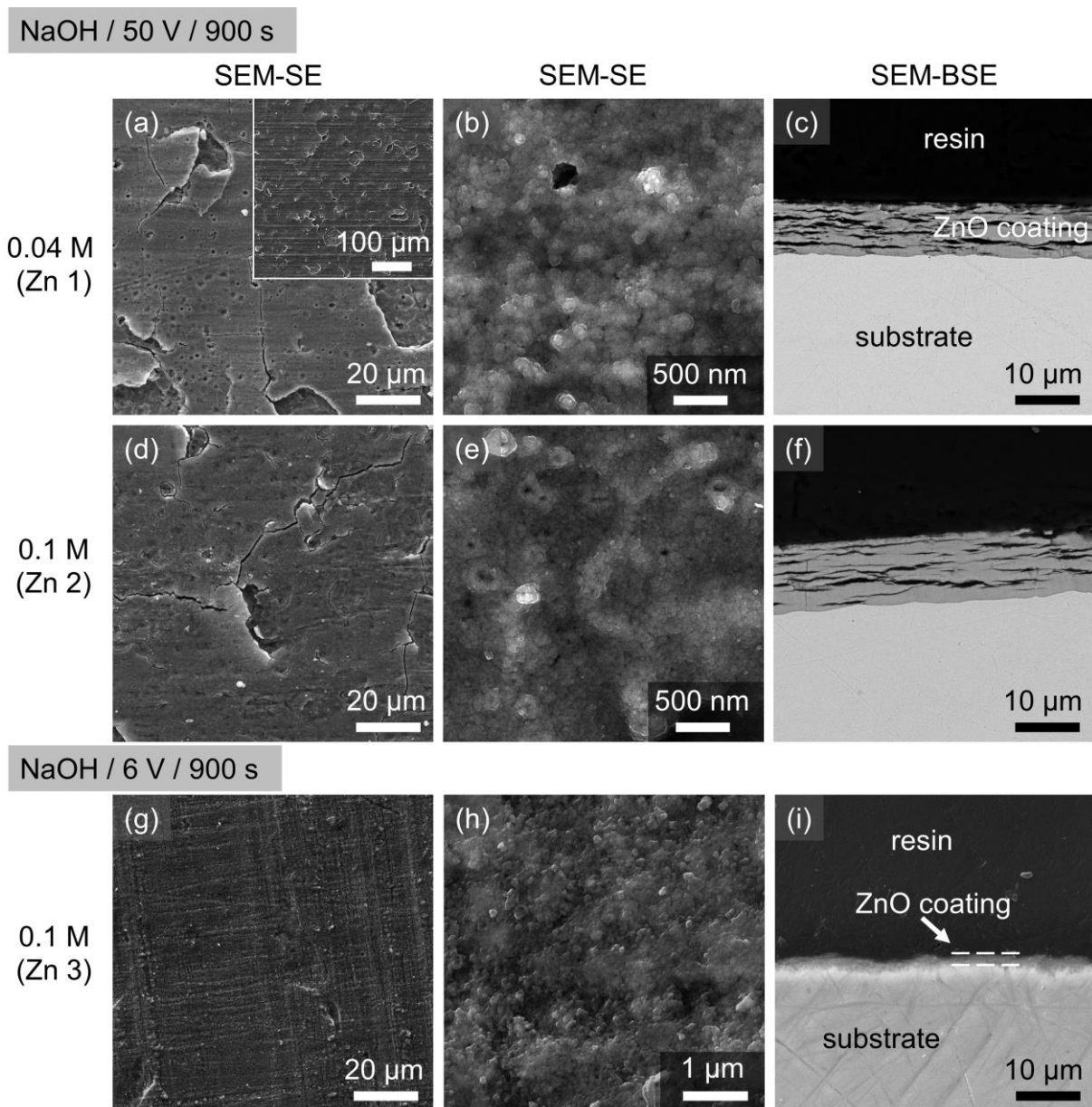
Fig. 48 Micrographs of the coating surface (left and middle) and its cross-section (right) after anodizing at 21 ºC for 900 s in the: (a-c) 0.04 M NaOH at 50 V, (d-f) 0.1 M NaOH at 50 V, and (g-i) 0.1 M NaOH at 6 V.
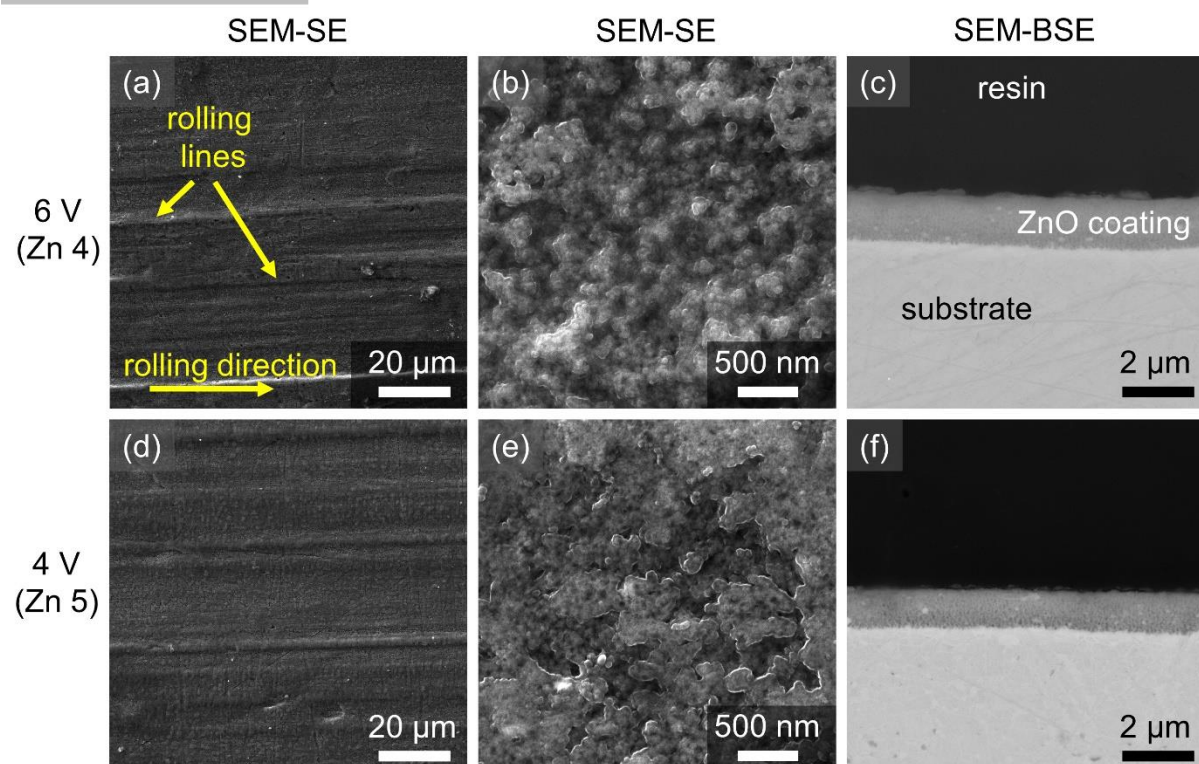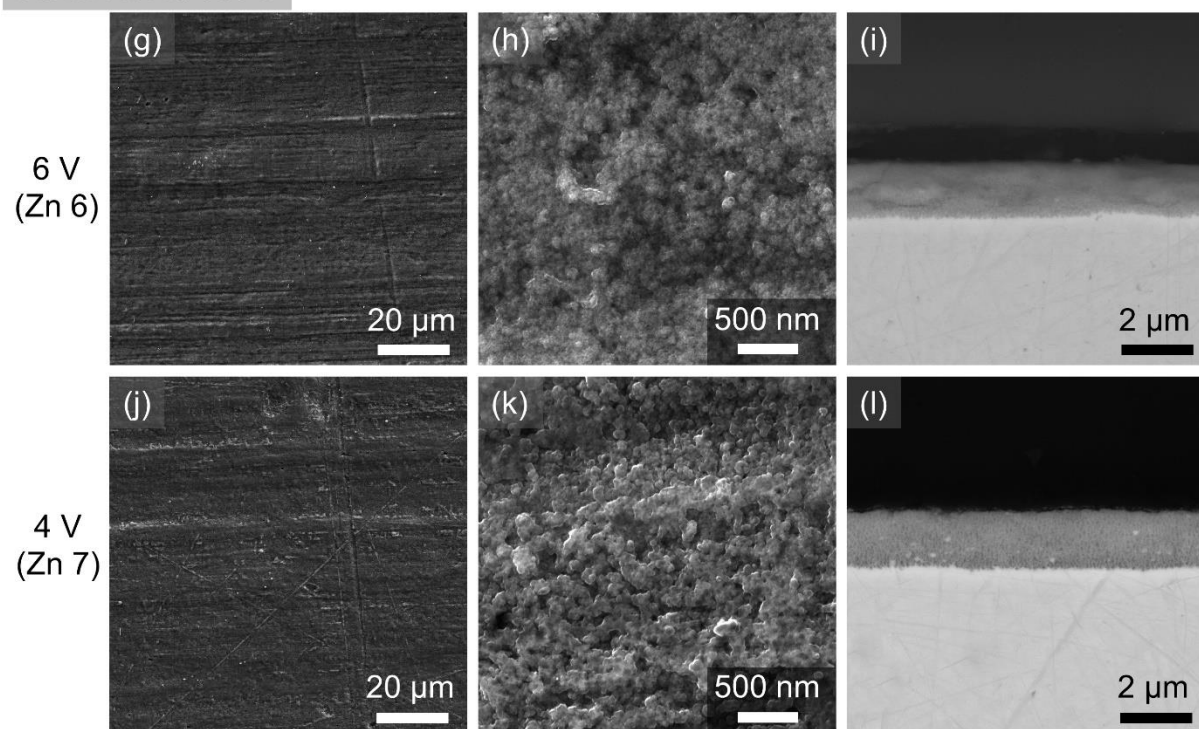
Fig. 49 *Micrographs of the coating surface (left and middle) and its cross-section (right) after anodizing at 21 °C for 900 s in the: (a-c) 0.3 M NaOH at 6 V, (d-f) 0.3 M NaOH at 4 V, (g-i) 0.3 M KOH at 6 V, and (j-l) 0.3 M KOH at 4 V.*

0.3 M C₂H₂O₄ / 600 s

SEM-SE   SEM-SE   SEM-BSE
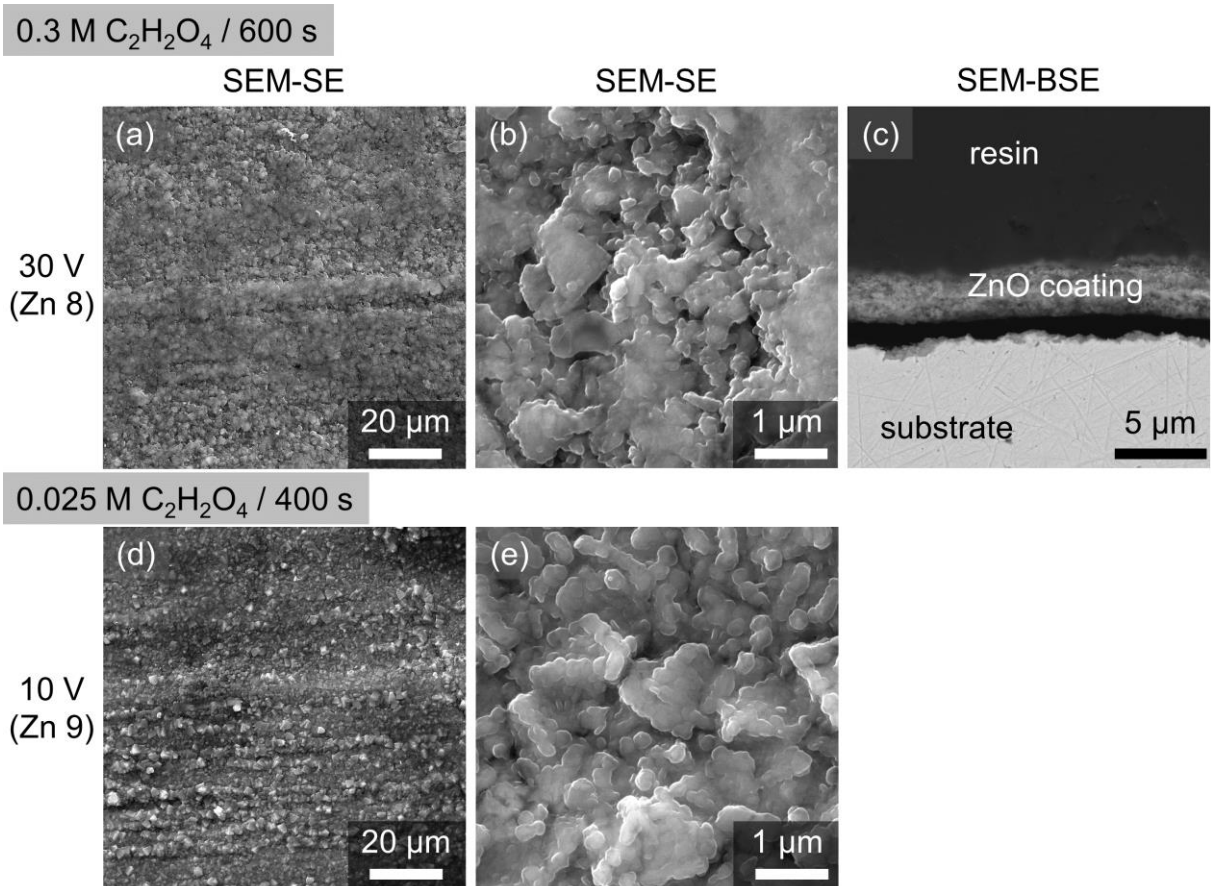
Fig. 50 Micrographs of the coating surface (left and middle) and its cross-section (right) after anodizing at 21 ºC in the: (a-c) 0.3 M C₂H₂O₄ at 6 V for 600 s, and (d, e) 0.025 M C₂H₂O₄ at 10 V for 400 s.

4.3.2. Effect of voltage, NaOH electrolyte concentration and anodizing time on the resulting morphology, structure and thickness of anodic coatings

In the previous set of experiments, it was easier to control the anodizing process that was carried out in the NaOH electrolyte, compared to other electrolytes. Therefore, further experimental work was designed in order to evaluate the effect of voltage, concentration of the NaOH electrolyte, and anodizing time on the resulting structure, morphology, and thickness of the produced anodic coatings. Various NaOH concentrations were used further to analyse the concentration effect on the anodizing process conditions. Coatings produced at 6 V exhibited a very low thickness; therefore, only 4 and 50 V were further used. Preferential anodizing conditions are summarized in Table 21.

Table 21 *Experimental conditions for the evaluation of the effect of the NaOH electrolyte concentration and voltage on the anodizing process of ZnTi2.*

Sample	Electrolyte $(C_{NaOH}$[¶]$)$	Voltage (V)	Anodizing time (s)	pH
Zn 1	0.04 M	50	900	12.6
Zn 10	0.04 M	50	1800	12.6
Zn 2	0.1 M	50	900	13.0
Zn 11	0.1 M	50	1800	13.0
Zn 12	1.0 M	4	1800	13.6
Zn 13	0.5 M	4	1800	13.4
Zn 14	0.3 M	4	1800	13.3
Zn 5	0.3 M	4	900	13.3
Zn 15	0.3 M	4	300	13.3

[¶]NaOH - sodium hydroxide

Anodizing process

The current density *vs* anodizing time curves recorded during the anodizing process of the ZnTi2 at different voltages and concentrations of the NaOH electrolyte, are in Fig. 51. When 50 V was applied, the current density rapidly decreased with anodizing time (Fig. 51a), compared to the case of lower voltage (4 V), as can be seen in Fig. 51b. With increasing

electrolyte concentration, the current density significantly increased, which can be explained by the presence of a higher amount of OH^-, O^{2-} ions and the mobility of the ions in the electrolyte, which are involved in the reaction. Also, the oxygen gas evolution was intense at 50 V, when compared to the lower voltage 4 V. Similar behaviour was observed by Rocca et al. [38] during their experiments in the 0.05 M KOH electr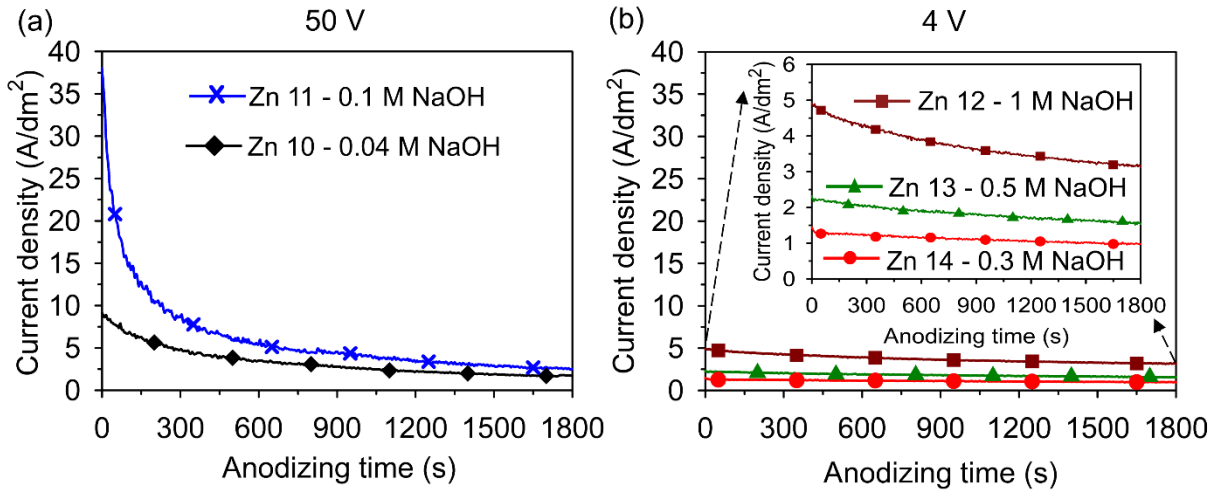olyte at 50 V. The formation mechanism of ZnO coatings is still unclear and not well described in the literature. Anodic coatings produced under the same conditions (namely samples Zn 15, Zn 5 and Zn 14 anodized for 300, 900 and 1800 s) exhibited similar electrochemical behaviour.

Fig. 51 *Current density vs time curves recorded during anodizing of ZnTi2 alloys at different NaOH electrolyte concentrations at 21 °C and at (a) 50 V and (b) 4 V.*

Characterization of the produced ZnO coatings

Effect of voltage and NaOH concentration on overall appearance, and the chemical and phase composition

The appearance of the initial material is shown in Fig. 52a. Due to the anodizing process, two different types of ZnO anodic coating were formed and referred to as "black" and "white" respectively, as shown in Figs. 52b and 52c, respectively. Samples anodized in the 0.04-0.1 M NaOH electrolytes at 50 V were white in appearance (Fig. 52b). The samples anodized in the 0.3-1 M NaOH electrolytes at 4 V were found to be black colour (Fig. 52c). The used voltage influenced the appearance of the produced anodic coatings, which can also relate to the evolution of oxygen. Mabon et al. [137] proposed that black ZnO anodic coatings produced in alkaline electrolytes exhibited good solar-selective properties for application as an absorber surface for low temperature photothermal solar energy conversion. Therefore, more attention should be paid to the overall appearance of the anodic coatings, which is closely connected to its optical properties. The influence of process conditions on the overall appearance (i.e. colour) of ZnO anodic coatings is not even discussed in the literature, and only a limited number of authors comment on the resulting appearance for a specific combination of process conditions. For example, Rocca et al. [38] observed the formation of grey ZnO anodic coatings in the 0.05 M KOH at 50 V. Zhang et al. [21] described that anodic coatings

93

of various colours, from white through grey to black, can be produced in NaOH and Na_2CO_3 aqueous solutions in dependence on the current density. Mika et al. [138] found that the dark nanoporous ZnO coatings could be obtained in the strongly alkaline electrolyte (i.e. 1 M NaOH) at 2 and 4 V.
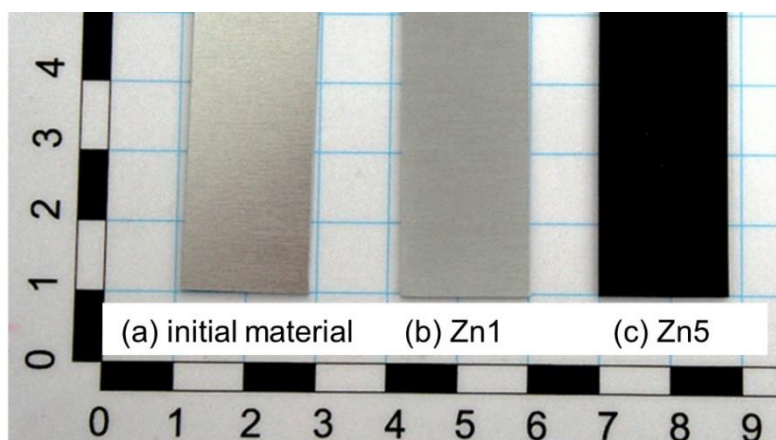
Fig. 52 *Influence of voltage on the appearance: (a) initial material, and samples anodized (b) in the 0.04 M NaOH electrolyte at 50 V (sample Zn 1), and (c) in the 0.3 M NaOH electrolyte at 4 V (sample Zn 5).*

X-ray diffraction was employed to confirm the crystal structure of the produced anodic coatings. As shown in Fig. 53, the less pronounced diffraction peaks (dots) can be indexed as ZnO (JCPDS card number 01-080-0075), while the more distinctive peaks (diamonds) correspond to the zinc substrate (JCPDS card number 03-065-5973). The diffraction peaks of coatings Zn 1, Zn 2 and Zn 5 correspond to (100), (002), (101), (102), (110), (103) and (112) Miller indices, indicating polycrystalline ZnO with hexagonal (wurtzite) structure. The EDX analysis confirmed the presence of Zn, O and Na.
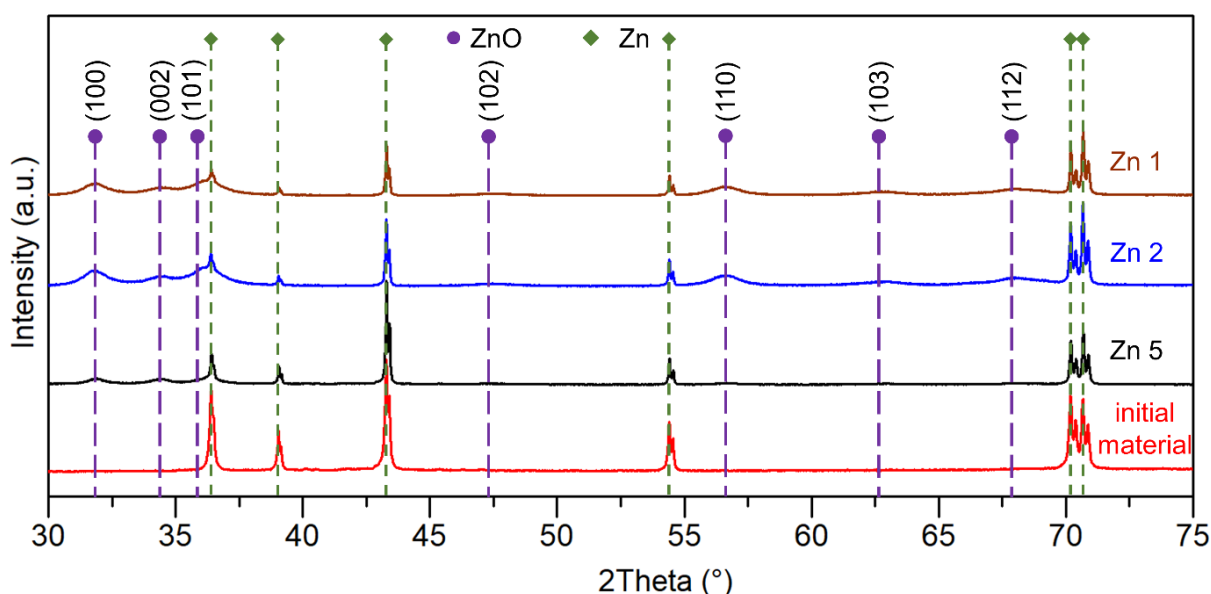
Fig. 53 *XRD pattern of the initial material (ZnTi2) and ZnO anodic coatings obtained by anodizing for 900 s (samples: Zn 1 - 0.04 M NaOH, 50 V; Zn 2 - 0.1 M NaOH, 50 V; Zn 5 - 0.3 M NaOH, 4 V).*

Effect of electrolyte concentration on the growth and thickness of ZnO coating

The effect of electrolyte concentration on the morphology of the ZnO coatings was investigated using (i) the 0.04 and 0.1 M NaOH electrolytes at 50 V and (ii) the 0.3, 0.5 and 1 M NaOH electrolytes at 4 V, the anodizing time was kept the same, i.e. 1800 s. The coating surface free morphology and cross-section micrographs are shown in Figs. 54 and 55, respectively.

At a high voltage of 50 V, coatings with the white appearance and similar surface morphology for both electrolyte concentrations, i.e. 0.04 and 0.1 M NaOH, were produced, see Fig. 54. In the high magnification micrographs of the coating surface (Fig. 54a,b) the granular structure can be seen. The presence of cracks on the free surface seems to be closely related to the horizontal cracks and gaps which were observed over the thickness of the whole coating (Fig. 54c,d). Even the coating thicknesses (16.4 μm and 17.7 μm) did not significantly change with the electrolyte concentration. Nevertheless, with the increasing concentration of the NaOH electrolyte, the bulk-like structure contained a lower number of horizontal cracks and gaps were formed, see Fig. 54c,d. Longer anodizing time did not affect the morphology of produced coatings compared to coatings Zn 1 and Zn 2 produced in the shorter anodizing time, i.e. 900 s, but had an effect on the coating thickness. With the anodizing time increasing from 900 s to 1800 s, the thickness of ZnO coatings increased from 8.3 to 16.4 μm and from 11.0 to 17.7 μm respectively.
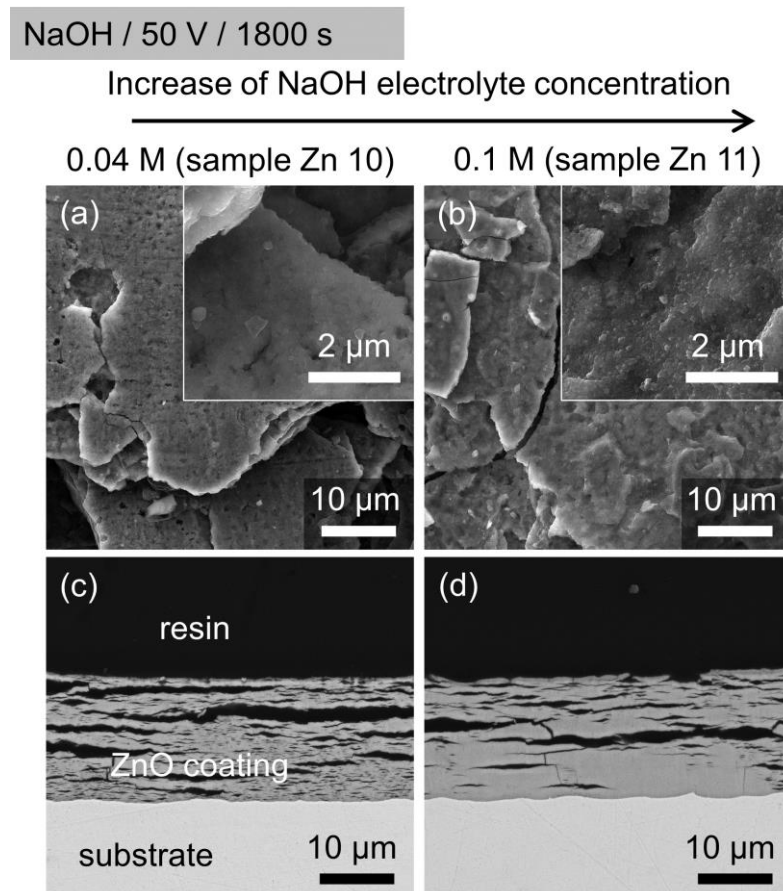
Fig. 54 *Micrographs of the (a, b) free surface (SEM-SE), and (c, d) cross-section (SEM-BSE)*
of ZnO coatings formed at 21 °C and at 50 V for 1800 s in the:
(a, c) 0.04 M NaOH, and (b, d) 0.1 M NaOH electrolyte.

Decreasing the voltage from 50 to 4 V led to the formation of anodic coatings that were different in structure and appearance, see Fig. 55. Anodic coatings produced at 4 V were dark black, and a sponge-like structure was produced, as can be seen in the cross-section in Fig. 55d-f. With the electrolyte concentration increasing from 0.3 to 1 M NaOH, the thickness of anodic coating increased non-linearly (2.5, 4.8 and 9.4 µm), and a coating with bulk-like structure and smaller pores was produced, as can be seen in the cross-section in Fig. 55d-f. On the other hand, the anodic coating formed in the 1 M NaOH electrolyte contained undesirable vertical microcracks, and the coating surface was smoother and had a finer granular structure. At higher electrolyte concentrations, a higher number of Zn^{2+} and OH^- ions participate in the formation of a coating, and therefore, the thicker coating can be produced. The effect of anodizing time (i.e. 300, 900 and 1800 s) during the anodizing process at 4 V in the 0.3 M NaOH was also studied. As might be expected, longer anodizing time led to the formation of thicker anodic coatings, from 2.5 to 4.8 up to 9.5 µm. Dong et al. [136] anodized pure Zn foil in the 0.1 M NaOH at 5-40 V and found that the ZnO coatings produced at lower voltages (< 9 V) were thinner, the thickness did not change with the voltage range from 5 to 9 V, and they exhibited a porous structure. ZnO coatings produced at 12 V were thicker and exhibited a nanorod structure. Dong et al. [136] explained the formation of the porous structure as the result of an insufficient supply of voltage. When the voltage was lower than 9 V, the migration of OH^- and O^{2-} ions was lower, and therefore these ions were unable to pass through the produced ZnO coating as in the case when 12 V was used. The residual ions tend to diffuse freely and attacked the formed ZnO coating randomly. When using a higher voltage, the ions could pass through the produced ZnO coating, and a thicker and regular nanorod structure could be produced, i.e. the oxidation and dissolution rates were in balance. With the voltage increasing from 20 to 40 V, the nanorod ZnO coating became thicker and contained horizontal cracks and gaps.

Increase of NaOH electrolyte concentration

0.3 M (sample Zn 14)   0.5 M (sample Zn 13)   1 M (sample Zn 12)
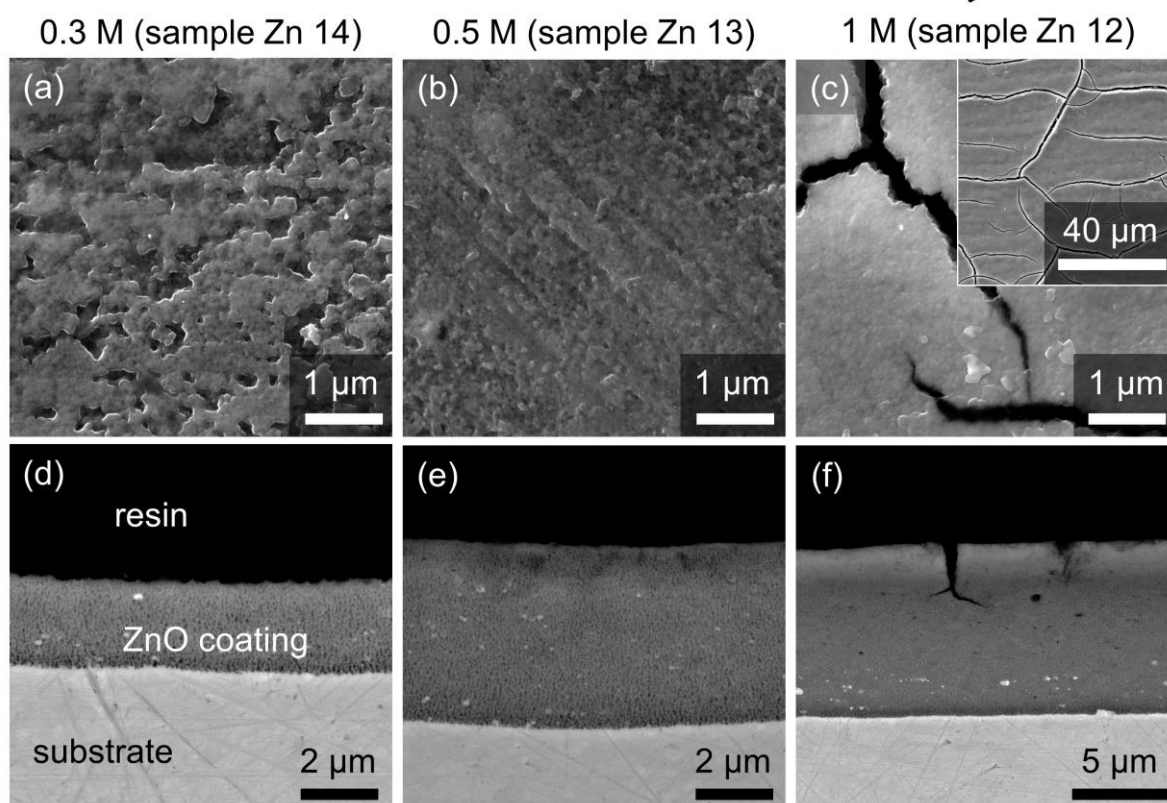

Fig. 55 *Micrographs of the (a-c) free surface (SEM-SE), and (d-f) cross-section (SEM-BSE) of ZnO coatings after anodizing at 21 °C, 4 V for 1800 s in the: (a, d) 0.3 M NaOH, (b, e) 0.5 M NaOH, and (c, f) 1 M NaOH.*

Anodic coatings Zn 11 (0.1 M NaOH, 50 V and 1800 s, "white") and Zn 14 (0.3 M NaOH, 4 V, 1800 s, "black") were investigated in detail by FESEM and HRTEM.

In Fig. 56 is shown a detail of the coating surface morphology of the samples Zn 11 and Zn 14. As can be seen in Fig. 56a, the coating surface morphology of Zn 11 contained densely arranged and piled up smaller globular nanoparticles compared to the coating Zn 14 (Fig. 56b).
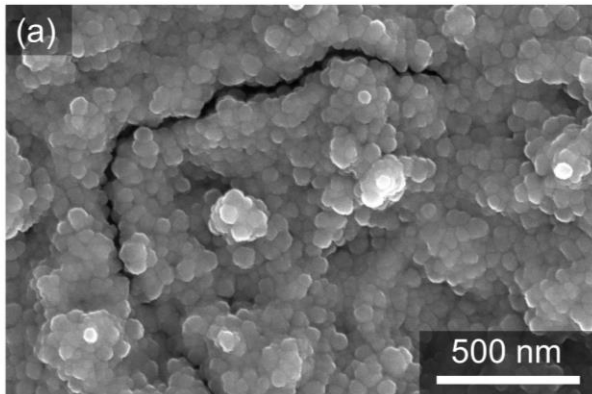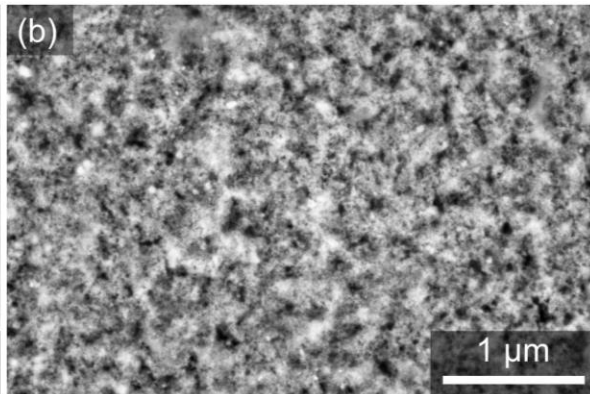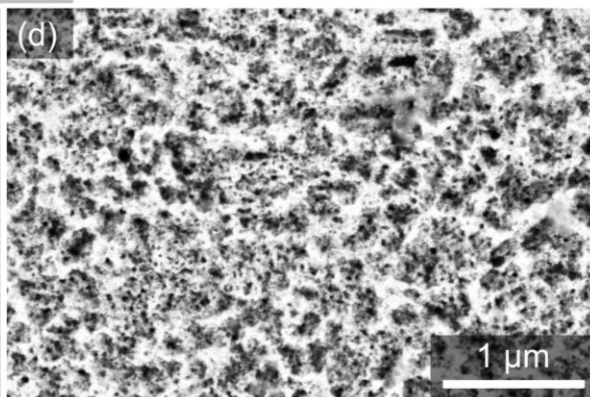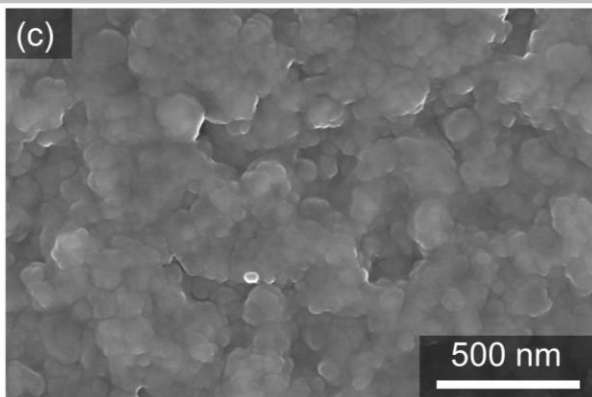
Fig. 56 *FESEM micrographs of the free surface of ZnO coatings after anodizing at 21 °C for 1800 s (a, b) in the 0.1 M NaOH at 50 V (sample Zn 11), and (c, d) in the 0.3 M NaOH at 4 V (sample Zn 14).*

A detailed analysis of Zn 11 coating is shown in Fig. 57. As can be seen in the cross-section, Figs. 57b and 57e, the produced coating is a channel-like structure which contains cracks and gaps. Inside the gaps, numerous granular nanoparticles were found that had a similar appearance to the granular surface. On the bottom of the lamella, a different structure of the coating, reminiscent of a compact coating, was found. Further and more detailed studies, focused on a careful examination of morphology and growth, are necessary. From the results, it is not possible to determine exactly whether the structure contained nanotubes or nanorods or a combination of both.

FESEM cross-section micrographs of the coating Zn 14 are shown in Fig. 58. All over the cross-section of the coating, numerous small pores were found. On the bottom part of the coating Zn 14, no different structure or compact coating was observed when compared to the coating Zn 11 produced at 50 V.

Fig. 57 *FESEM micrographs of ZnO coating Zn 11 formed in the 0.1 M NaOH at 50 V, 21 ^{o}C for 1800 s: (a-d) cross-section, and (e) bottom part; FESEM-SE.*

Fig. 58 *FESEM cross-section micrographs of ZnO coating Zn 14 formed in the 0.3 M NaOH at 4 V, 21 ^{o}C for 1800 s: (a) overview, and (b) detail of lamella - middle part; FESEM-SE.*

Figure 59 shows the TEM micrographs of the cross-sections of anodic coatings Zn 11 (Fig. 59a,b) and Zn 14 (Fig. 59c,d). Both ZnO coatings consist of overlapping ZnO crystalline grains. Based on the results, it can be assumed that the coating Zn 11 produced at 50 V is made up of nanorods rather than nanotubes. The EELS spectra for both coatings were identical.

0.1 M NaOH / 50 V / 1800 s (sample Zn 11)
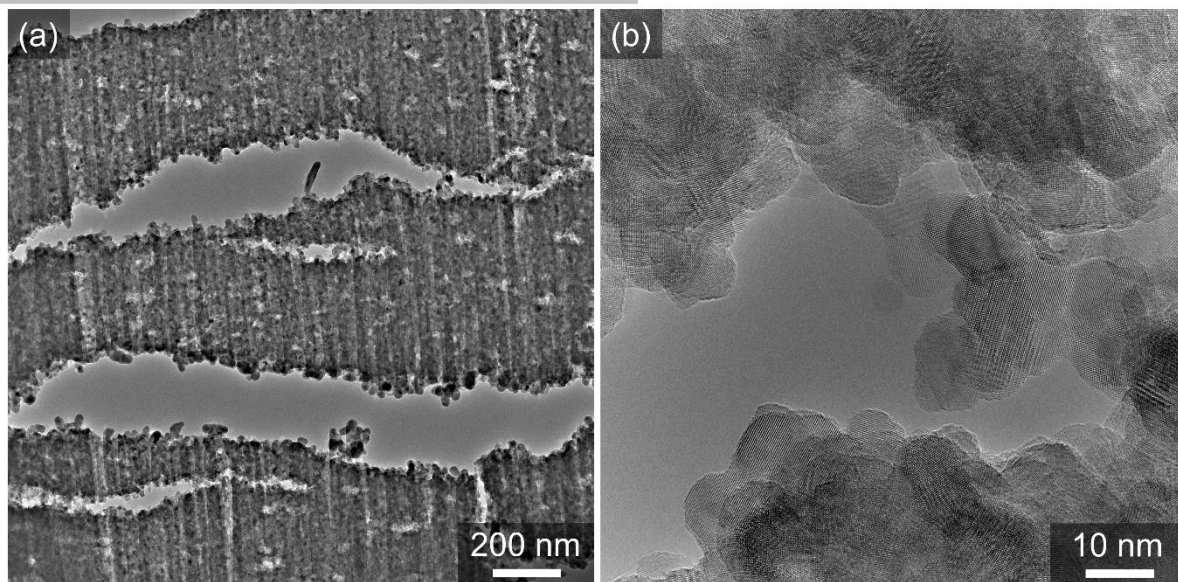
0.3 M NaOH / 4 V / 1800 s (sample Zn 14)
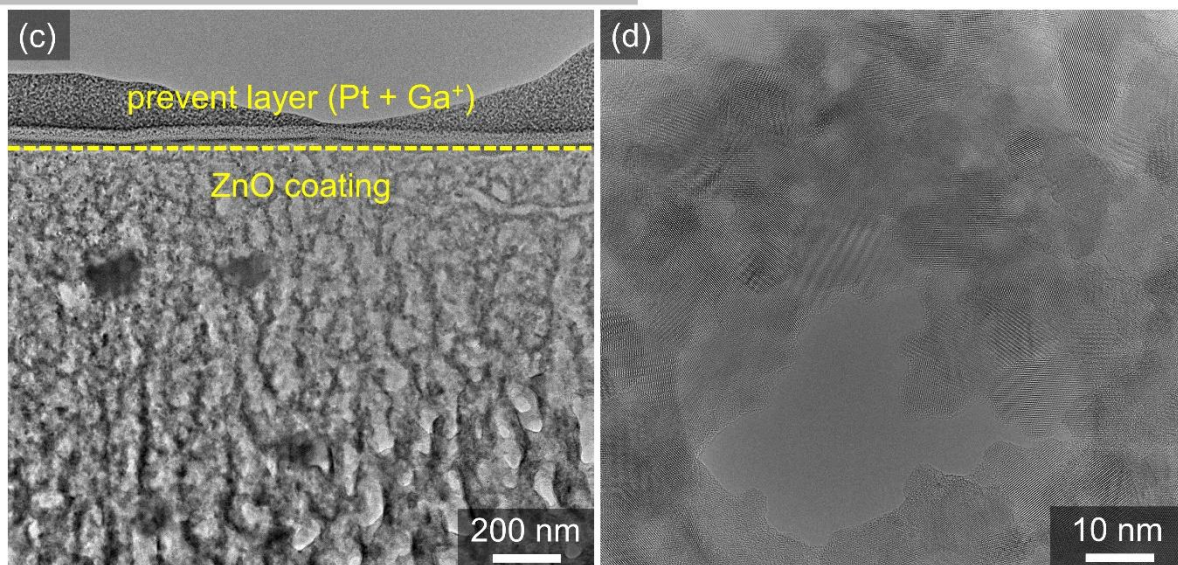
Fig. 59 *TEM cross-section micrographs of ZnO coatings (a, b) Zn 11, and (b, c) Zn 14.*

Further analysis of the Zn 11 ("white") and Zn 14 ("black") coating was performed by Raman spectra, and the results are shown in Fig. 60. The Raman spectra were found to be almost identical and are in agreement with the Raman spectra which were recorded by Mika et al. [138], who then anodized pure zinc in the 1 M NaOH at 2 and 4 V. In general, spectra were recorded in the range between 300 cm^{-1} and 650 cm^{-1} (LO mode). These bands are related to the vibrations of Zn and oxygen sub-lattices. In addition, a low-intensity signal

at $\sim$435 cm^{-1} is a high-frequency E_2 mode associated with vibrations of the oxygen sub-lattice. This peak typically dominates the spectra of crystalline zinc oxide [138].
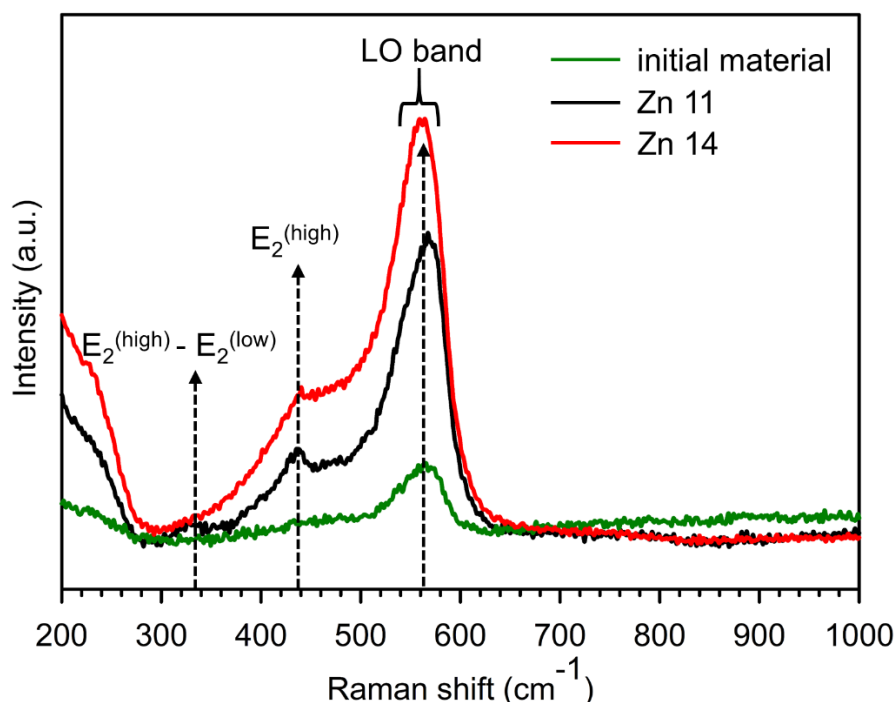
***Fig. 60** Raman spectra of ZnTi2 substrate and ZnO coatings.*

4.3.3. Composite anodic coatings containing Al₂O₃ particles on ZnTi2 alloy

The sodium hydroxide electrolyte (0.5 M) with 6 g/L Al$_2$O$_3$ particles and two types of agitation were used; (i) compressed air and (ii) magnetic stirring to produce the composite anodic coatings (voltage 4 V). The distance between the anode and the cathode was (i) 70 and (ii) 40 mm. The conditions of all experiments are summarized in Table 23.

***Table 23** Summary of the experimental conditions for composite anodic coating formation.*

Sample	Electrolyte	Temperature (°C)	Voltage (V)	Anodizing time (s)	Type of agitation
Zn 17	0.5 M NaOH¶ + 0.6 g/L SDBS# + 6 g/L Al₂O₃£	21	4	1800	compressed air
Zn 18	0.5 M NaOH + 0.6 g/L SDBS + 6 g/L Al₂O₃	21	4	1800	magnetic stirring

¶NaOH - sodium hydroxide; CH$_3$(CH$_2$)$_{11}$C$_6$H$_4$SO$_3$Na - #SDBS - sodium dodecylbenzenesulfonate; £Al$_2$O$_3$ - aluminium oxide

Anodizing process

The current density *vs* anodizing time curves for ZnTi2 alloy in the 0.5 M NaOH electrolyte with or without Al_2O_3 particles, utilizing different agitation mechanisms for anodic composition coating formation, are shown in Fig. 61. Addition of 6 g/L Al_2O_3 particles and 0.6 g/L sodium dodecylbenzenesulfonate (SDBS) to the 0.5 M NaOH electrolyte (Zn 17, Fig. 61), agitated by compressed air, led to a slight decrease in the current density when compared to the process without Al_2O_3 particles and SDBS addition (Zn 13, Fig. 61). Magnetic stirring and the shorter distance between the cathode and the anode led to a decrease in the current density (Zn 18, Fig. 61), and the anodizing curve was found to be much smoother than for the sample Zn 17. The decrease in current density can lead to the formation of a thinner coating.
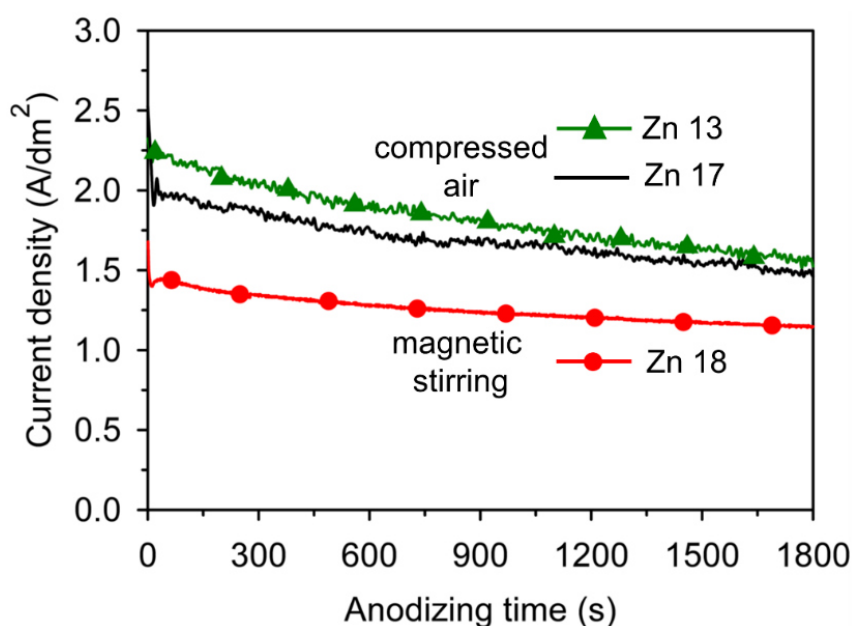
Fig. 61 *Current density vs anodizing time curves recorded during anodizing of ZnTi2 alloys at 21 °C, 4 V in the 0.5 M NaOH without Al_2O_3 particles (sample Zn13) and with Al_2O_3 particles under different agitation mechanisms, i.e. compressed air (sample Zn 13 and Zn 17) and magnetic stirring (sample Zn 18).*

Effect of anodizing conditions on the morphology and thickness of the produced anodic composite coating

The free surfaces and cross-sections of the produced composite anodic coatings utilizing different agitation mechanisms, i.e. compressed air or magnetic stirring, are shown in Fig. 62a-c and Fig. 62d-i, respectively. On the coating surface (Fig. 62a,b) produced with compressed air agitation, uniformly distributed and aggregated Al_2O_3 particles were observed. Addition of Al_2O_3 particles to the 0.5 M NaOH electrolyte did not affect the morphology and thickness of the produced composite anodic coatings when compared to the coating Zn 13 without Al_2O_3 particles (Fig. 55b,e). On the other hand, magnetic stirring affected the morphology of the produced anodic composite coating. On the coating surface (Fig. 62d-h),

non-uniformly distributed Al_2O_3 particles and cracks were found. During the magnetic stirring, the flow of electrolyte caused inhomogeneities whose shape resembled loops. These inhomogenities in the coating were produced due to the high stirring rate. The chemical composition loops and "normal" coatings were similar. More Al_2O_3 particles were deposited in the composite anodic coating during anodizing with using compressed air agitation when compared to magnetic stirring (see Table 24).

0.5 M NaOH + 6 g/L Al_2O_3 / 4 V / 1800 s / compressed air (sample Zn 17)
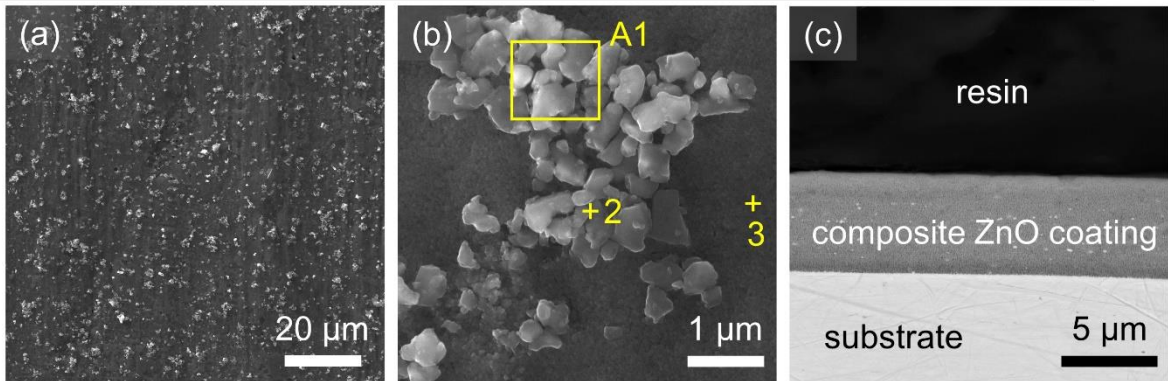
0.5 M NaOH + 6 g/L Al_2O_3 / 4 V / 1800 s / magnetic stirring (sample Zn 18)
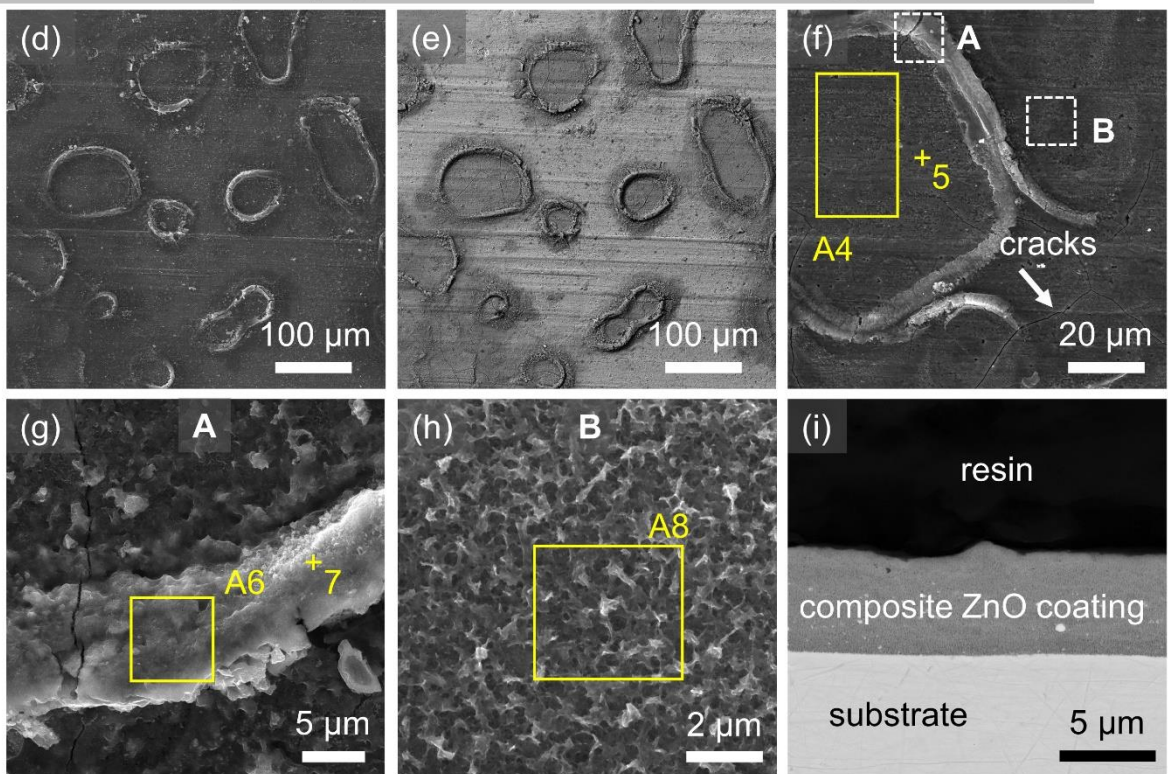
Fig. 62 Micrographs of composite anodic coatings (a, b, d-h) top surface, and (c, i) cross-section produced in the composite electrolyte under different types of agitation of the electrolyte during anodizing - (a-d) compressed air, (a-h) magnetic stirring; (a, b, d, f-h) SEM-SE, (c, e, i) SEM-BSE.

Table 24 EDX analysis of anodized samples (Zn 17 and Zn 18) and selected points and larger areas after anodizing under different conditions. The points and areas are shown in Fig. 62.

	Position	Element (wt.%)			
		O	Zn	Na	Al
surface analysis (0.64 mm²)	compressed air	16.7	76.4	3.3	3.6
	magnetic stirring	17.2	78.1	4.1	0.6
local analysis	A1	26.2	48.6	1.6	23.6
	2	30.1	40.3	1.1	28.5
	3	15.1	82.2	1.8	0.9
	A4	14.6	83.0	1.3	1.1
	5	15.7	79.6	2.5	2.2
	A6	22.3	74.4	2.1	1.2
	7	25.7	69.8	4.0	0.5
	A8	20.9	76.9	1.8	0.4

4.3.4. Closing remarks on anodizing of ZnTi2 alloy

Anodizing conditions, including the type and concentration of the electrolyte, voltage, anodizing time, and the agitation mechanism on the deposition of Al_2O_3 particles from the electrolyte, have been applied to ZnTi2 substrate to produce anodic oxide coatings. The effect of the above-mentioned conditions on the resulting morphology, structure and thickness was examined, and the conclusions can be listed as follow:

Effect of the type of electrolyte:

- Anodic coatings were successfully produced *via* a one-step potentiostatic anodizing process of ZnTi2 sheet in the NaOH, KOH, and $C_2H_2O_4$ electrolytes at 21 °C and in a voltage range of 4-50 V.
- Using the NaOH and KOH electrolyte, a similar electrochemical behaviour during the anodizing processes was recorded (i.e. current density decreased with anodizing time) and similar coatings with granular surface morphology were produced.
- When the $C_2H_2O_4$ electrolyte was used, the anodizing process was speedy (i.e. current density rapidly decreased with anodizing time). Thinner coatings with nano-rock or nano-flower surface morphology were produced.
- Based on earlier results, the NaOH solution was selected as a suitable electrolyte for the following experiments.

Effect of applied voltage:

- The higher voltage (50 V) resulted in vigorous gas evolution during the anodizing process, which led to the appearance of horizontal cracks and gaps inside the coatings.
- Decreasing the voltage from 50 to 4 V resulted in the production of a thinner coating with a different structure and appearance. Coatings produced at 50 V in the NaOH electrolyte were white in appearance with cracks and nanorod bulk-like structure, while coatings produced at ≤ 6 V were black with porous sponge-like structure. A finer and more granular surface structure was found for coatings produced at higher voltages. Both types of coatings were polycrystalline ZnO with hexagonal (wurtzite) structure and consisted of overlapping ZnO crystalline grains.
- The applied voltage played a crucial role in determining the morphology and structure of ZnO coating and also had a more significant effect on the coating thickness than the electrolyte concentration. The structure of the formed coating is related to the appearance of the formed coating.

Effect of NaOH electrolyte concentration:

- With increasing electrolyte concentration, thicker coatings with bulk-like structure, smoother granular morphology and vertical cracks were produced.
- Electrolyte concentration affected the structure only slightly.

Effect of anodizing time:

- With increasing the anodizing time, thicker ZnO coatings were produced. At the higher anodizing voltage of 50 V, the increase in thickness was not so significant as in the case of applying the lower voltage of 4 V.

Effect of agitation mechanism on Al_2O_3 particles deposition directly from the electrolyte:

- Addition of Al_2O_3 particles directly to electrolyte did not affect the morphology and thickness of the produced composite anodic coatings.
- Using compressed air agitation during the anodizing process resulted in uniform distribution of Al_2O_3 particles in the coating.
- Using the magnetic stirring mechanism during the anodizing process had a negative effect on the deposition of non-uniform Al_2O_3 particles and on the inhomogeneous surface morphology of produced coatings.

5. Conclusions

To summarize, this thesis dealt with the development of technological process of anodizing of aluminium alloy (AA1050), pure magnesium (99.9% Mg) and zinc alloy (ZnTi2). The aim was to produce anodic coatings with higher hardness and tribological properties compared to the initial substrate and to systematically study and understand the effect of mechanical pre-treatment and individual anodizing conditions, i.e. current density/voltage, temperature, concentration and composition of the electrolyte, on the properties of produced coatings. One of the essential tasks was to prepare stable electrolyte containing Al_2O_3 particles or a mixture of Al_2O_3 and PTFE particles. This was achieved by using the SDBS (sodium dodecylbenzenesulfonate) anionic surfactant, Al_2O_3 nanoparticles and 60% PTFE suspension.

The first experimental part of the thesis is focused on aluminium alloy (AA1050), which contains intermetallic phase particles based on Al-Fe and Al-Fe-Si compounds, with irregular-shape and round-shape. The results showed that the electrolyte temperature and current density had a significant effect on the properties of produced porous anodic aluminium oxide (PAAO) coatings. Decreasing the temperature during the galvanostatic anodizing at 3 A/dm^2 in the sulfuric-oxalic acid electrolyte led to the formation of thicker and harder PAAO coatings, which however contained microcracks and hillocks on the coating surfaces. At a higher anodizing current density, the increased sulfur content suggested the incorporation of sulfate ions in the PAAO coating. In the current *vs* time curves after reaching the voltage maximum, an unusual area was recorded for the higher current densities 3 and 2 A/dm^2, which was ascribed to the incorporation of the sulfate ions in the growing coating. The porous composite AAO coating without structural defects (hillocks and microcracks) and with the best combination of mechanical properties, such as high hardness, low COF, and high wear resistance was produced by the galvanostatic anodizing process at a low current density (1 A/dm^2), and low temperature (10 °C) in an electrolyte with the addition of 6 g/L Al_2O_3 and 15 mL/L 60% PTFE suspension. Intermetallic phase particles were preferably oxidized at the low electrolyte temperature, and the oxidation rate of these phase particles was lower when a lower anodizing current density was applied.

The second set of experiments were focused on anodizing of pure magnesium in the sodium hydroxide (NaOH) electrolyte. The use of voltage had a significant effect on the morphology and thickness of the produced anodic coatings. A thicker and denser magnesium hydroxide ($Mg(OH)_2$) coating was produced with a rough surface at a lower voltage of 4 V. The coating produced in the NaOH electrolyte containing Al_2O_3 and PTFE particles at 4 V was non-compact. On the other hand, coatings produced at a higher voltage ($\geq$ 10 V) were compact and contained Al_2O_3 and PTFE particles. Further investigation and testing are necessary to be done in this area topic; for example, applying lower voltage, corrosion resistance testing and nanoindentation testing.

The final experiments were focused on anodizing of ZnTi2. Two different types of coatings were produced, referred to as "black" and "white". Black, thinner and porous coatings with the sponge-like structure were produced at a lower voltage of 4 V in the 0.3-1 M NaOH

electrolyte. White, thicker coatings composed of nanorod bulk-like structure with compact granular morphology on the surface were produced at 50 V in the 0.04 and 0.1 M NaOH electrolyte. Due to higher oxygen evolution during the anodizing process at the higher voltage, produced coatings contained horizontal cracks and gaps. The applied voltage plays an important role in determining the morphology and appearance while higher concentrations and longer anodizing times give rise to bulk-like ZnO coatings with smaller pore size. The compressed air agitation during the anodizing process in the stable electrolyte containing 6 g/L Al_2O_3 particles led to the formation of a composite coating with uniform distribution of Al_2O_3 particles in the coating.

The anodizing process of aluminium, magnesium and zinc cannot be compared because each material requires a different pre-treatment and different anodizing conditions (i.e. type and temperature of the electrolyte, voltage/current density). Aluminium is preferably anodized in the acidic bath, commonly containing sulfuric acid, oxalic acid or their mixture, yielding a porous anodic aluminium oxide coating with parallel hexagonal pores oriented normal to the surface. At low electrolyte temperatures and high current densities, thicker and harder coatings are produced. Magnesium and zinc are preferably anodized in an alkaline electrolyte (i.e. NaOH, KOH). With increasing voltage, smoother and thinner anodic magnesium hydroxide coatings are produced. Darker anodic ZnO coatings with the sponge-like structure are produced at a low voltaklage and higher concentration of the NaOH electrolyte. On the other hand, white anodic ZnO coatings with bulk-like structure and horizontal cracks and gaps are produced at a high voltage and low electrolyte concentration. Addition of secondary particles (Al_2O_3 and PTFE) directly to the electrolyte have a positive effect on the hardness and tribological properties.

6. Suggested future work

Although the anodizing process has been known for decades, there is still room for research and development, for both academic and industrial reasons. Further research in this field can continue; for example, anodizing of zinc is still not sufficiently described in the literature. Zinc oxide is a promising material for biomedicine, photoelectrochemical and photocatalytic applications, sensor devices and thus, systematic studies are required among others. For example, the study of the effect of current density/voltage and type, temperature, and electrolyte concentration on ZnO coating growth and morphology attract attention. Adding secondary particles directly to the electrolyte has proved to be a suitable way to achieve the required properties of produced anodic coatings, but only a few scientific papers have been published in this respect.

References

[1]   SALMAN, S. A. and M. OKIDO. Anodization of magnesium (Mg) alloys to improve corrosion resistance. *Corrosion Prevention of Magnesium Alloys*. Elsevier, 2013, pp. 197-231. ISBN 9780857094377. DOI: 10.1533/9780857098962.2.197

[2]   SONG, G.-L. and Z. SHI. Anodization and corrosion of magnesium (Mg) alloys. *Corrosion Prevention of Magnesium Alloys*. Elsevier, 2013, pp. 232-281. ISBN 9780857094377. DOI: 10.1533/9780857098962.2.197

[3]   GOUEFFON, Y., L. ARURAULT, C. MABRU, C. TONON and P. GUIGUE. Black anodic coatings for space applications: Study of the process parameters, characteristics and mechanical properties. *Journal of Materials Processing Technology*. 2009, vol. 209, no. 11, pp. 5145-5151. DOI: 10.1016/j.jmatprotec.2009.02.013

[4]   BRALLA, J. G. *Handbook of manufacturing processes: how products, components and materials are made*. New York: Industrial Press, 2007. ISBN 9780831131791

[5]   GROOVER, M. P. *Fundamentals of modern manufacturing: materials, processes and systems*. New York: Wiley Global Education, 2012. ISBN 9781118476550

[6]   VOON, C. H., M. N. DERMAN, U. HASHIM, B. Y. LIM, S. T. SAM, K. L. FOO and S. T. TEN. Synthesis of Nanoporous Zinc Oxide by Anodizing of Zinc in Distilled Water. *Applied Mechanics and Materials*. 2015, vol. 754-755, pp. 1126-1130. DOI: 10.4028/www.scientific.net/AMM.754-755.1126

[7]   SULKA, G. D. Highly Ordered Anodic Porous Alumina Formation by Self-Organized Anodizing. *Nanostructured Materials in Electrochemistry*. Weinheim, Germany: Wiley-VCH Verlag, 2008. ISBN 9783527621507. DOI: 10.1002/9783527621507.ch1

[8]   EDITED BY H. DONG. *Surface engineering of light alloys aluminium, magnesium and titanium alloys*. Boca Raton: CRC Press, 2010. ISBN 9781845699451

[9]   JIANG, B. L. and Y. F. GE. Micro-arc oxidation (MAO) to improve the corrosion resistance of magnesium (Mg) alloys. *Corrosion Prevention of Magnesium Alloys*. Elsevier, 2013, pp. 163-196. DOI: 10.1533/9780857098962.2.163

[10]   P. G. SHEASBY. *The surface treatment and finishing of aluminium and its alloys*. 6. ed. Metals, Ohio: ASM International, 2001. ISBN 0904477215

[11]   VAGASKÁ, A., E. FECHOVÁ, P. MICHAL and M. GOMBÁR. The Influence of Input Factors of Aluminium Anodizing Process on Resulting Thickness and Quality of Aluminium Oxide Layer. *Procedia Engineering*. 2016, vol. 149, pp. 512-519. DOI: 10.1016/j.proeng.2016.06.699

[12]   WIELAGE, B., G. ALISCH, T. LAMPKE and D. NICKEL. Anodizing - A Key for Surface Treatment of Aluminium. *Key Engineering Materials*. 2008, vol. 384, pp. 263-281. DOI: 10.4028/www.scientific.net/KEM.384.263

[13] SU, Z. and W. ZHOU. Porous Anodic Metal Oxides. *Science Foundation in China*. 2008, vol. 16, no. 1, pp. 36-53. DOI: 10.1088/1005-0841/16/1/004

[14] LEE, W. and S.-J. PARK. Porous Anodic Aluminum Oxide: Anodization and Templated Synthesis of Functional Nanostructures. *Chemical Reviews*. 2014, vol. 114, no. 15, pp. 7487-7556. DOI: 10.1021/cr500002z

[15] SU, Z., G. HÄHNER and W. ZHOU. Investigation of the pore formation in anodic aluminium oxide. *Journal of Materials Chemistry*. 2008, vol. 18, no. 47, pp. 5787-5795. DOI: 10.1039/b812432a

[16] MIZUTANI, Y., S. J. KIM, R. ICHINO and M. OKIDO. Anodizing of Mg alloys in alkaline solutions. *Surface and Coatings Technology*. 2003, vol. 169-170, pp. 143-146. DOI: 10.1016/S0257-8972(03)00214-7

[17] KIM, S. J. and M. OKIDO. The electrochemical properties and mechanism of formation of anodic oxide films on Mg-Al alloys. *Bulletin-Korean chemical society*. 2003, vol. 24, no. 8, pp. 975-980. DOI: 10.5012/bkcs.2003.24.7.975

[18] GILANI, S., M. GHORBANPOUR and A. PARCHEHBAF JADID. Antibacterial activity of ZnO films prepared by anodizing. *Journal of Nanostructure in Chemistry*. 2016, vol. 6, no. 2, pp. 183-189. DOI: 10.1007/s40097-016-0194-1

[19] HU, Z., Q. CHEN, Z. LI, Y. YU and L.-M. PENG. Large-Scale and Rapid Synthesis of Ultralong ZnO Nanowire Films via Anodization. *The Journal of Physical Chemistry C*. 2010, vol. 114, pp. 881-889. DOI: 10.1021/jp9094744

[20] RAMIREZ-CANON, A., D. O. MILES, P. J. CAMERON and D. MATTIA. Zinc oxide nanostructured films produced via anodization: a rational design approach. *RSC Advances*. 2013, vol. 3, pp. 25323-25330. DOI: 10.1039/C3RA43886D

[21] ZHANG, X. G. *Corrosion and electrochemistry of zinc*. New York: Plenum Press, 1996. ISBN 0306453347

[22] MILES, D. O., P. J. CAMERON and D. MATTIA. Hierarchical 3D ZnO nanowire structures via fast anodization of zinc. *Journal of Material Chemistry A*. 2015, vol. 3, pp. 17569-17577. DOI: 10.1039/C5TA03578C

[23] FERREIRA, M. G. S., M. L. ZHELUDKEVICH and J. TEDIM. Advanced protective coatings for aeronautical applications. *Nanocoatings and Ultra-Thin Films*. Elsevier, 2011, pp. 235-279. DOI: 10.1533/9780857094902.2.235

[24] EDITED BY D. DILLARD. *Advances in structural adhesive bonding*. Cambridge: Woodhead Pub, 2010. ISBN 9781845698058

[25] EBNESAJJAD, S. and C. F. EBNESAJJAD. *Surface Treatment of Materials for Adhesive Bonding*. 2nd ed. Burlington: Elsevier Science, 2013. ISBN 9780323265041

[26] KOCK, E., M. BENEKE, C. GERLACH and AIRBUS DEUTSCHLAND GMBH. *Method for anodizing aluminum materials: CA2491095 C*. 2004.

[27]   EDITED BY L. J. DURNEY. *Electroplating engineering handbook*. 4th ed. London: Chapman & Hall, 1996. ISBN 9780412741104

[28]   *Aluminum and aluminum alloys*. Materials Park, OH: ASM International, 1993. ISBN 9780871704962

[29]   EDITED BY M. G. FONTANA and R. W. STAEHLE. *Advances in Corrosion Science and Technology Volume 1*. Boston, MA: Springer US, 1995. ISBN 9781461582526

[30]   TOTTEN, G. E. and D. S. MACKENZIE. *Handbook of aluminum*. Basel: M. Dekker, 2003. ISBN 0824708962

[31]   HENLEY, V. F. *Anodic oxidation of aluminium and its alloys*. New York: Pergamon Press, 1982. ISBN 0080267262

[32]   YLI-PENTTI, A. Electroplating and Electroless Plating. *Comprehensive Materials Processing*. Elsevier, 2014, pp. 277-305. DOI:10.1016/B978-0-08-096532-1.00413-1

[33]   MANG, T., K. BOBZIN and T. BARTELS. *Industrial tribology: tribosystems, friction, wear and surface engineering, lubrication*. Weinheim: Wiley-VCH, 2011. ISBN 9783527320578

[34]   GHALI, E. *Corrosion resistance of aluminum and magnesium alloys: understanding, performance, and testing*. Hoboken: Wiley, 2010. ISBN 9780471715764

[35]   FRIEDRICH, H. E. and B. L. MORDIKE. *Magnesium technology: metallurgy, design data, applications*. New York: Springer, 2006. ISBN 9783540205999

[36]   PORTER, F. *Corrosion resistance of zinc and zinc alloys*. New York: M. Dekker, 1994. ISBN 0824792130

[37]   VOON, C. H., B. Y. LIM, U. HASHIM, M. K. MD ARSHAD, S. T. SAM, K. L. FOO and S. T. TEN. Effect of Temperature of Distilled Water on the Morphology of Nanoporous Zinc Oxide Synthesized by Anodizing. *Applied Mechanics and Materials*. 2015, vol. 754-755, pp. 1131-1135. DOI: 10.4028/www.scientific.net/AMM.754-755.1131

[38]   ROCCA, E., D. VEYS-RENAUX and K. GUESSOUM. Electrochemical behavior of zinc in KOH media at high voltage: Micro-arc oxidation of zinc. *Journal of Electroanalytical Chemistry*. 2015, vol. 754, pp. 125-132. DOI: 10.1016/j.jelechem.2015.06.021

[39]   YAMAGUCHI, Y., M. YAMAZAKI, S. YOSHIHARA and T. SHIRAKASHI. Photocatalytic ZnO films prepared by anodizing. *Journal of Electroanalytical Chemistry*. 1998, vol. 442, pp. 1-3. DOI: 10.1016/S0022-0728(97)00354-9

[40]   SHETTY, A. and K. K. NANDA. Synthesis of zinc oxide porous structures by anodization with water as an electrolyte. *Applied Physics A*. 2012, vol. 109, pp. 151-157. DOI: 10.1007/s00339-012-7023-2

[41]   DIOMIDIS, N. and J.-P. CELIS. Effect of hydrodynamics on zinc anodizing in silicate-based electrolytes. *Surface and Coatings Technology*. 2005, vol. 195, no. 2-3, pp. 307-313. DOI: 10.1016/j.surfcoat.2004.07.100

[42]   SPATHIS, P. and I. POULIOS. The corrosion and photocorrosion of zinc and zinc oxide coatings. *Corrosion Science*. 1995, vol. 37, no. 5, pp. 673-680. DOI: 10.1016/0010-938X(95)80001-8

[43]   SINGH, M. and G. DAS. Highly ordered anodic porous alumina membrane and its surface modification approaches for biomedical application. *Journal of Applied Chemistry*. 2014, vol. 7, pp. 17-34. DOI: 10.9790/5736-07111734

[44]   SALMAN, S. A., R. MORI, R. ICHINO and M. OKIDO. Effect of Anodizing Potential on the Surface Morphology and Corrosion Property of AZ31 Magnesium Alloy. *Materials transactions*. 2010, vol. 51, no. 6, pp. 1109-1113. DOI: 10.2320/matertrans.M2009380

[45]   SILVA, L. F. M., A. ÖCHSNER and R. D. ADAMS. *Handbook of adhesion technology*. Heidelberg: Springer, 2011. ISBN 9783642011689

[46]   EVANGELISTI, F., M. STIEFEL and O. GUSEVA. Electronic and structural characterization of barrier-type amorphous aluminium oxide. *Electrochimica Acta*. 2017, vol. 224, pp. 503-516. DOI: 10.1016/j.electacta.2016.12.090

[47]   KANNADASSAN, D., R. KARTHIK, M. S. BHAGINI and P. S. MALLICK. Nanostructured Barrier Type Anodic Oxide Metal-Insulator-Metal Capacitors. *Journal of Nanoelectronics and Optoelectronics*. 2012, vol. 7, no. 4, pp. 400-404. DOI: 10.1166/jno.2012.1317

[48]   HERNÁNDEZ-LÓPEZ, J. M., A. NĚMCOVÁ and X. L. ZHONG. Formation of barrier-type anodic films on ZE41 magnesium alloy in a fluoride/glycerol electrolyte. *Electrochimica Acta*. 2014, vol. 138, pp. 124-131. DOI: 10.1016/j.electacta.2014.05.147

[49]   LIN, Y., Q. LIN, X. LIU, Y. GAO, J. HE, W. WANG and Z. FAN. A Highly Controllable Electrochemical Anodization Process to Fabricate Porous Anodic Aluminum Oxide Membranes. *Nanoscale Research Letters*. 2015, vol. 10, no. 495, pp. 1-8. DOI: 10.1186/s11671-015-1202-y

[50]   KELLER, F., M. S. HUNTER and D. L. ROBINSON. Structural Features of Oxide Coatings on Aluminum. *Journal of the Electrochemical Society*. 1953, vol. 100, no. 9, pp. 411-419.

[51]   WU, C. S., Z. ZHANG, F. H. CAO, L. J. ZHANG, J. Q. ZHANG and C. N. CAO. Study on the anodizing of AZ31 magnesium alloys in alkaline borate solutions. *Applied Surface Science*. 2007, vol. 253, no. 8, pp. 3893-3898. DOI: 10.1016/j.apsusc.2006.08.020

[52]   KOBAYASHI, Y., H. ASOH and S. ONO. Structure and Photocatalytic Property of Zinc Oxide Film Prepared by Anodizing. *Journal of the Surface Finishing Society of Japan*. 2009, vol. 60, no. 3, pp. 202-207. DOI: 10.4139/sfj.60.202

[53]   PENG, L. and M. LI. Improved Technology for Hard Anodizing Dissolution of Aluminum Alloy Part. *The Open Materials Science Journal*. 2015, vol. 9, pp. 82-85. DOI: 10.2174/1874088X01509010082

[54]   LOSIC, D. and A. SANTOS, ed. *Nanoporous Alumina: Fabrication, Structure, Properties and Applications*. Springer. 2015, vol. 219. DOI: 10.1007/978-3-319-20334-8.

[55]   ARYSLANOVA, E. M., A. V. ALFIMOV and S. A. CHIVILIKHIN. Modelling the growth process of porous aluminum oxide film during anodization. *Journal of Physics: Conference Series*. IOP Publishing. 2015, vol. 643, pp. 1-4. DOI: 10.1088/1742-6596/643/1/012008

[56]   PARKHUTIK, V. P. and V. I. SHERSHULSKY. Theoretical modelling of porous oxide growth on aluminium. *Journal of Physics D: Applied Physics*. 1992, vol. 25, no. 8, pp. 1258-1263. DOI: 10.1088/0022-3727/25/8/017

[57]   CHAUSSUMIER, M., C. MABRU, R. CHIERAGATTI and M. SHAHZAD. Fatigue Life Model for 7050 Chromic Anodized Aluminium Alloy. *Procedia Engineering*. 2013, vol. 66, pp. 300-312. DOI: 10.1016/j.proeng.2013.12.085

[58]   ŠTEFAN, M, I. LUKÁČ, V. OČENÁČEK, R. KOŘENÝ, J. DRÁPAL, H. SCHNEIDER AND A. MIŠKUFOVÁ. *Encyklopedie hliníku*. Děčín: Alcan Děčín Extrusions, 2005. ISBN 8089041884

[59]   VEYS-RENAUX, D., N. CHAHBOUN and E. ROCCA. Anodizing of multiphase aluminium alloys in sulfuric acid: in-situ electrochemical behaviour and oxide properties. *Electrochimica Acta*. 2016, vol. 211, pp. 1056-1065. DOI: 10.1016/j.electacta.2016.06.131

[60]   RIDDAR, F., S. HOGMARK and A. K. RUDOLPHI. Comparison of anodised aluminium surfaces from four fabrication methods. *Journal of Materials Processing Technology*. 2012, vol. 212, no. 11, pp. 2272-2281. DOI: 10.1016/j.jmatprotec.2012.06.007

[61]   KAYE, A. and A. STREET. *Die Casting Metallurgy: A volume in Butterworths Monographs in Materials*. Elsevier, 1982. ISBN 9781483163390

[62]   KHAN, S. A., Y. MIYASHITA, Y. MUTOH and T. KOIKE. Effect of anodized layer thickness on fatigue behavior of magnesium alloy. *Materials Science and Engineering: A*. 2008, vol. 474, no. 1-2, pp. 261-269. DOI: 10.1016/j.msea.2007.04.078

[63]   KREIBICH V. and V. OSTRÁ. Chyby při eloxování hliníku a jeho slitin. *Povrcháři*. 2009, vol. 3, pp. 3-5. ISSN 1802-9833

[64]   PROBERT, R. H. *Aluminum how to: The Chromatizing, Anodizing, Hard Coating Handbook*. Tailored Text, 2005

[65]   THEOHARI, S. and C. KONTOGEORGOU. Effect of temperature on the anodizing process of aluminum alloy AA 5052. *Applied Surface Science*. 2013, vol. 284, pp. 611-618. DOI: 10.1016/j.apsusc.2013.07.141

[66]   DE OLIVEIRA, M. C. L., V. S. M. PEREIRA, O. V. CORREA and R. A. ANTUNES. Corrosion Performance of Anodized AZ91D Magnesium Alloy: Effect of the Anodizing Potential on the Film Structure and Corrosion Behavior. *Journal of Materials Engineering and Performance*. 2014, vol. 23, no. 2, pp. 593-603. DOI: 10.1007/s11665-013-0755-0

[67]   ZHANG, D., Y. GOU, Y. LIU and X. GUO. A composite anodizing coating containing superfine Al2O3 particles on AZ31 magnesium alloy. *Surface and Coatings Technology*. 2013, vol. 236, pp. 52-57. DOI: 10.1016/j.surfcoat.2013.04.059

[68]   AERTS, T., T. DIMOGERONTAKIS, I. DE GRAEVE, J. FRANSAER and H. TERRYN. Influence of the anodizing temperature on the porosity and the mechanical properties of the porous anodic oxide film. *Surface and Coatings Technology*. 2007, vol. 201, no. 16-17, pp. 7310-7317. DOI: 10.1016/j.surfcoat.2007.01.044

[69]   SANKARA NARAYANAN, T. S. N. and M. H. LEE. Incorporation of ZrO2 particles in the oxide layer formed on Mg by anodizing: Influence of electrolyte concentration and current modes. *Journal of Colloid and Interface Science*. 2016, vol. 464, pp. 36-47. DOI: 10.1016/j.jcis.2015.11.011

[70]   CHEN, S., C. KANG, J. WANG, C. LIU and K. SUN. Synthesis of anodizing composite films containing superfine Al2O3 and PTFE particles on Al alloys. *Applied Surface Science*. 2010, vol. 256, no. 22, pp. 6518-6525. DOI: 10.1016/j.apsusc.2010.04.040

[71]   CHENG, T.-C. and C.-C. CHOU. The Electrical and Mechanical Properties of Porous Anodic 6061-T6 Aluminum Alloy Oxide Film. *Journal of Nanomaterials*. 2015, vol. 2015, pp. 1-5. DOI: 10.1155/2015/371405

[72]   GUEZMIL, M., W. BENSALAH, A. KHALLADI, K. ELLEUCH, M. DEPETRIS-WERY and H.F. AYEDI. Friction coefficient and microhardness of anodized aluminum alloys under different elaboration conditions. *Transactions of Nonferrous Metals Society of China*. 2015, vol. 25, no. 6, pp. 1950-1960. DOI: 10.1016/S1003-6326(15)63803-1

[73]   SAENZ DE MIERA, M., M. CURIONI, P. SKELDON and G.E. THOMPSON. The behaviour of second phase particles during anodizing of aluminium alloys. *Corrosion Science*. 2010, vol. 52, no**.** 7, pp. 2489-2497. DOI: 10.1016/j.corsci.2010.03.029

[74]   PALAGONIA, M. S., A. NĚMCOVA, I. KUBĚNA. Behavior of Alloying Elements during Anodizing of Mg-Cu and Mg-W Alloys in a Fluoride/Glycerol Electrolyte. *Journal of the Electrochemical Society*. 2015, vol. 162, no. 9, pp. C487-C494. DOI: 10.1149/2.0761509jes

[75]   SCHLÖGL, C. M. and H. ANTREKOWITSCH. Impact of different alloying additives and pre-treatments on the anodising behaviour of AA2007. *Surface and Interface Analysis*. 2016, vol. 48, no. 8, pp. 939-945. DOI: 10.1002/sia.5899

[76]   ZHU, B., S. SEIFEDDINE, P. O. A. PERSSON, A. E. W. JARFORS, P. LEISNER and C. ZANELLA. A study of formation and growth of the anodised surface layer on cast Al-Si alloys based on different analytical techniques. *Materials and Design*. 2016, vol. 101, pp. 254-262. DOI: 10.1016/j.matdes.2016.04.013

[77]   FORN, A., J. A. PICAS, M. T. BAILE, E. MARTIN and V.G. GARCÍA. Microstructure and tribological properties of anodic oxide layer formed on Al–Si alloy produced by semisolid processing. *Surface and Coatings Technology*. 2007, vol. 202, no. 4, pp. 1139-1143. DOI: 10.1016/j.surfcoat.2007.07.070

[78]   LI, X., X. NIE, L. WANG and D. O. NORTHWOOD. Corrosion protection properties of anodic oxide coatings on an Al–Si alloy. *Surface and Coatings Technology*. 2005, vol. 200, no. 5-6, pp. 1994-2000. DOI: 10.1016/j.surfcoat.2005.08.019

[79]   RATILA-APACHITEI, L. E., F. D. TICHELAAR, G. E. THOMPSON, H. TERRYN, P. SKELDON, J. DUSZCZYK and L. KATGERMAN. A transmission electron microscopy study of hard anodic oxide layers on AlSi(Cu) alloys. *Electrochimica Acta*. 2004, vol. 49, no. 19, pp. 3169-3177. DOI: 10.1016/j.electacta.2004.02.030

[80]   FRATILA-APACHITEI, L. E., H. TERRYN, P. SKELDON, G. E. THOMPSON, J. DUSZCZYK and L. KATGERMAN. Influence of substrate microstructure on the growth of anodic oxide layers. *Electrochimica Acta*. 2004, vol. 49, no. 7, pp. 1127-1140. DOI: 10.1016/j.electacta.2003.10.024

[81]   SHAHZAD, M., M. CHAUSSUMIER, R. CHIERAGATTI, C. MABRU and F. REZAI-ARIA. Influence of anodizing process on fatigue life of machined aluminium alloy. *Procedia Engineering*. 2010, vol. 2, no. 1, pp. 1015-1024. DOI: 10.1016/j.proeng.2010.03.110

[82]   SHAHZAD, M., M. CHAUSSUMIER, R. CHIERAGATTI, C. MABRU and F. REZAI ARIA. Influence of surface treatments on fatigue life of Al 7010 alloy. *Journal of Materials Processing Technology*. 2010, vol. 210, no. 13, pp. 1821-1826. DOI: 10.1016/j.jmatprotec.2010.06.019

[83]   RAYMOND F. WEGMAN and J. TWISK. *Surface Preparation Techniques for Adhesive Bonding*. 2nd ed. Burlington: Elsevier Science, 2013. DOI: 10.1016/C2012-0-02158-8

[84] SASTRI, V. S. *Green corrosion inhibitors theory and practice*. Hoboken, N.J: Wiley, 2013. ISBN 9781118015414

[85] BONONI, M., R. GIOVANARDI, A. B. OZZA and P. MATTIOLI. Pulsed current effect on hard anodizing process of 2024-T3 aluminium alloy. *Surface and Coatings Technology*. 2016, vol. 289, pp. 110-117. DOI: 10.1016/j.surfcoat.2016.01.056

[86] SAIJO, A., K. MURAKAMI, M. HINO and T. KANADANI. Effect of Environmentally Friendly Anodization on the Mechanical Properties and Microstructure of AZ91D Magnesium Alloy. *Materials transactions*. 2008, vol. 49, no. 5, pp. 903-908. DOI: 10.2320/matertrans.MC200733

[87] KIM, M., H. YOO and J. CHOI. Non-nickel-based sealing of anodic porous aluminum oxide in NaAlO2. *Surface and Coatings Technology*. 2017, vol. 310, pp. 106-112. DOI: 10.1016/j.surfcoat.2016.11.100

[88] WANG, S., H. PENG, Z. SHAO, Q. ZHAO and N. DU. Sealing of anodized aluminum with phytic acid solution. *Surface and Coatings Technology*. 2016, vol. 286, pp. 155-164. DOI: 10.1016/j.surfcoat.2015.12.024

[89] ZUO, Y., P.-H. ZHAO and J.-M. ZHAO. The influences of sealing methods on corrosion behavior of anodized aluminum alloys in NaCl solutions. *Surface and Coatings Technology*. 2003, vol. 166, no. 2-3, pp. 237-242. DOI: 10.1016/S0257-8972(02)00779-X

[90] HAO, L. and B. R. CHENG. Sealing processes of anodic coatings-Past, present, and future. *Metal Finishing*. 2000, vol. 98, no. 12, pp. 8-18. DOI: 10.1016/S0026-0576(01)80002-7

[91] LEE, J., Y. KIM, H. JANG and W. CHUNG. Cr2O3 sealing of anodized aluminum alloy by heat treatment. *Surface and Coatings Technology*. 2014, vol. 243, pp. 34-38. DOI: 10.1016/j.surfcoat.2012.05.071

[92] SHANG, Y., WANG L., LIU Z., NIU D. and Y. WANG. The Effects of Different Sealing Techniques for Anodic Film of Al-12.7Si-0.7Mg Alloys. *International Journal of Electrochemical Science*. 2016, vol. 11, pp. 5234-5244. DOI: 10.20964/2016.06.85

[93] MAHALLAWY, N. A. E., M. A. SHOEIB and M. H. ABOUELENAIN. AZ91 Magnesium Alloys: Anodizing of Using Environmental Friendly Electrolytes. *Journal of Surface Engineered Materials and Advanced Technology*. 2011, vol. 1, pp. 62-72. DOI: 10.4236/jsemat.2011.12010

[94] LI, Q., J. LIANG and Q. WANG. Plasma Electrolytic Oxidation Coatings on Lightweight Metals. *Modern Surface Engineering Treatments*. InTech. 2013, pp. 75-99. DOI: 10.5772/55688

[95] EDITED BY S. C. CHA and A. ARDEMIR. *Coating Technology for Vehicle Applications*. Springer, 2015. ISBN 9783319147710

[96]   SANKARA NARAYANAN, T. S. N., I. S. PARK and M.-H. LEE. *Surface modification of magnesium and its alloys for biomedical applications*. Waltham, MA: Elsevier/Woodhead Publishing, 2015. DOI: 10.1016/C2013-0-16448-3

[97]   XIA, G., H. JIANG, R. LIU and Y. ZHAI. Effects of surfactant on the stability and thermal conductivity of Al2O3/de-ionized water nanofluids. *International Journal of Thermal Sciences*. 2014, vol. 84, pp. 118-124. DOI: 10.1016/j.ijthermalsci.2014.05.004

[98]   LI, S., M. ZHU, J. LIU, M. YU, L. WU, J. ZHANG and H. LIANG. Enhanced tribological behavior of anodic films containing SiC and PTFE nanoparticles on Ti6Al4V alloy. *Applied Surface Science*. 2014, vol. 316, pp. 28-35. DOI: 10.1016/j.apsusc.2014.07.088

[99]   REMEŠOVÁ, M., L. KLAKURKOVÁ, M. HORYNOVÁ, L. ČELKO and J. KAISER. Preparation of Metallographic Samples with Anodic Layers. *Materials Science Forum*. 2017, vol. 891, pp. 106-110. DOI: 10.4028/www.scientific.net/MSF.891.106

[100]   ASTM G99-95a(2000)e1, Standard test method for wear testing with a pin-on-disk apparatus, ASTM International, West Conshohocken, PA, 2000. DOI: 10.1520/G0099-95AR00E01

[101]   GASTÓN-GARCÍA, B., E. GARCÍA-LECINA, J. A. DÍEZ, M. BELENGUER and C. MÜLLER. Local Burning Phenomena in Sulfuric Acid Anodizing: Analysis of Porous Anodic Alumina Layers on AA1050. *Electrochemical and Solid-State Letters*. 2010, vol. 13, no. 11. DOI: 10.1149/1.3478482

[102]   JARIYABOON, M., P. MØLLER, R.E. DUNIN-BORKOWSKI and R. AMBAT. FIB-SEM investigation of trapped intermetallic particles in anodic oxide films on AA1050 aluminium. *Anti-Corrosion Methods and Materials*. 2011, vol. 58, no. 4, pp. 173-178. DOI: 10.1108/00035591111148885

[103]   MONTERO-MORENO, J.M., M. SARRET and C. MÜLLER. Self-ordered porous alumina by two-step anodizing at constant current: Behaviour and evolution of the structure. *Microporous and Mesoporous Materials*. 2010, vol. 136, no. 1-3, pp. 68-74. DOI: 10.1016/j.micromeso.2010.07.022

[104]   KOROLEVA, E., G. E. THOMPSON, G. HOLLRIGL and M. BLOECK. Surface morphological changes of aluminium alloys in alkaline solution. *Corrosion Science*. 1999, vol. 41, no. 8, pp. 1475-1495. DOI: 10.1016/S0010-938X(98)00188-7

[105]   WITKOWSKA, M., G. E. THOMPSON, T. HASHIMOTO and E. KOROLEVA. Assessment of the surface reactivity of AA1050 aluminium alloy. *Surface and Interface Analysis*. 2013, vol. 45, no. 10, pp. 1585-1589. DOI: 10.1002/sia.5271

[106]   BU, S. D., Y. C. CHOI, J. Y. HYEON and T. S. BAE. Effects of Anodizing Voltages on the Pore Morphology Formation of Porous Anodic Aluminas and Corresponding Current Density Variations. *Journal of the Korean Physical Society*. 2009, vol. 55, pp. 835-840. DOI: 10.3938/jkps.55.835

[107]   TSANGARAKI-KAPLANOGLOU, I., S. THEOHARI, T. DIMOGERONTAKIS, Y.-M. WANG, H.-H. KUO and S. KIA. Effect of alloy types on the anodizing process of aluminum. *Surface and Coatings Technology*. 2006, vol. 200, no. 8, pp. 2634-2641. DOI: 10.1016/j.surfcoat.2005.07.065

[108]   MICHALSKA-DOMAŃSKA, M., M. NOREK, W. J. STĘPNIOWSKI and B. BUDNER. Fabrication of high quality anodic aluminum oxide (AAO) on low purity aluminium-A comparative study with the AAO produced on high purity aluminum. *Electrochimica Acta*. 2013, vol. 105, pp. 424-432. DOI: 10.1016/j.electacta.2013.04.160

[109]   ABDEL REHIM, S. S., H. H. HASSAN and M. A. AMIN. Galvanostatic anodization of pure Al in some aqueous acid solutions Part I: Growth kinetics, composition and morphological structure of porous and barrier-type anodic alumina films. *Journal of Applied Electrochemistry*. 2002, vol. 32, pp. 1257-1264. DOI: 10.1023/A:1021662814303

[110]   SULKA, G. D., S. STROOBANTS, V. MOSHCHALKOV, G. BORGHS and J.-P. CELIS. Synthesis of Well-Ordered Nanopores by Anodizing Aluminum Foils in Sulfuric Acid. *Journal of The Electrochemical Society*. 2002, vol. 149, no. 7. DOI: 10.1149/1.1481527

[111]   STĘPNIOWSKI, W. J., M. NOREK, M. MICHALSKA-DOMAŃSKA, A. BOMBALSKA, A. NOWAK-STĘPNIOWSKA, M. KWAŚNY and Z. BOJAR. Fabrication of anodic aluminum oxide with incorporated chromate ions. *Applied Surface Science*. 2012, vol. 259, pp. 324-330. DOI: 10.1016/j.apsusc.2012.07.043

[112]   PARKHUTIK, V. P., J. M. ALBELLA, Y. E. MAKUSHOK, I. MONTERO, J. M. MARTINEZ-DUART and V. I. SHERSHULSKII. Study of aluminium anodization in sulphuric and chromic acid solutions—I. Kinetics of growth and composition of oxides. *Electrochimica Acta*. 1990, vol. 35, no. 6, pp. 955-960. DOI: 10.1016/0013-4686(90)90027-W

[113]   HAKIMIZAD, A., K. RAEISSI and F. ASHRAFIZADEH. Characterization of aluminum anodized layers modified in sulfuric and phosphoric acid baths and their effect on conventional electrolytic coloring. *Surface and Coatings Technology*. 2012, vol. 206, no. 8-9, pp. 2438-2445. DOI: 10.1016/j.surfcoat.2011.10.046

[114]   WEI, P.-S. and T.-S. SHIH. Monitoring the Progressive Development of an Anodized Film on Aluminum. *Journal of The Electrochemical Society*. 2007, vol. 154, no. 11. DOI: 10.1149/1.2780864

[115] AERTS, T., I. DE GRAEVE and H. TERRYN. Study of initiation and development of local burning phenomena during anodizing of aluminium under controlled convection. *Electrochimica Acta*. 2008, vol. 54, no. 2, pp. 270-279. DOI: 10.1016/j.electacta.2008.08.004

[116] ROA, J. J., B. GASTÓN-GARCÍA, E. GARCÍA-LECINA and C. MÜLLER. Mechanical properties at nanometric scale of alumina layers formed in sulphuric acid anodizing under burning conditions. *Ceramics International*. 2012, vol. 38, no. 2, pp. 1627-1633. DOI: 10.1016/j.ceramint.2011.09.053

[117] REMEŠOVÁ, M., S. TKACHENKO, D. KVARDA, I. ROČŇÁKOVÁ, B. GOLLAS, M. MENELAOU, L. ČELKO and J. KAISER. Effects of anodizing conditions and the addition of Al2O3/PTFE particles on the microstructure and the mechanical properties of porous anodic coatings on the AA1050 aluminium alloy. *Applied Surface Science*. 2020, vol. 513. DOI: 10.1016/j.apsusc.2020.145780

[118] CHUNG, I. C., C. K. CHUNG and Y. K. SU. Effect of current density and concentration on microstructure and corrosion behavior of 6061 Al alloy in sulfuric acid. *Surface and Coatings Technology*. 2017, vol. 313, pp. 299-306. DOI: 10.1016/j.surfcoat.2017.01.114

[119] MOUTARLIER, V, M. P GIGANDET, J. PAGETTI and B. NORMAND. Influence of oxalic acid addition to chromic acid on the anodising of Al 2024 alloy. *Surface and Coatings Technology*. 2004, vol. 182, no. 1, pp. 117-123. DOI: 10.1016/S0257-8972(03)00875-2

[120] YOSHIMOTO, M., Y. MORIZONO, S. TSUREKAWA and T. BABA. Anodizing of aluminum in sulfuric acid and oxalic acid solutions with percarboxylic acid-based additive. *Journal of the Ceramic Society of Japan*. 2012, vol. 120, no. 1403, pp. 276-279. DOI: 10.2109/jcersj2.120.276

[121] FRATILA-APACHITEI, L. E., J. DUSZCZYK and L. KATGERMAN. Vickers microhardness of AlSi(Cu) anodic oxide layers formed in H2SO4 at low temperature. *Surface and Coatings Technology*. 2003, vol. 165, no. 3, pp. 309-315. DOI: 10.1016/S0257-8972(02)00750-8

[122] ZHANG, P. and Y. ZUO. Effects of pore parameters on performance of anodic film on 2024 aluminum alloy. *Materials Chemistry and Physics*. 2019, vol. 231, pp. 9-20. DOI: 10.1016/j.matchemphys.2019.04.008

[123] LIANG, J., L. HU and J. HAO. Preparation and characterization of oxide films containing crystalline TiO2 on magnesium alloy by plasma electrolytic oxidation. *Electrochimica Acta*. 2007, vol. 52, no. 14, pp. 4836-4840. DOI: 10.1016/j.electacta.2007.01.059

[124] LI, S.-M., X.-M. YU, J.-H. LIU, M. YU, L. WU and K. YANG. Microstructure and abrasive wear behaviour of anodizing composite films containing SiC nanoparticles on Ti6Al4V alloy. *Journal of Central South University*. 2014, vol. 21, no. 12, pp. 4415-4423. DOI: 10.1007/s11771-014-2443-0

[125] CHEN, M. H., K. C. KAO, M. W. TU and D. N. ZHANG. Self-Lubricating SiC/PTFE Composite Coating Formation on Surface of Aluminium Alloy. *Advanced Materials Research*. 2012, vol. 490-495, pp. 3511-351. DOI: 10.4028/www.scientific.net/AMR.490-495.3511

[126] ESCOBAR, J., L. ARURAULT and V. TURQ. Improvement of the tribological behavior of PTFE-anodic film composites prepared on 1050 aluminum substrate. *Applied Surface Science*. 2012, vol. 258, no. 20, pp. 8199-8208. DOI: 10.1016/j.apsusc.2012.05.022

[127] LU, J., G. WEI, Y. YU, C. GUO and L. JIANG. Aluminum alloy AA2024 anodized from the mixed acid system with enhanced mechanical properties. *Surfaces and Interfaces*. 2018, vol. 13, pp. 46-50. DOI: 10.1016/j.surfin.2018.08.003

[128] ZHU, B. and C. ZANELLA. Hardness and corrosion behaviour of anodised Al-Si produced by rheocasting. *Materials and Design*. 2019, vol. 173. DOI: 10.1016/j.matdes.2019.107764

[129] LI, S.-M., Y.-D. LI, Y. ZHANG, J.-H. LIU and M. YU. Effect of intermetallic phases on the anodic oxidation and corrosion of 5A06 aluminum alloy. *International Journal of Minerals, Metallurgy, and Materials*. 2015, vol. 22, no. 2, pp. 167-174. DOI: 10.1007/s12613-015-1057-3

[130] WU, H., Y. MA, W. HUANG, X. ZHOU, K. LI, Z. WANG and L: LIU. Effect of Iron-Containing Intermetallic Particles on Film Structure and Corrosion Resistance of Anodized AA2099 Alloy. *Journal of The Electrochemical Society*. 2018, vol. 165, no. 9, pp. C573-C581. DOI: 10.1149/2.1361809jes

[131] Páleníček, M., M. Papula, M. Remešová, D. Jech, I. Ročňáková and L. Čelko. Anodizing of Pure Magnesium in Sodium Hydroxide Electrolyte Solution. In Metallography and Fractography XVII. Materials Science Forum. Switzerland: Trans Tech Publications Ltd. 2019. ISBN: 978-3-0357-1018-2, in press.

[132] SALMAN, S. A., R. ICHINO and M. OKIDO. A Comparative Electrochemical Study of AZ31 and AZ91 Magnesium Alloy. *International Journal of Corrosion*. 2010, pp. 1-7. DOI: 10.1155/2010/412129

[133] KIM, S.-J., M. OKIDO, Y. MIZUTANI, R. ICHINO, S. TANIKAWA and S. HASEGAWA. Formation of Anodic Films on Mg-Al Alloys in NaOH solutions at Constant Potentials. *MATERIALS TRANSACTIONS*. 2003, vol. 44, no. 5, pp. 1036-1041. DOI: 10.2320/matertrans.44.1036

[134] BEEDRI, N. I., Y. A. INAMDAR, S. A. SAYYED, A. V. SHAIKH, S. R. JADKAR, and H. M. PATHAN. Electrochemical Anodization of Nano Crystalline ZnO Films in Acidic Bath and Their Properties. *Advanced Science Letters*, 2014, vol. 20, no. 5-6, pp. 1147-1150. DOI: 10.1166/asl.2014.5500

[135] REMEŠOVÁ, M., L. KLAKURKOVÁ, L. ČELKO, L. SLÁDKOVÁ, D. JECH and J. KAISER. Anodizing of Zinc-Titanium Alloy in NaOH and KOH Baths. *Solid State Phenomena*. 2016, vol. 258, pp. 399-402. DOI: 10.4028/www.scientific.net/SSP.258.399

[136] DONG, J., Z. LIU, J. DONG, D. ARIYANTI, Z. NIU, S. HUANG, W. ZHANG and W. GAO. Self-organized ZnO nanorods prepared by anodization of zinc in NaOH electrolyte. *RSC Advances*. 2016, vol. 6, no. 77, pp. 72968-72974. DOI: 10.1039/C6RA16995C

[137] MABON, J.C. and O.T. INAL. Optimization and evaluation of black zinc selective solar absorber surfaces. *Thin Solid Films*. 1984, vol. 115, no. 1, pp. 51-73. DOI: 10.1016/0040-6090(84)90316-X

[138] MIKA, K., R. P. SOCHA, P. NYGA, E. WIERCIGROCH, K. MALEK, M. JAROSY, T. UCHACY, G. S. SULKA and L. ZARASKA Electrochemical synthesis and characterization of dark nanoporous zinc oxide films. *Electrochimica Acta*. 2019, vol. 305, pp. 349-359. DOI: 10.1016/j.electacta.2019.03.052

List of abbreviations and symbols

Abbreviations

AA	aluminium alloy
AAO	anodic aluminium oxide
AC	alternating current
AMHC	anodic magnesium hydroxide coating
CAC	composite anodic coating
COF	coefficient of friction
DC	direct current
EDX	energy-dispersive X-ray spectroscopy
EELS	electron energy loss spectroscopy
FESEM	field emission scanning electron microscope/microscopy
FIB	focused ion beam
HRTEM	high-resolution transmission electron microscope
HV	Vicker hardness
MAO	micro-arc oxidation
PAAO	porous anodic aluminium oxide
PC	pulse current
PEO	plasma electrolytic oxidation
PTFE	polytetrafluoroethylene
SDBS	sodium dodecylbenzenesulfonate
SEM	scanning electron microscope/microscopy
SEM-BSE	backscattered electron mode of scanning electron microscope/microscopy
SEM-SE	secondary electron mode of scanning electron microscope/microscopy
TEM	transmission electron microscope/microscopy
XRD	X-ray difraction

Symbols

A	Ampere
C_{NaOH}	concentration of sodium hydroxide
cm	centimetre
dm^2	squere decimeter
g	gram
I	current
keV	kiloectron volts
L	litre
M	molar concentration
min	minute/minutes
mL	mililitre
mm	milimeter
N	Newton
nm	nanomilimeter
^{o}C	degree Celsium
pH	potential of hydrogen
s	seconds
t	time
V	Volt
wt.%	weight percent
μm	micrometre

A. List of authors scientific achievements

Authors scientific identifiers

Research ID: G-9563-2014
ORCID ID: 0000-0003-1678-5618

A.1. Publications in impact journal

REMEŠOVÁ, M.; TKACHENKO, S.; KVARDA, D.; ROČŇÁKOVÁ, I.; GOLLAS, B.; MENELAOU, M.; ČELKO, L.; KAISER, J. Effects of anodizing conditions and the addition of Al2O3/PTFE particles on the microstructure and the mechanical properties of porous anodic coatings on the AA1050 aluminium alloy. *Applied Surface Science,* 2020. DOI: 10.1016/j.apsusc.2020.145780

SLÁMEČKA, K.; JECH, D.; KLAKURKOVÁ, L; TKACHENKO, S.; REMEŠOVÁ, M.; GEJDOŠ, P.; ČELKO, L. Thermal cycling damage in pre-oxidized plasma-sprayed MCrAlY + YSZ thermal barrier coatings: Phenomenon of multiple parallel delamination of the TGO layer. *Surface and Coatings Technology.* 2020. DOI: 10.1016/j.surfcoat.2019.125328

HORYNOVÁ, M.; REMEŠOVÁ, M.; KLAKURKOVÁ, L.; DVOŘÁK, K.; ROČŇÁKOVÁ, I.; YAN, S.; ČELKO, L.; SONG, G. L. Design of tailored biodegradable implants: The effect of voltage on electrodeposited calcium phosphate Coatings on pure magnesium. *Journal of the American Ceramic Society,* 2019, pp. 123-135. DOI: 10.1111/jace.15888

ČELKO, L.; MENELAOU, M.; CASAS LUNA, M.; HORYNOVÁ, M.; MUSÁLEK, T.; REMEŠOVÁ, M.; DÍAZ DE LA TORRE, S.; MORSI, K.; KAISER, J. Spark Plasma Extrusion and the Thermal Barrier Concept. *Metallurgical and Materials Transactions B-process metallurgy and materials processing science,* 2019, pp. 656-665. DOI: 10.1007/s11663-018-1493-3

ROČŇÁKOVÁ, I.; SLÁMEČKA, K.; MONTUFAR JIMENEZ, E.; REMEŠOVÁ, M.; DYČKOVÁ, L.; BŘÍNEK, A.; JECH, D.; DVOŘÁK, K.; ČELKO, L.; KAISER, J. Deposition of Hydroxyapatite and Tricalcium Phosphate Coatings by Suspension Plasma Spraying: Effects of Torch Speed. *Journal of the European Ceramic Society,* 2018, pp. 5489-5496. DOI: 10.1016/j.jeurceramsoc.2018.08.007

KLAKURKOVÁ, L.; HORYNOVÁ, M.; JULIŠ, M.; GEJDOŠ, P.; SKALKA, P.; REMEŠOVÁ, M.; ČELKO, L. Failure analysis of massively failed compressed air cartridge. *ENGINEERING FAILURE ANALYSIS,* 2017, pp. 776-782. DOI: 10.1016/j.engfailanal.2017.07.016

SLÁDKOVÁ, L.; PROCHAZKA, D.; POŘÍZKA, P.; ŠKARKOVÁ, P.; REMEŠOVÁ, M.; HRDLIČKA, A.; NOVOTNÝ, K.; ČELKO, L.; KAISER, J. Improvement of the Laser-Induced Breakdown Spectroscopy method sensitivity by the usage of combination of Ag-nanoparticles and vacuum conditions. *Spectrochimica Acta Part B,* 2017, pp. 48-55. DOI: 10.1016/j.sab.2016.11.005

A.2. Contributions to conference proceedings indexed in WoS or Scopus

JECH, D.; REMEŠOVÁ, M.; KOMAROV, P.; TKACHENKO, S.; ČESÁNEK, Z.; SCHUBERT, J.; HOUDKOVÁ, Š.; ČELKO, L. Evaluation of Microstructure, Phase Composition and Hardness of Alternative Abradable Ceramic Coating Systems Produced by Means of Atmospheric Plasma Spraying. In *Binders, Materials and Technologies in Modern Construction V. Solid State Phenomena.* Switzerland: Trans Tech Publications, 2019, pp. 161-166. ISSN: 1662-9779.

DYČKOVÁ, L.; KOMAROV, P.; REMEŠOVÁ, M.; DYČKA, M.; DVOŘÁK, K.; MENELAOU, M.; ČELKO, L. Optimization of Molybdenum Powder Milling Parameters. *ОБРАБОТКА МЕТАЛЛОВ,* 2018, pp. 109-122. ISSN: 1994-6309.

REMEŠOVÁ, M.; KLAKURKOVÁ, L.; ROČŇÁKOVÁ, I.; DYČKOVÁ, L.; ČELKO, L.; KAISER, J. Application of Metallographic Analysis Techniques for Detection and Identification of Spray Paint Defects. In *Přínos metalografie pro řešení výrobních problémů. Solid State Phenomena.* 14. Switzerland: Trans Tech Publications, 2017, pp. 118-123. ISSN: 1662-9779.

DYČKOVÁ, L.; KLAKURKOVÁ, L.; GEJDOŠ, P.; REMEŠOVÁ, M.; JULIŠ, M.; ČELKO, L. Causal analysis of damage of a cover. In *Přínos metalografie pro řešení výrobních problémů. Solid State Phenomena.* 14. Switzerland: Trans Tech Publications, 2017, pp. 57-62. ISSN: 1662-9779.

PAVLOUŠKOVÁ, Z.; HORYNOVÁ, M.; KLAKURKOVÁ, L.; JULIŠ, M.; GEJDOŠ, P.; REMEŠOVÁ, M. Influence of microstructure on machinability of material and its final surface quality. In *Přínos metalografie pro řešení výrobních problémů. Solid State Phenomena.* 14. Switzerland: Trans Tech Publications, 2017, pp. 112-117. ISSN: 1662-9779.

HORYNOVÁ, M.; REMEŠOVÁ, M.; KLAKURKOVÁ, L.; JULIŠ, M.; GEJDOŠ, P.; DYČKOVÁ, L. Evaluation of surface degradation of deoxidized AW-AlMg0.7Si alloy. In *Přínos metalografie pro řešení výrobních problémů. Solid State Phenomena.* 14. Switzerland: Trans Tech Publications, 2017, pp. 136-141. ISSN:1662-9779.

ČELKO, L.; JECH, D.; KOMAROV, P.; REMEŠOVÁ, M.; DVOŘÁK, K.; ŠULÁK, I.; SMETANA, B.; OBRTLÍK, K. Failure mechanism of yttria stabilized zirconia atmospheric plasma sprayed thermal barrier coatings subjected to calcia-magnesia-aluminosilicate environmental attack. In *Přínos metalografie pro řešení výrobních problémů. Solid State Phenomena.* 14. Switzerland: Trans Tech Publications, 2017, pp. 39-44. ISSN: 1662-9779.

REMEŠOVÁ, M.; KLAKURKOVÁ, L.; HORYNOVÁ, M.; ČELKO, L.; KAISER, J. Preparation of Metallographic Samples with Anodic Layers. In *Metallography XVI. Materials Science Forum.* Switzerland: Trans Tech Publications Ltd., 2017, pp. 106-110. ISSN: 0255-5476.

GEJDOŠ, P.; KLAKURKOVÁ, L.; JULIŠ, M.; HORYNOVÁ, M.; REMEŠOVÁ, M.; HÉGR, E. Analysis of Surface Layer Defects on Carburezed Steel Component after Alkaline Blackening. In *Metallography XVI. Materials Science Forum.* Switzerland: Trans Tech Publications Ltd., 2017, pp. 274-277. ISSN: 0255-5476.

ŠVEJCAR, J.; KLAKURKOVÁ, L.; JULIŠ, M.; GEJDOŠ, P.; REMEŠOVÁ, M.; DYČKOVÁ, L. Analysis of causes of fractures of terminal board bolts. In *Přínos metalografie pro řešení výrobních problémů. Solid State Phenomena.* 14. Switzerland: Trans Tech Publications, 2017, pp. 93-98. ISSN: 1662-9779.

REMEŠOVÁ, M.; KLAKURKOVÁ, L.; ČELKO, L.; SLÁDKOVÁ, L.; JECH, D.; KAISER, J. Anodizing of Zinc-Titanium Alloy in NaOH and KOH Baths. In *Materials Structure & Micromechanics of Fracture VIII. Solid State Phenomena.* Solid State Phenomena. Switzerland: Trans Tech Publications, 2017, pp. 399-402. ISSN: 1012-0394.

A.3. Active conferences, workshops and internship

14th Conference on Contribution of Metallography to Production Problem Solutions, Mariánské Lázně, Czech Republic, 2017

International Conference on Materials Structure and Micromechanics of Fracture, Brno, Czech Republic, 2016

16th International Symposium on Metallography and Materials Science in Slovakia, 2016

International Conference on Engineering Failure Analysis, Leipzig, Germany, 2016

International workshop, Progressive and non-traditional technologies of surface treatment, Brno, Czech Republic, 2018

Nanoindentation workshop, CEITEC Nano RI, Brno, Czech Republic, 2017

International workshop, Progressive and non-traditional technologies of surface treatment, Brno, Czech Republic, 2017

International workshop, Progressive and non-traditional technologies of surface treatment, Brno, Czech Republic, 2016

Electrochemistry workshop, COST MP 1407, Cracow, Poland, 2015

4.2.-30.4.2019 Erasmus+ Traineeship, Institute for Chemistry and Technology of Materials, Graz University of Technology, traineeship title: *Activation of aluminium electrodes in deep eutectic solvents*, coordinator - Assoc. Prof. Dr. Bernhard Gollas

A.4. Participation in research projects

Student project STI-J-18-5308, Brno University of Technology, CEITEC, Czech Republic, Výzkum a vývoj technologie anodické oxidace hliníkové slitiny EN AW-1050A za účelem přípravy dopovaných konverzních vrstev, coordinator - Prof. Jozef Kaiser

MPO no. FV20232 Biodegradovatelné strukturované implantáty vyrobené metodou 3D tisku kovů - MPO, FV - TRIO

MPO no. FV10897 VaV speciálních typů brusiv pro broušení ložiskových kroužků se zaměřením dodržení požadované integrity broušení oběžných drah - MPO, FV - TRIO

MPO no. FV30335 Výzkum a vývoj pokročilých typů pojiv pro speciální brousicí nástroje - MPO, FV - TRIO

GAČR no. 19-22662S In situ precipitace hydroxyapatitu uvnitř hierarchických titanových struktur - GAČR

MPO no. FV10477 Technologie kombinovaného zdroje plasmatu pro vznik pokročilých povrchových úprav MPO, FV - TRIO